12
RF

PNL-2921
UC-70

Characterization of the Hanford 300 Area Burial Grounds

Task III - Fluid Transport and Modeling

G. W. Gee
C. S. Simmons

August 1979

Prepared for the U.S. Department of Energy
under Contract EY-76-C-06-1830

Pacific Northwest Laboratory
Operated for the U.S. Department of Energy
by Battelle Memorial Institute

Battelle

PNL-2921

NOTICE

This report was prepared as an account of work sponsored by the United States Government. Neither the United States nor the Department of Energy, nor any of their employees, nor any of their contractors, subcontractors, or their employees, makes any warranty, express or implied, or assumes any legal liability or responsibility for the accuracy, completeness or usefulness of any information, apparatus, product or process disclosed, or represents that its use would not infringe privately owned rights.

The views, opinions and conclusions contained in this report are those of the contractor and do not necessarily represent those of the United States Government or the United States Department of Energy.

PACIFIC NORTHWEST LABORATORY
operated by
BATTELLE
for the
UNITED STATES DEPARTMENT OF ENERGY
Under Contract EY-76-C-06-1830

Printed in the United States of America
Available from
National Technical Information Service
United States Department of Commerce
5285 Port Royal Road
Springfield, Virginia 22151

Price: Printed Copy $____*; Microfiche $3.00

*Pages	NTIS Selling Price
001-025	$4.00
026-050	$4.50
051-075	$5.25
076-100	$6.00
101-125	$6.50
126-150	$7.25
151-175	$8.00
176-200	$9.00
201-225	$9.25
226-250	$9.50
251-275	$10.75
276-300	$11.00

PNL-2921
UC-70

3 3679 00046 5643

CHARACTERIZATION OF THE HANFORD 300 AREA BURIAL GROUNDS.

TASK III - FLUID TRANSPORT AND MODELING

G. W. Gee
C. S. Simmons

August 1979

Prepared for the U.S. Department of Energy
Under Contract EY-76-C-06-1830

Pacific Northwest Laboratory
Richland, Washington 99352

PREFACE

The United States Department of Energy (DOE) is considering decontamination and decommissioning alternatives for its retired nuclear facilities in order to provide adequate protection from radioactive and other hazardous materials potentially originating from such sources. Decontamination and decommissioning of these facilities may involve the selective removal of radioactive or other materials from retired nuclear facilities and selection of the ultimate disposition of the facilities. Among the facilities being evaluated are retired radioactive waste burial grounds at DOE's Hanford Site, Richland, Washington.

The "Characterization of the Hanford 300 Area Burial Grounds" project was initiated to provide an assessment of retired radioactive waste burial grounds prior to selection of decontamination and decommissioning alternatives at the Hanford Site. The project was sponsored by the U.S. Department of Energy, Division of Environmental Control Technology and was conducted by Pacific Northwest Laboratory from 1975 through 1978.

The original intent of this project was to develop technology and methods for characterization of waste burial sites and to apply them to the 300 Area Burial Grounds. During the course of the study, the scope was broadened to include development of recommendations pertaining to buried waste disposition alternatives.

Project tasks were initiated to provide the necessary technology and to characterize burial ground sites. These tasks included:

Task I - Geophysical Evaluation
Task II - Geochemical Analysis
Task III - Fluid Transport Characterization and Modeling
Task IV - Biological Transport

Topical reports from each of these tasks have been issued under separate cover.

Two other reports have been issued: "Decontamination and Decommissioning" provides an overview of the 300 Area Burial Grounds, project results and recommendations. "Decontamination and Decommissioning Regulatory Issues" details regulatory issues to be considered when evaluating the alternatives.

SUMMARY

When evaluating radionuclide migration from burial sites, interaction of radionuclides with water and fluid transport through the geologic media must be considered. Fluid transport includes both liquid and vapor (evaporation) phase flow. In arid areas, such as the Department of Energy's Hanford Site, evaporation is often the dominant phase.

In Task III, Fluid Transport and Modeling, a computer model was developed and applied to the 300 Area Burial Grounds to analyze the influence of potential evaporation and rainfall patterns on drainage. The model describes one-dimensional unsaturated flow.

Fluid transport equations were evaluated to describe the driving forces of fluid flow. The data indicate that the major processes are evaporative drying, capillarity, and gravity flow. Thermally induced transport does not appear significant in the subsurface sediments of the area.

Several empirical evaporation methods are available for assessing potential evaporation/evapotranspiration. Four methods were used with the unsaturated flow model. Ultimately, the Blaney-Criddle method was chosen for subsequent simulation examples because it relies only on the climatic data available and gave results comparable to the other methods tested.

Simulations showed that a dry layer formation is important in controlling the soil-water balance in the profile. The surface dry layer acts as a mulch to retard the evaporative water losses and increase water storage.

The most important climatic factor in determining drainage appears to be yearly rainfall distribution. When rainfall is distributed in fall or winter, during periods of low potential evaporation, both water storage and drainage are increased. Summer showers, on the other hand, were shown to add little to the annual water storage. Rainfall occurring in one year influences the subsequent annual drainage for several succeeding years because of annual changes in water storage capacity and the transient nature of unsaturated flow in the storage zone.

CONTENTS

PREFACE iii
SUMMARY v
FIGURES ix
TABLES xii
INTRODUCTION 1
CONCLUSIONS 3
DESCRIPTION OF GEOHYDROLOGIC SYSTEM 5
STRATIGRAPHY. 5
HYDROLOGY 5
Ground Water 7
Unsaturated Zone 7
FLUID TRANSPORT 10
FLUID TRANSPORT EQUATIONS 10
POTENTIAL EVAPORATION 15
Blaney-Criddle Method 16
Radiation Method 16
Penman Method 17
Modified Penman Method 17
Pan Evaporation Method 17
ACTUAL EVAPORATION 18
UNSATURATED ZONE SIMULATION MODEL 21
MATHEMATICAL FORMULATION 21
FINITE DIFFERENCE FORMULATION 23
Water Mass Balance 24
Hydraulic Properties 25
Surface Flux Control 26
MODEL APPLICATION TO SHALLOW LAND BURIAL SITE AT HANFORD . . . 28
SOIL PROFILE 28
SOIL HYDRAULIC PROPERTIES 28
POTENTIAL EVAPORATION CALCULATIONS 34

CONTENTS (contd)

BOUNDARY CONDITIONS 45
INITIAL CONDITIONS 45
HYDROPHOBIC SURFACE LAYER SENSITIVITY 50
HYDRAULIC CONDUCTIVITY SENSITIVITY 51
POTENTIAL EVAPORATION SENSITIVITY 70
TOTAL RAINFALL SENSITIVITY 73
EFFECT OF RAINFALL DISTRIBUTION 74
EFFECTS OF SOIL PROFILE CONFIGURATION 98
REFERENCES 109

FIGURES

1 Geologic Cross Sections of the 300 Area at Hanford . . . 6

2 Soil-Water Characteristic Curve for Fine Sand 30

3 Hydraulic Conductivity Computed by the Millington-Quirk Method for Fine Sand 31

4 Soil-Water Characteristic Curve for Coarse Sand 32

5 Hydraulic Conductivity Computed by the Millington-Quirk Method for Coarse Sand 33

6 Cumulative Potential Evaporation by Four Methods for 1947 35

7 Cumulative Potential Evaporation by Four Methods for 1948 36

8 Daily Potential Evaporation by Four Methods for 1947 . . . 37

9 Daily Potential Evaporation by Four Methods as in Figure 8 but for 1948 41

10 Water Content Profiles for Days 1, 50, 200, and 365 During Simulation of a Transient State Using 1948 Climate . . . 47

11 Cumulative Seepage at Selected Depths During Simulation of a Transient State Using 1948 Climate 48

12 Soil-Water Storage Difference from Initial Values During Simulation of a Transient State Using 1948 Climate. . . . 49

13 Water Content Profiles for Selected Days for Simulation without a Hydrophobic Surface Layer 52

14 Water Content Profiles for Selected Days for Simulation with a Hydrophobic Surface Layer 53

15 Water Content Profiles for Selected Days Following Rainfall--without Surface Layer 54

16 Water Content Profiles for Selected Days Following a Rainfall--with Surface Layer 55

FIGURES (contd)

17 Simulation of Water Movement without Surface Layer . . . 56

18 Simulation of Water Movement with a Surface Layer . . . 58

19 Water Content Profiles Near the Surface without Surface Layer During Drying 60

20 Water Content Profiles beneath a Hydrophobic Surface Layer During Drying 61

21 Water Content Profiles for 1, 50, 200, 365 Days Using 1/10 Conductivity 62

22 Water Content Profiles for 1, 6, 8, 20 Days Using 1/10 Conductivity 63

23 Water Content Profiles for 1, 50, 200, and 365 Days Using 1/100 Conductivity 64

24 Water Content Profiles for 1, 6, 8, and 20 Days Using 1/100 Conductivity 65

25 Simulated Soil-Water Movement Using 1/100 Conductivity and 1948 Climate 66

26 Simulated Soil-Water Movement Using 1/100 Conductivity and 1948 Climate 68

27 Simulated Soil-Water Movement Using Penman PET and 1948 Climate 71

28 Water Content Profiles for 1, 50, 200, 365 Days Using 2X Rainfall of 1948 75

29 Water Content Profiles for 1, 6, 8, 20 Days and Conditions of Figure 28 76

30 Water Content Profiles for 1, 6, 8, 20 Days Using 1.5X Rainfall of 1948 77

31 Water Content Profiles for 1, 6, 8, 20 Days Using 0.3X Rainfall of 1948 78

32 Simulated Soil-Water Movement for a 6-year Rainfall Sequence 79

FIGURES (contd)

33 Six-year Rainfall Sequence 81

34 Six-year Rainfall Sequence 83

35 Six-year Rainfall Sequence 85

36 Six-year Rainfall Sequence 87

37 Six-year Rainfall Sequence 89

38 Simulation of Soil-Water Movement for a Three-Year Sequence Based on Consecutive 1947 and 1948 Climates with a Repeated 1948 Year 91

39 Year 2 of Figure 38 93

40 Year 3 of Figure 38 95

41 Simulation of Soil-Water Movement for a Three-Year Sequence Based on Repeated 1947 Climate 99

42 Year 3 of Figure 41 101

43 Cumulative Seepage at Selected Depths for 1947 Climate and Blaney-Criddle PET, 800-cm-deep Water Table 103

44 Cumulative Seepage at Selected Depths for 1947 Climate and Blaney-Criddle PET, 700-cm-deep Water Table 104

45 Cumulative Seepage at Selected Depths for 1947 Climate and Blaney-Criddle PET; Sand Layer Removed from Profile . . . 105

46 Water Content Profiles for Selected Days in 1947 . . . 107

47 Water Content Profiles for Selected Days in 1947 with Coarse Sand Layer Removed 108

TABLES

1 Water Flow in Response to Thermal Gradients at Shallow Land Burial Grounds on the Hanford Site 13

2 Soil-Water Characteristics for the Fine and Coarse Sands . . 29

3 Standard Initial Conditions Derived from Simulation of a Transient State Using 1948 Climate 46

4 Simulation of 1948 Climate, with and without a Hydrophobic Surface Layer 50

5 Simulations Based on 1948 Climate, without Hydrophobic Surface Layer 70

6 Simulation of Six Consecutive Years Based on Multiples of Rainfall in 1948 73

7 Simulation of a Three-Year Rainfall Sequence Based on Consecutive 1947 and 1948 Climates with a Repeated 1948 Year 97

8 Simulation of a Three-Year Rainfall Sequence on Repeated 1947 Climate 97

9 Simulations Using 1947 Climate and Blaney-Criddle Pet Method, Assuming Presence of a Hydrophobic Layer for Three Cases 106

INTRODUCTION

Both decontamination and decommissioning of burial sites require an assessment of radionuclide migration from the burial site to the biosphere. The single most important factor affecting containment capability of a burial site is the interaction of water with the radionuclides and subsequent radionuclide migration induced by water transport through the geologic media which surrounds the buried waste (Gilmore, 1977). In addition to determining the location, quantity and type of radionuclide present, a thorough knowledge of the site geology and hydrology is required.

Hydrologic assessment is now required as a portion of the licensing procedure for all commercial burial sites, and hydrologic studies are in progress at all existing or planned burial grounds at Department of Energy (DOE) operated facilities (Gilmore, 1977). Although geohydrologic conditions vary dramatically from site to site throughout the country, certain assessments can be made that will allow managers of waste facilities to properly monitor and subsequently predict radionuclide transport from shallow land burial sites.

Assessment of fluid transport at burial grounds requires a consideration of the mechanisms of transport governing both liquid and vapor phase flow. In arid regions, evaporation is often the dominant mechanism for fluid transport, with a major portion of the annual precipitation being transported to and evaporated from the soil surface. Mechanisms for flow are principally, isothermal and Darcian in nature but also include thermal gradients which exist at the soil surface and geothermal gradients which are present within the sediments. The influence of thermally induced water transport on the overall annual water balance needs to be evaluated.

The study reported here is primarily an unsaturated zone water transport modeling effort specific to an arid region site, namely, the 300 Area Burial Grounds at DOE's Hanford Site. However, the methodology described includes measurement and modeling techniques that can be applied to other burial sites to characterize the water migration and hence be used as a framework from which radionuclide migration can be predicted.

The report contains:

- a description of the geohydrologic setting of the 300 Area Burial Grounds
- a review of generalized transport equations used to identify mechanisms for fluid transport at arid zone burial grounds
- an evaluation of thermally induced water transport using soil characteristics typical of the 300 Area Burial Grounds
- a description of several empirical evaporation models used in assessing potential evapotranspiration from arid region sites
- a description of UNSAT, a finite difference computer model, used to predict water balance at arid zone burial grounds. UNSAT simulates evaporation from bare, or vegetated surfaces, and has a mass balance capability of ± 0.1 cm water on an annual basis
- simulation runs of water balance, including evaporation losses and deep seepage, in response to changes in climatic variables
- simulation runs of water balance, including evaporation losses and deep seepage in response to changes in soil hydraulic conductivity and soil layering.

CONCLUSIONS

The work in this task consisted of characterizing the geohydrologic system and applying a computer model to describe unsaturated zone fluid flow. The results of the study are summarized in the following conclusions.

- Evaporative drying, capillarity, and gravity flow are the dominant forces moving fluid through sediments at Hanford.
- Thermally induced water flow is insignificant in subsurface sediments at Hanford. Vapor transport due to thermal gradients in subsurface sediments will seldom exceed 0.06 mm/yr.
- Isothermal models of fluid transport are acceptable for seasonal predictions of water flow. Additional evaporation data will be required to adequately test models for use in long-term simulations.
- Simulation modeling demonstrated the importance of a dry layer formation in controlling soil-water balance in the profile. Such a layer may determine the actual evaporation possible as a fraction of the potential evapotranspiration. The thickness and persistence of this layer is subject to additional research.
- Levels of expected drainage into a simulated 8-m-deep water table below the 300 Area Burial Grounds can vary between about 0.5 cm extracted by evaporation to 1 cm of seepage, depending on the yearly rainfall and its distribution. Perhaps the most important climatic factor in determining drainage probability is the annual rainfall distribution - not the yearly quantity nor the potential evapotranspiration. The high conductivity of the surface material will transport excess water beyond the reach of potential evaporation when intensity is high.
- Effects of previous rainfall history have a significant influence on the drainage and water balance in following years. Storage excesses from previous years can continue to drain and support current water balance conditions.

- Effects of soil layering can be demonstrated with the simulation model. Engineered and geologic barriers to water movement can be modeled if hydraulic properties of the barriers are known. The example simulations have demonstrated that coarse sand layers can retard soil-water flow, and hence act as dynamic soil-water barriers.
- It is believed that the example simulations clarify an indispensable need for using model simulation as an approach to estimating drainage, because direct field measurement using neutron probes and other instrumentation may prove inadequate due to measurement error and uncertainty.

DESCRIPTION OF GEOHYDROLOGIC SYSTEM

The geology and hydrology of the 300 Area Burial Grounds, described in part by Lindberg and Bond (1979), can be summarized as follows.

STRATIGRAPHY

Geologic formations present in the 300 Area are, in ascending order:

1. Columbia River Basalt Group, including the Yakima Basalt Subgroup
2. Ringold Formation
3. Glaciofluvial deposits
4. Eolian sediments.

These formations are shown in Figure 1.

The Columbia River Basalt Group and older basalts extend to depths greater than 3,500 m. The Ringold Formation overlies the topmost basalt flow (some 47 to 49 m below the Columbia River surface). The Ringold Formation is largely quartzitic gravel and quartz- and mica-rich sands with some basalt sands and gravels intermixed. The lower member of the formation is comprised of silts and clays. The Ringold Formation beneath the 300 Area is about 46 m thick. The lower 12 m are composed largely of silt and clay with some gravel and sand intermixed. The glaciofluvial deposits overlying the Ringold Formation are called Pasco Gravels. The Pasco Gravels underlying the 300 Area display two cycles of graded bedding except that the finer portion of the upper cycle is absent (removed by erosion by the Columbia River). The surface sediments are largely wind-transported sands and silts. These sediments have been deposited in dunes up to 3 m deep. These dunes are prominent features of the landscape.

HYDROLOGY

Both the ground water and the unsaturated zone are important hydrologic considerations.

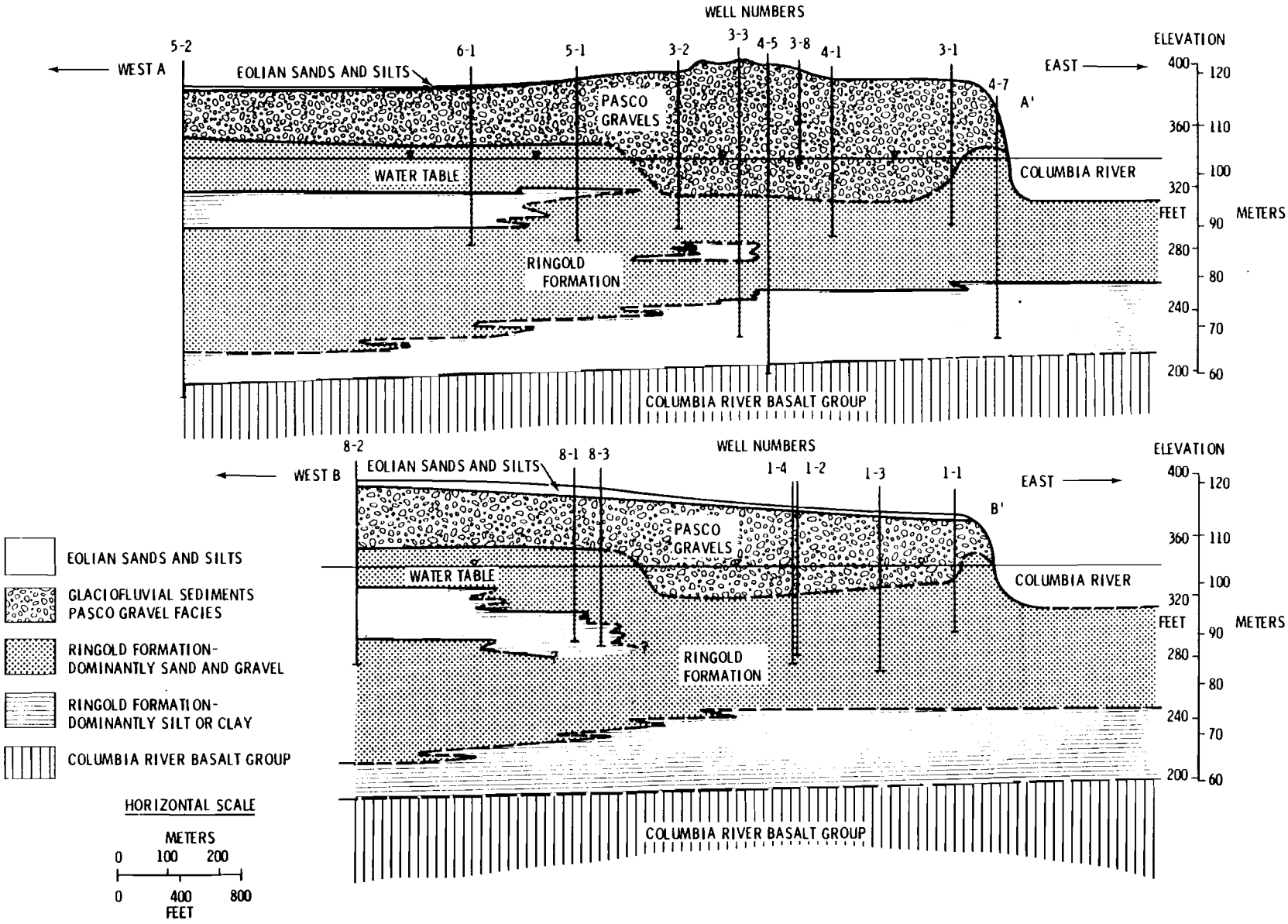

FIGURE 1. Geologic Cross Sections of the 300 Area at Hanford (Lindberg and Bond, 1979)

Ground Water

Ground water beneath the 300 Area occurs in confined aquifers within the Columbia River Basalt sequence and in the unconfined aquifer in the Ringold Formation and Pasco Gravels. The boundary between confined and unconfined aquifers is the lowermost silt and clay member of the Ringold Formation. The low permeability of this layer allows little interchange of ground water between confined and unconfined aquifers. The confined aquifers in the 300 Area are under slight artesian pressure. The 300 Area is close to an area where mixing of two ground water sources occurs in the unconfined aquifer: 1) ground water flowing southeasterly from the central portion of the Hanford Site and 2) ground water recharged by the Yakima River and flowing generally east to southeast into the Columbia River.

Eight burial grounds were designated for storage of dry wastes of uranium-contaminated materials. These wastes were emplaced well above the water table at various times since 1944. At present there is no evidence that contaminants from any of these dry wastes have been leached by water percolating from the ground surface.

Sources for potential groundwater contamination in the 300 Area include: 1) routine discharge of wastewater into the processing water trench, and 2) leaking pipes containing wastewater, steam condensate or fresh water. Several unplanned releases have occurred (Paas, 1955), but monitoring has failed to confirm an association of these releases with observed concentrations of uranium in the ground water. Major contaminants beneath the 300 Area are nitrate, fluoride, chloride, uranium and beta emitters. Details of concentration levels and location of these contaminants are described by Lindberg and Bond (1979).

Unsaturated Zone

The unsaturated zone above the ground water in the 300 Area consists of well-drained coarse sediments. The water holding capacity of the surface sediments is low and, hence, little water is available to sustain more than a

sparse cover of cheatgrass/sagebrush type vegetation. The annual precipitation is 160 mm of water mostly in the form of rain showers occurring predominantly in the fall and early spring. About half of the winter precipitation occurs as snow.

How much of the annual precipitation is transmitted to the ground water via deep drainage is an important but unresolved question. At Hanford it is generally assumed that virtually all of the annual precipitation is lost to evaporation and that only in unusually wet years is there any likelihood that drainage to the water table occurs (Brownell et al., 1975). However, Wallace (1978) using an evaporation model calibrated for arid sites (Morton, 1976) predicted that precipitation would exceed evaporation by as much as 11.6 mm, an excess of about 7% of the annual precipitation. This annual precipitation excess of 11.6 mm is not lost to surface runoff since the infiltration capacity of the soil is high; therefore, under long-term steady conditions the excess precipitation should drain through the unsaturated zone to the ground water.

Extensive monitoring of a lysimeter site in the 200 Area at Hanford (Brownell et al., 1975) has shown that little water movement occurs in sediments below about 4 m. The precision of the measuring devices (neutron moisture probes) was such that small amounts of water drainage could not be detected until water content changes exceeded about 0.01 cm/cm in the sediments studied. Changes below the 4-m depth in a closed-bottom, 18-m deep lysimeter used to capture and store gravity-drained water were not greater than ± 0.01 cm/cm after 4 years, (Brownell et al., 1975). It would take over 17 years for water to accumulate in sufficient quantities to be detected if 11.6 mm of precipitation was accumulating annually and was stored in the lysimeter soil volume in a relatively uniform fashion.

The low rates of unsaturated water movement observed at the Hanford Site (Brownell et al., 1975) suggest that long-term studies will be required for a complete assessment of radionuclide migration. Computer simulation of the fluid transport at specified burial sites provides a way to quickly assess contaminant migration which may occur slowly and for extended periods of time

(centuries or longer). However, it is first necessary to understand the mechanisms of transport and the limitations of the existing methods and models used to predict water migration under conditions characteristic of the Hanford Site.

FLUID TRANSPORT

Fluid transport at burial sites is concerned primarily with the movement of the soil solution to either the ground water or the atmosphere through unsaturated sediments in which radionuclides and waste materials have been placed. The flow of water may result from a number of driving forces. Among these are forces of gravity and capillarity, as well as osmotic and thermal energy forces.

FLUID TRANSPORT EQUATIONS

The flow of water must be considered in both the liquid and vapor states. A generalized equation for fluid transport which considers water, solute, and thermal interactions can be written:

$$J_w = J_w^{\ell} + J_w^{\nu} = -L_{ww}^{\ell} (X_w + \beta^{\ell} X_q + \sigma X_s) - L_{ww}^{\nu} (X_w + \beta^{\nu} X_q + \sigma^{\nu} X_s) \quad (1)$$

where

J_w = total water transport

J_w^{ℓ}, J_w^{ν} = liquid and vapor transport, respectively

L_{ww}^{ℓ} and L_{ww}^{ν} = the transport coefficients for liquid and vapor, respectively

X_w, X_q, X_s = the driving forces related to water, heat, and solute transport

β^{ℓ}, β^{ν} = heat of transport coefficients for liquid and vapor, respectively.

σ^{ℓ}, σ^{ν} = solute reflection coefficients for liquid and vapor, respectively.

This equation has been developed for water flow in soils by Taylor and Cary (1964) and Letey (1968) and can be written in terms of known hydraulic conductivities and measurable matric, gravity, osmotic and thermal potential gradients as:

$$J_w = -\left[K(\theta) + \frac{D_v \rho^\circ_v}{RT}\right]\left[\left(\frac{\partial \psi m}{\partial z}\right) + \frac{\partial \psi g}{\partial z}\right]$$

$$-\left[\sigma K(\theta) + \frac{D_v \rho^\circ_v}{RT}\right]\left(\frac{\partial \psi o}{\partial z}\right) - \left[K(\theta)\frac{\partial \psi m}{\partial T} + \frac{D_v \rho^\circ \lambda}{RT^2}\right]\frac{\partial T}{\partial z} \qquad (2)$$

where

$K(\theta)$ = hydraulic conductivity

D_v = vapor diffusivity in soil

ρ°_v = saturation vapor density

R = specific gas constant for water

T = Kelvin temperature

ψ_m, ψ_g, ψ_o = matric, gravity, osmotic potential

λ = latent heat of vaporization

When salt concentration and thermal gradients are absent the second and third terms are zero. If significant transport occurs from these driving forces then simultaneous transport of water, heat, and solute must be accounted for. Equations similar in form to Equation (2) can be developed to describe the simultaneous transport of heat and solute. In addition, if solutes are ionic and of sufficient concentration, additional sets of equations must be developed to describe the flow of electricity and its interacting effect on water flow. The general solution of the flow equation is difficult to obtain. However, assessment of the magnitude of the various terms often provides for suitable simplification. This approach is used in the following discussion to evaluate thermally induced flow in burial ground soils.

Components of Equation (2) can be assessed to describe fluid transport in soils typical of the 300 Area and 300 North Burial Grounds. From Phillips et al. (1977) and data presented in Task IV of this project, Biological Transport, the soils in the 300 Area Burial Grounds can be classed as well drained, coarse textured sediments (>70% sand, <5% clay). The sediments are low in salts and drained water contents range from 0.05 cm/cm to 0.10 cm/cm.

Seasonal thermal gradients and water content changes are virtually damped out in the top 5 m of soil at typical burial sites at Hanford (Brownell et al., 1975). For transport below the top 5 m of soil, i.e., in the zone where most waste is stored, the equation for flow can be reduced to:

$$J_w = K(\theta) \frac{\partial \psi g}{\partial z} + \left[\beta' L(T) \frac{\partial T}{\partial z}\right] \tag{3}$$

where

β' = an enhancement factor which combines the effect of porous material and thermal gradient interactions on water vapor transport

$L(T)$ = temperature dependence factor for water vapor

= $0.0732 \exp [0.0547(T-273.15)]$

Recently, Jury and Letey (1979) have shown that enhancement factors for a wide variety of sediments nearly always range between 1.0 and 2.0. Table 1 illustrates the water transport in response to thermal gradients in soils typical of the 300 North Burial Ground. The values were calculated at several field water contents for soil at 5 m depth. A -1.0 (cm/cm) water potential gradient was assumed.

The data indicate that the dominant driving force is the gravity gradient. Downward flow persists even at very low water contents (0.035 cm/cm) although the flow rates are reduced to almost insignificant values (0.01 to 0.04 mm/yr). Changes in the enhancement factor, β', from 1 to 2 only slightly affect flow at water potentials of -0.7 bar. At -16 bar water potential there is a larger influence of β' changes on the net flow, but in a practical sense these rate differences would be unmeasurable. These data support earlier work by Enfield et al. (1973) who estimated that net flow rates in drained soils at Hanford should not exceed 10 mm/yr.

TABLE 1. Water Flow in Response to Thermal Gradients at Shallow Land Burial Grounds on the Hanford Site

Water Potential, -cm x 10^6	Water Content, cm/cm	K,[a] mm/yr	β'	dT/dz,[b] C/cm x 10^{-4}	J_w,[c] mm/yr
0.7	0.055	1.21	1.0	4.6	1.18
0.7	0.055	1.21	1.5	4.6	1.17
0.7	0.055	1.21	2.0	4.6	1.15
4.1	0.040	0.205	1.0	4.6	0.175
4.1	0.040	0.205	1.5	4.6	0.165
4.1	0.040	0.205	2.0	4.6	0.145
16.0	0.035	0.074	1.0	4.6	0.044
16.0	0.035	0.074	1.5	4.6	0.034
16.0	0.035	0.074	2.0	4.6	0.014

(a) Estimated from water characteristics of soil typical of 300 Area Burial Ground Sediments

(b) Geothermal gradient

(c) Flow is positive downward.

Calculations similar to those shown in Table 1 yield the following observations:

1. Thermally induced water flow is insignificant at the normal, drained water content values in subsurface sediments.

2. When water contents drop below drained water content values as a result of plant root extraction or some other drying means, thermally enhanced vapor flow may tend to dominate the slow process; however, flow rates at these water contents are so low that transport upward due to vapor would seldom exceed 0.06 mm/yr (this rate is 4 x 10^{-4} times the estimated annual evaporation rate).

3. Larger thermal gradients would produce greater thermally induced flow, but significant thermal gradients exist only in the top 2 m of the soil profile.

These observations suggest that fluid transport in subsurface sediments at burial ground sites at Hanford can be modeled by considering only Darcian flow. This approach is described in detail later, see for example, Equation (10). Equation (2) reduces to Darcy's law when the thermal, osmotic, and vapor terms are set to zero. Only at low water contents (below 0.05 cm/cm for the soil illustrated in Table 1) would vapor flow be significant.

The need for including thermally induced flow in modeling of soil-water evaporation has been considered by a number of workers (Cary, 1966; Hanks et al., 1967; Feddes, 1971; Jackson et al., 1976). A complete model of evaporation must include thermal effects since diurnal temperature gradients are large, particularly at the soil surface. However, the net daily flow of thermally driven water is generally small in comparison to total daily evaporation (Jackson et al., 1976). The most comprehensive field investigation of nonisothermal water flow at an arid region site has been conducted by Jackson and coworkers (Jackson, 1973; Jackson et al., 1973, 1974, 1975; and Kimball et al., 1976). Their results indicate that surface water contents are affected by diurnal heat cycling, but that both water and heat transport could be predicted by models which do not incorporate the coupling effects of heat and water. Their results tend to support work of others (Gardner and Gardner, 1969 and Hanks et al., 1967) which have shown that seasonal evaporation rates can be predicted with reasonable accuracy using empirical isothermal evaporation models.

Because there is a paucity of data on annual evaporation, the effects of thermally induced flow during winter months at arid sites is not known. Recent work by Fuchs et al. (1978) suggests that in partially saturated soil considerable upward transport of water can take place in response to temperature gradients as a result of dramatic increases in the apparent thermal conductivity and heat capacity of the soil. This response occurs primarily near saturation at temperatures slightly below freezing and is damped significantly as soils dry to normal field water contents. These results have not been

experimentally verified, and field data are needed to assess the magnitude of this effect on the annual water balance. Until further data are available it is reasonable to assume that, as in the case of thermally induced near-surface flow in the summer months, the water profile in the top 1 m of soil can be altered by thermal effects but the net transport is not significantly affected. Subsequently, isothermal flow models can be used to predict fluid transport during the entire year.

Some of the isothermal models that are available for arid zone evaporation predictions are discussed in the following section. Models developed to predict long-term evaporation losses from arid sites require inputs that will allow accurate estimation of both the atmospheric or energy-limited potential evaporation rates, which are governed by atmospheric variables, and the soil-limited evaporation rates, which are governed by the hydraulic properties of the soil.

POTENTIAL EVAPORATION

Numerous methods have been developed to estimate evaporation from wet plant and soil surfaces. During periods when surfaces are wet, evaporation proceeds to a maximum or potential rate. When plants are included in the surface (vegetated) the concept of potential evapotranspiration is used. According to Rosenberg (1974)

> Potential evapotranspiration (PET) is the evaporation from an extended surface of short green crop which fully shades the ground, exerts little or negligible resistance to the flow of water, and is always well supplied with water. Potential evapotranspiration cannot exceed free water evaporation under the same weather conditions.

When no cover crop exists, i.e., bare wet soil, PET is set equal to potential evaporation, PE.

Under arid conditions potential evaporation rates are seldom achieved, since surfaces are most often dry or drying and vegetation is sparse. However, the concept of PE is still useful since it describes the upper limit for evaporation and actual evaporation is computed as some fraction of PE. Virtually all evaporation models are based on the potential evaporation concept.

These models incorporate empiricisms that relate PE to measured climatic variables. The most common variables considered are mean daily temperature, mean daily relative humidity, daily wind run, and daily total radiation (solar or net). Five methods for calculating potential evaporation from climatic variables are described below.

Blaney-Criddle Method

Potential evapotranspiration can be computed for areas where climatic data are limited and air temperature data are the only weather records available (Blaney and Criddle, 1962). The Blaney-Criddle method has been used extensively for irrigation scheduling (Doorenbos and Pruitt, 1977):

$$ET_0 = c' \, [p(0.46T + 8)] \text{ mm/day} \tag{4}$$

where

T = mean daily temperatures in °C over the month considered.

p = mean daily percentage of the total annual daytime hours estimated for a given month and latitude.

c' = adjustment factor which depends upon minimum relative humidity sunshine hours and daytime wind estimates

Radiation Method

This method is proposed where weather records are sufficient that temperature, solar radiation, or sunshine duration and cloudiness data are available (Makkink, 1957; Doorenbos and Pruitt, 1977). The equation used to estimate potential evaporation is:

$$ET_0 = c'' \, (W' \cdot R_s) \tag{5}$$

where

R_s = solar radiation in mm/day evaporation equivalents

W' = weighting factor depending upon temperature and latitude

c'' = adjustment factor depending upon mean humidity and daytime wind conditions

Penman Method

Soil-water evaporation from wet soil surfaces has been modeled extensively. Penman (1948) proposed a model based on an energy balance at the soil surface. The model is composed of two terms, the energy term and the aerodynamic term. The relative importance of each term varies with climatic conditions.

The Penman equation can be written:

$$ET_o = [W \cdot R_n + (1-w)\ f(u)\ (e_a - e_d)] \qquad (6)$$

(Energy term) (Aerodynamic term)

where

ET_o = potential evaporation

W = temperature-related weighting factor = $\Delta/(\Delta + \gamma)$; where γ = psychrometric constant, Δ = slope of saturation vapor pressure temperature

R_n = net radiation in mm/day equivalent evaporation

$f(u)$ = wind function = $0.27\ (1 + u/100)$

U = 24 hr wind run in km/day at 2 m height.

$e_a - e_d$ = difference between saturation vapor pressure at mean air temperature and mean actual vapor pressure of the air (in mbars)

Modified Penman Method

This is identical to the above method except the equation is multiplied by a correction factor, c; c is an adjustment factor to compensate for effects of day and night weather conditions. Tabulated values for c under varying humidity and day/night wind conditions are given by Doorenbos and Pruitt (1977). Under low relative humidity ($\leq$30%) conditions c is always unity.

Pan Evaporation Method

Potential evaporation from wet surfaces can also be computed from pan evaporation data (Thornthwaite and Mather, 1955; Doorrenbos and Pruitt, 1977). The equation can be written:

$$ET_o = K_p \cdot E_{pan} \tag{7}$$

E_{pan} = daily pan evaporation in mm/day

K_p = pan coefficient (tabulated values are available for weather bureau class A and Colorado sunken type pans).

ACTUAL EVAPORATION

Empirical relations have also been used extensively to describe bare soil evaporation. Tanner and Fuchs (1968) used a modified Penman approach using the surface temperature to calculate the saturation deficit and from it the potential evaporation rate. Correlation was good for wet soil surfaces, but their formulation did not predict the actual evaporation rate when the surface dried. Jury (1973) attributed the discrepancy to the fact that the Tanner-Fuchs (1968) equations did not account for simultaneous heat and water transport. In contrast, Staple (1974) used a Penman approach modified for surface humidity at soil surface and found good agreement between measured and calculated evaporation rates.

Soil limiting evaporation has also been modeled by empirically assuming a time-dependent function for the evaporation rate (Black et al., 1969; Gardner and Gardner, 1969; Ritchie, 1972; Tanner and Jury, 1976). The relation between evaporation and time can be written:

$$\int E dt = c\ (t-t_c)^{1/2} \tag{8}$$

where

E = bare soil evaporation rate

c = a constant determined for each soil for a given climate

t_c = the time at which the soil water content drops below a critical value and a falling rate of evaporation ensues (Tanner and Jury, 1976).

Most investigators have observed that Equation (8) works reasonably well for short-term studies (Black et al., 1969; Tanner and Jury, 1976). Agreement between observed and measured values is often within 5 to 10% for evaporation periods up to 60 days. However, estimates of evaporation losses on an annual

basis will be in error unless the calibration constant is carefully determined for both soil type and seasonal variations. Because of the uncertainties involved and its empirical nature this method does not appear to hold promise for long-term generic studies of bare soil evaporation for sites which have not been intensively studied.

Idso et al. (1975) proposed a procedure for calculating daily evaporation rates from both wet and dry soils using as input data, solar radiation, maximum and minimum air temperatures, moist surface albedo and maximum and minimum surface temperatures. For Arizona desert conditions, Idso et al. (1975) formulated the method to be independent of season. They demonstrated that seasonal fluctuations in wind speed and other important climatic variables such as vapor pressure, which varied by a factor of 5 or more, were accounted for in the measured surface-air temperature differences, hence, were automatically corrected by the simple regression relations developed. In addition, they indicated that their method was independent of soil or surface type and could be used even on vegetated surfaces.

A recent treatment by Hillel (1977) and van Bavel and Hillel (1977) suggests ways that bare soil evaporation might be handled under the special circumstances of a dry hydrophobic surface mulch. The governing equation for dry soil evaporation model used by Hillel et al. (1975) can be written as follows:

$$E_m = \frac{PE\ (e + 1)}{e + 1 + r_m/r_a} \tag{9}$$

where $$PE = \frac{e(Rn - S)/L + d_z/r_a}{e + 1}$$

and Rn = net radiant flux density

S = heat flux density into soil

L = heat of vaporization

d_z = saturation deficit at elevation z above surface

$r_a = (\ln(z/z_0))^2/(0.16\ Uz)$ where z_0 is the roughness parameter and U_z is wind speed at z

$e = \Delta/\gamma$

Δ = slope of saturation vapor density-temperature curve

γ = psychrometric constant

$r_m = M/Dft$

where M = the mulch (dry soil) thickness

D = vapor diffusivity of bulk air

f = mulch porosity

t = tortuosity.

This model assumes that the temperature profile is uniform, the wind profile is logarithmic, and the value of e can be taken at $T = T_z$ (temperature at elevation z). Also, it assumes that the dry layer is completely dry and does not transmit any water by capillary flow.

The Hillel model has not been experimentally verified for long-term (annual) evaporation conditions. Until additional experimental data have been collected, simple models should be tested. However, as evaporation data from buried sites become available, it is likely that more sophisticated models will be required to account for annual evaporation losses. We have chosen to develop a model similar in principle to the hydrophobic layer model of Hillel but requiring less input data. The development of a water flow model that includes a dry surface layer is described in the following section.

UNSATURATED ZONE SIMULATION MODEL

Questions regarding the influence of potential evaporation and rainfall patterns on drainage through the unsaturated zone were analyzed quantitatively by using a computer model describing one-dimensional unsaturated flow. Flow governed by liquid phase capillary conductivity was assumed, and nonisothermal effects within the soil profile were disregarded. Because reasonable predictions should not exceed the complexity of available data, a one-dimensional bare soil profile was simulated using an empirically developed mechanism to control evaporation and water balance within the soil profile. This controlled evaporation layer was required in as much as the desert climate of the 300 Area Burial Grounds imposes extreme desiccating conditions.

MATHEMATICAL FORMULATION

The model used in the application to the 300 Area Burial Grounds was a modified version of the unsaturated flow computer model UNSAT (Gupta et al. 1978). This model can simulate infiltration, vertical drainage, and extraction by plant roots as related to the hydraulic properties of a soil, soil layering, and the root growth characteristics in a particular soil for given evapotranspiration rates and water application rates.

Unsaturated vertical soil water flow is described by the one-dimensional Darcy's law:

$$q = K(\theta)\frac{dH}{dz} \tag{10}$$

for hydraulic conductivity $K(\theta)$

where

q = volumetric flux (positive down) (cm/hr)

$H = h + z$ is the hydraulic potential (cm)

z = depth (positive downward) (cm)

h = suction head (soil-water tension) (cm)

θ = volumetric water content of soil (cm water/cm soil)

The hydraulic conductivity, which depends on the water content θ, can also depend explicitly on z, and thus describe a heterogeneous soil profile.

The equation of continuity is given by:

$$\frac{\partial \theta}{\partial t} = - \frac{\partial q}{\partial z} - S(z, t) \tag{11}$$

where

t = time (hr)

$S(z,t)$ = plant root sink term in (cm water/cm soil/hr).

Expressing conductivity as a function of h and combining Equations (10) and (11) gives the basic equation for vertical soil water flow:

$$C(h) \frac{\partial h}{\partial t} = \frac{\partial}{\partial z} \left[K(h) \left(\frac{\partial h}{\partial z} + 1\right)\right] + S(z,t) \tag{12}$$

where

$$C(h) = - \frac{d\theta}{dh} \tag{13}$$

is the soil water capacity (cm^{-1}), and K is expressed explicitly as a function of h. The functional relation between h and θ for each depth used to define Equation (13) is called the soil-water characteristic curve or retention relation. Since for this application the soil profile does not include plants, the sink term vanishes in Equations (11) and (12).

The basic Equation (12) is solved subject to the following boundary conditions imposed at the soil profile's extremities and for a presumed initial water distribution within the profile.

Initial Condition:

Determined by prescribing the suction head $h(z,o)$ or water content $\theta(z,o)$ for each depth z at the beginning of simulation.

Surface Boundary Condition:

Determined by prescribing the suction head (h) or flux at the surface for each time step. Rainfall rate and evaporation rate establish the surface flux.

Lower Boundary Condition:

A variety of conditions are possible.

1. A static water table has a constant suction head approximately equal to zero at the water table's depth.
2. A variable water table has variable depth.
3. A dynamic water table has prescribed flux at the water table's depth.
4. Unit hydraulic gradient drainage conditions prevail if the water table is far below the base of the simulated soil profile. This permits drainage.

Condition (1) was assumed throughout this application of the model.

FINITE DIFFERENCE FORMULATION

A numerical solution of Equation (12) subject to initial and boundary conditions was obtained by using separate profiles for depth and time. The finite difference equation is:

$$- C_i^{j-1/2} \left(\frac{h_i^j - h_i^{j-1}}{\Delta t_j} \right) = \frac{1}{z_{i+1} - z_{i-1}} \left[\left\{ \left(\frac{h_i^{j-1} - h_{i-1}^{j-1} + \Delta z_i}{\Delta z_i} \right) K_{i-1/2}^{j-1} \right.\right.$$

$$\left. - \left(\frac{h_{i+1}^{j-1} - h_i^{j-1} + \Delta z_{i+1}}{\Delta z_{i+1}} \right) K_{i+1/2}^{j-1} \right\} + \left\{ \left(\frac{h_i^j - h_{i-1}^j + \Delta z_i}{\Delta z_i} \right) K_{i-1/2}^j \right.$$

$$\left.\left. - \left(\frac{h_{i+1}^j - h_i^{j-1} + \Delta z_{i+1}}{\Delta z_{i+1}} \right) K_i^j + 1/2 \right\} \right] \qquad (14)$$

for $\Delta z_i = z_i - z_{i-1}$, $(z_o = 0)$

where i denotes the node of depth z_i and j represents the j'th time step with increment $\Delta t_j = t_j - t_{j-1}$, $(t_o = 0)$.

The internodal flux for each time step is:

$$q_i^j = \frac{1}{2}\left[K_{i+1/2}^{j-1}\left(1 + \frac{h_i^{j-1} - h_{i-1}^{j-1}}{\Delta z_i}\right) + K_{i+1/2}^{j}\left(1 + \frac{h_i^{j} - h_{i-1}^{j}}{\Delta z_i}\right)\right] \tag{15}$$

where

$i = 0$ denotes the surface.

Equation (14) constitutes an implicit finite difference scheme, which is non-linear in suction head (h). Solution is by iteration using the previous values C^{j-1} and K^{j-1} to estimate the present values C^j and K^j; h^j is obtained by solving this tridiagonal linear system equation defined over the nodes and subjected to the boundary conditions. Water content for each node is then calculated from the soil-water characteristic curve.

Water Mass Balance

Soil-water storage for each time step is:

$$W_j = \sum_{i=1}^{n} (\theta_i^j + \theta_{i-1}^j)\ \Delta z_i/2 \tag{16}$$

where

$z_i = z_i - z_{i-1}$ for n nodes.

Letting ΔI_j, ΔE_j, and ΔD_j denote infiltration, evaporation, and drainage, respectively, for each time step, the water mass balance error is calculated as:

$$\varepsilon = |\Delta I_j - \Delta E_j - \Delta D_j - \Delta W_j| \tag{17}$$

Cumulative surface flux (ΔQ_j) during the time increment Δt_j is:

$$\Delta Q_j = \Delta I_j - \Delta E_j\ . \tag{18}$$

The program maintains computational accuracy by adjusting the time step so that mass balance error Equation (17) remains less than a prescribed limit. The continuously changing time step is restricted to specified limits, however. Those limits are provided by the user as minimum and maximum time steps in hours. An option to use a reduced time step during water application is also provided. Model computations proceed with the maximum time step and use a reduced time step as required to maintain the prescribed mass balance error, selected to be 0.1 cm.

Hydraulic Properties

Inasmuch as the hydraulic properties of coarse soils and sands exhibit extreme ranges of variation including steep gradients, a special representation in terms of polynomial functions was adopted. For each soil type the suction head domain is divided by a value h_1 into wet and dry regions. Within each region the hydraulic properties are expressed as follows.

Soil-water characteristic:

$$\theta - \theta_o = \sum_{k=1}^{p} a_k (h - h_o)^k, \quad h_o \leq h \leq h_1 \tag{19}$$

$$\theta - \theta_f = \sum_{k=1}^{m} b_k (\ell n\ h - \ell n\ h_f)^k, \quad h_1 < h \leq h_f \tag{20}$$

Soil-water capacity:

$$C\ (h) = - \sum_{k=1}^{p} k\ a_k\ (h - h_o)^{k-1}\ , \quad h_o \leq h \leq h_1 \tag{21}$$

$$C\ (h) = - \sum_{k=1}^{m} k\ b_k\ (\ell n\ h - \ell n\ h_f)^{k-1}/h\ , \quad h_1 < h \leq h_f \tag{22}$$

Conductivity:

$$K\ (h) = K_o + \sum_{k=1}^{r} a_k\ (h - h_o)^k, \quad h_o \leq h \leq h_1 \tag{23}$$

$$K\ (h) = \ell n\ K_f + \sum_{k=1}^{l} b_k\ (\ell n\ h - \ell n\ h_f), \quad h_1 < h \leq h_f \tag{24}$$

where "o" and "f" denote minimum and maximum values.

Equations (19) through (24) are defined for positive pressure head (h). Coefficients in the equations are evaluated for a specific soil by least squares fitting with the constraint of continuity at the value h_1. Moreover, the fit of Equations (19) and (20) for the soil-water characteristic is constrained so that capacity is positive and θ is monotonic. Polynomial expressions used in the computer program avoid storage of measurements and

provide simplified extrapolation. Such expressions have the advantage of fitting nearly any data set; however, a disadvantage when they are compared to analytical functions describing physical models of hydraulic properties is that extrapolation beyond the measurement range is not generally possible.

Surface Flux Control

In vertical unsaturated flow, surface flux constitutes the major influence on water movement. Rainfall and evaporation rates comprise that surface flux. Thus, the flow equation is solved with a surface flux boundary condition (Neuman condition) for all times, except when soil dryness will not allow the given flux to be sustained. Therefore, if a certain dry limit head is attained, the simulation proceeds with a potential boundary condition (Dirichlet condition) by setting the surface head equal to that limit. When the dry limit suction head is established, surface flux is then estimated consistent with Darcy's law.

To simulate the behavior of a desiccated surface layer, an additional program option was included. When the suction head at the surface ($z = 0$) is greater than a specified limit value, the surface flux assumes a given value characteristic of vapor transport through a hydrophobic layer. During that vapor transmission state, the layer is viewed as being above $z = 0$, where the Darcian flow region begins. Once the layer has formed it remains until the next water application event, and following its formation, Darcian flow redistribution of soil-water beneath the layer takes place. The layer offers no flow resistance during water application or under wet soil conditions that allows potential evaporation rates, and detailed flow within the layer is not modeled. Thus, effects of layer thickness are not accounted for. In summary, the surface flux q_s was modeled as follows:

Define

q^j_s = surface flux at $z = 0$, time step j

q_1 = characteristic vapor transmission rate of hydrophobic layer

q_R = rainfall rate

Ep = potential evaporation rate

h_s = surface suction head at $z = 0$

h_d = suction head for dry limit of soil

h_1 = initial suction head limit beneath layer when formation occurs for $h_1 \leq h_d$

Then:

$$q_s^j = q_R \text{ if rainfall occurs } (q_R \geq 0)$$

$$= -Ep \text{ if } h_s^{j-1} < h_1$$

$$= -q_1 \text{ if } h_d \geq h_s^K \geq h_1 \text{ at some } k = j$$

$$\text{and } q^m_s < 0,\ k \leq m < j$$

$$= q_o, \text{ Equation (12) with } h_o j = h_d \text{ if } h_s \geq h_d$$

Note that during rainfall, evaporation is considered to be nil. In addition to an evaporation rate control, the model includes an infiltration control. If rainfall rate is high and exceeds infiltrability the excess water is assumed to constitute runoff. Surface runoff can enter the soil through ponding.

The total evaporation representing the dynamic interaction of soil and atmosphere is calculated as the integral of the surface flux, q_s, over periods when it is negative. A positive q_s indicates surface infiltration and downward transport. The potential evaporation required as input can be obtained directly from lysimeter measurements or by methods based on climatological data. These methods have been described previously.

MODEL APPLICATION TO SHALLOW LAND BURIAL SITES AT HANFORD

The computer model that was applied to the 300 Area Burial Grounds required the following list of input information:

1. depth of simulated soil profile and location of various soil layers
2. measured soil-water characteristics and hydraulic conductivity for each soil type layer present in the profile
3. potential evapotranspiration and rainfall for each day of the simulated period; pattern of diurnal variation
4. hydrophobic layer's surface evaporation control parameters: suction head dryness limit for which layer formation occurs and characteristic vapor transport rate through the layer
5. lower boundary conditions describing the type of water table or free drainage
6. initial conditions provided as suction head or water content distribution over the soil profile.

SOIL PROFILE

An 800-cm-deep soil profile terminated by a static water table and including a 50-cm coarse sand layer beginning at 600-cm was simulated. The nodal system used 20-cm increments in the first 100 cm and 50-cm increments from 100 to 800 cm, except for an additional 625-cm node at the center of the layer. Thus, there were 21 nodes with 3 nodes defining the layer.

SOIL HYDRAULIC PROPERTIES

The model parameters most difficult to obtain are the soil hydraulic properties. Each soil material involved must be described. Soil-water characteristics for the fine sand (eolian) material (typical of the 300 Area) and layered coarse sand material were determined from soil samples by measuring water content at known applied suction head. Table 2 contains values for the measured characteristics.

TABLE 2. Soil-Water Characteristics for the Fine and Coarse Sands

Fine Sand		Coarse Sand	
Water Content (cm/cm)	Suction Head (cm)	Water Content (cm/cm)	Suction Head (cm)
0.321	2	0.255	5
0.320	5	0.168	15
0.289	15	0.113	20
0.127	25	0.043	25
0.084	35	0.022	35
0.077	45	0.009	45
0.066	105	0.006	105
0.020	15,000	0.002	15,000
0.013	1,000,000		
Saturated Conductivity (cm/hr)			
169.2		324.0	

Field measurements of hydraulic conductivity are particularly difficult to obtain since extensive instrumentation is required to monitor moisture movement over a sufficient range of water content. Moreover, the solution of the inverse problem for conductivity satisfying Equation (12) is excessively difficult as a consequence of confounding by measurement uncertainty. To avoid that difficulty, hydraulic conductivity was estimated by the Millington-Quirk method by matching calculation and measurement at the saturated conductivity (Reisenauer, 1972).

Figures 2 through 5 show the soil hydraulic properties for the fine and coarse sands. The curves were least squares fit to Equations (19) through (24) and the parameters were input to the model. Implementation of the Millington-Quirk method and the least squares fit utilized linear extrapolation between the characteristic measurements of Table 2.

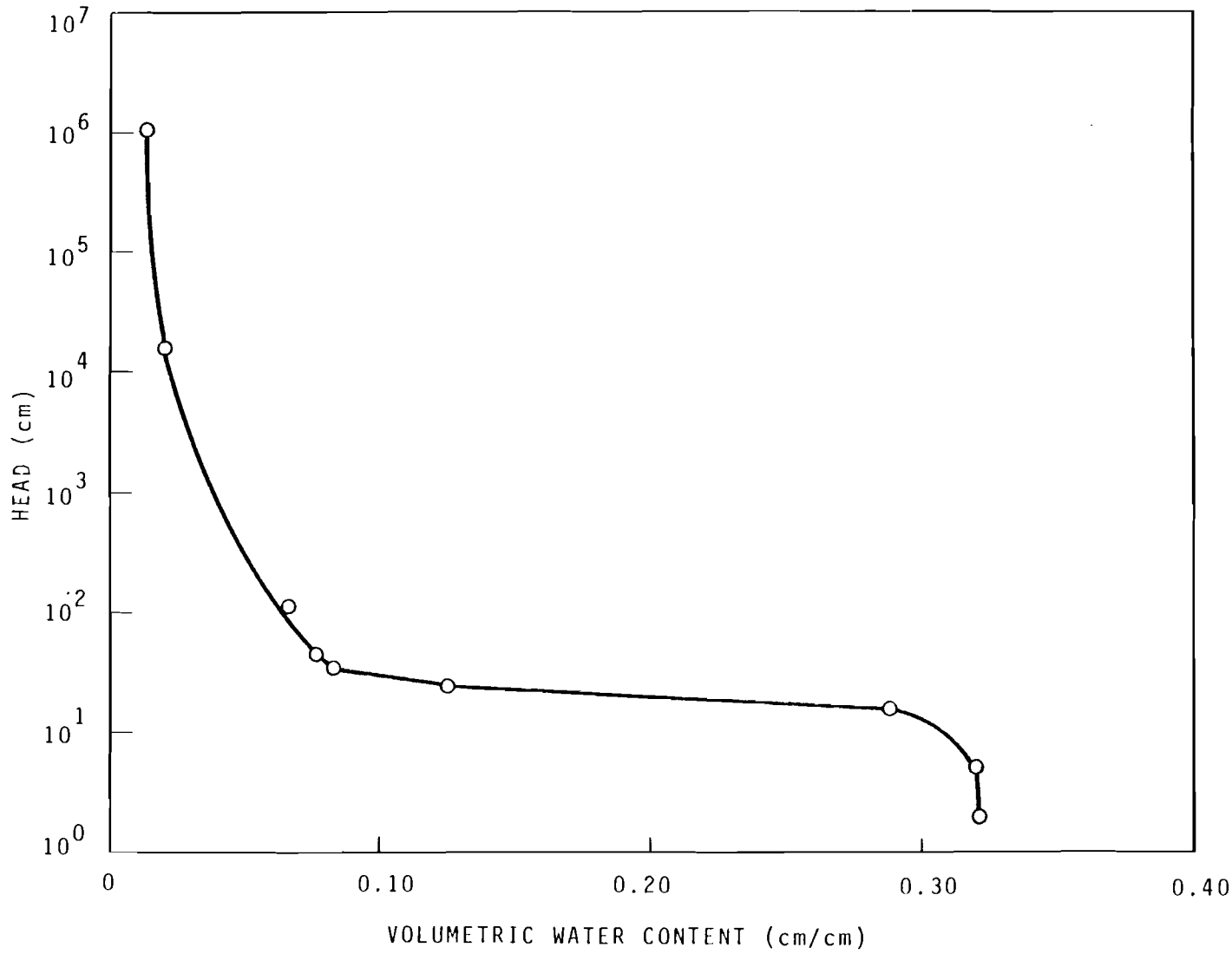

FIGURE 2. Soil-Water Characteristic Curve for Fine Sand

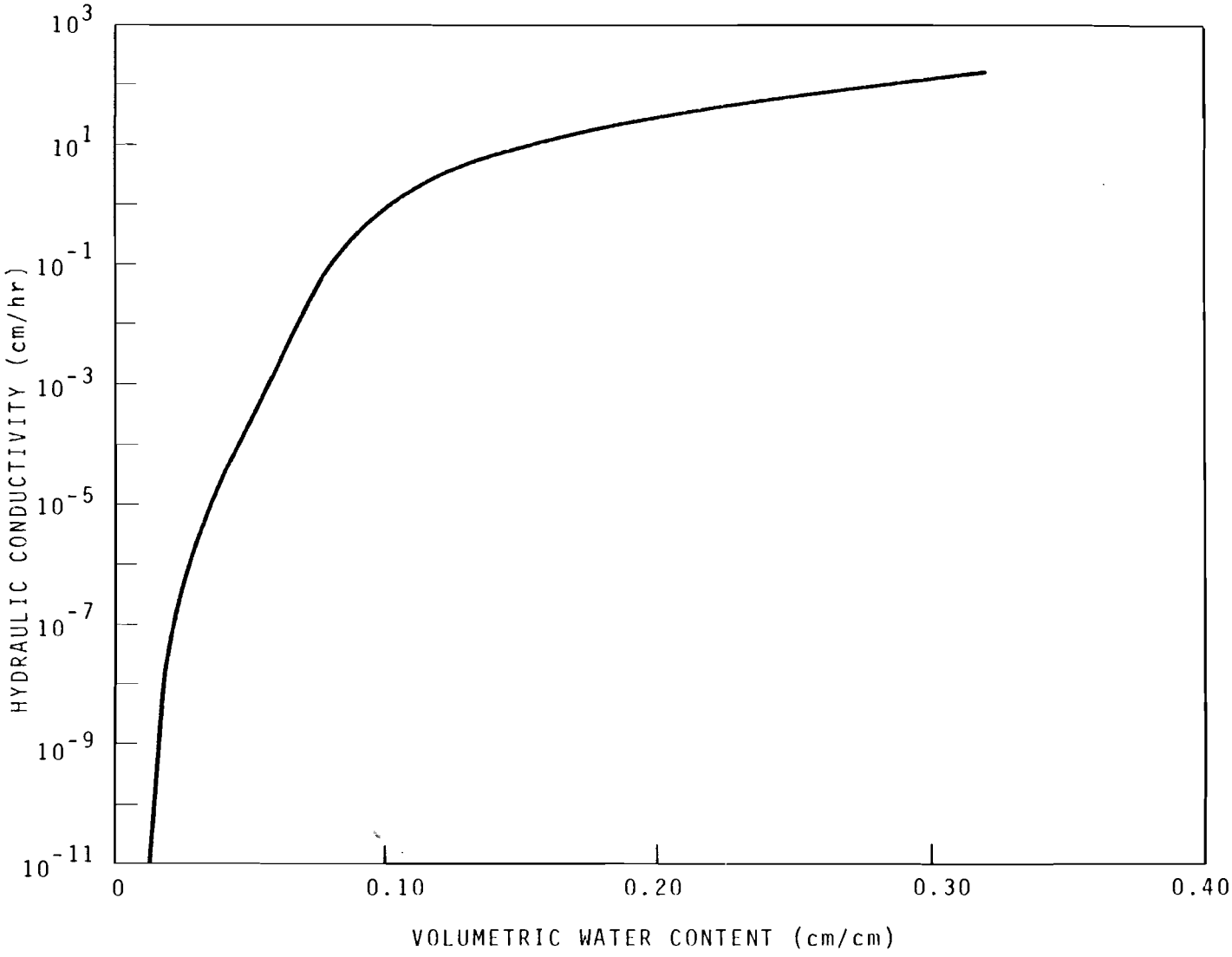

FIGURE 3. Hydraulic Conductivity Computed by the Millington-Quirk Method for Fine Sand

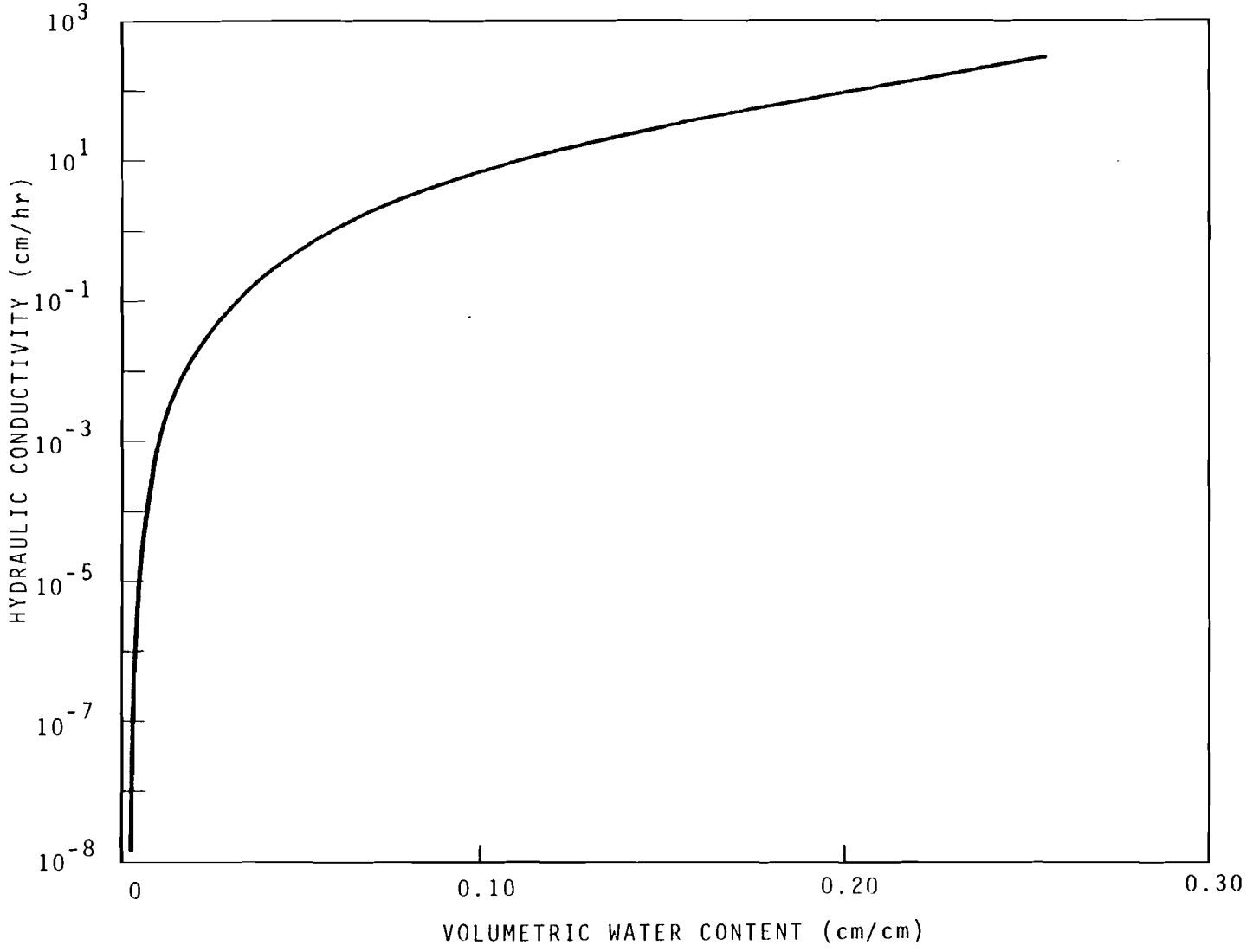

FIGURE 4. Soil-Water Characteristic Curve for Coarse Sand

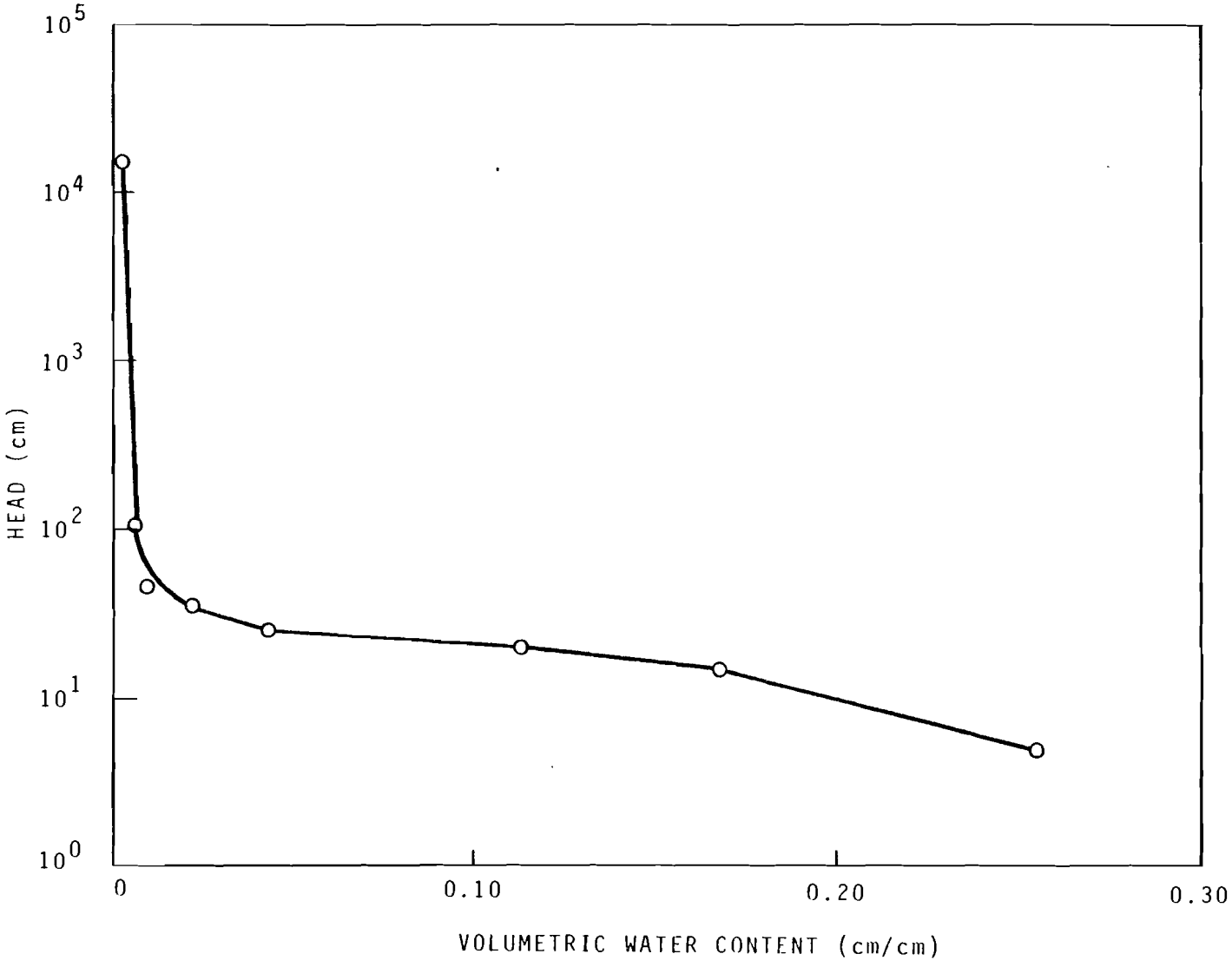

FIGURE 5. Hydraulic Conductivity Computed by the Millington-Quirk Method for Coarse Sand

POTENTIAL EVAPORATION CALCULATIONS

The computer program developed by Gupta et al. (1978), hereafter designated as the FAO Program, provided daily estimates of potential evapotranspiration (PET) calculated by four methods. Because these methods actually describe potential evaporation regardless of removal from plant or soil under saturated conditions, the potential evaporation is equal to potential evapotranspiration and used interchangeably. It is expected that the estimated potential evaporation would exceed that for a bare dry soil. The following climatic data were used for the test case years 1947 and 1948 at Hanford:

- minimum and maximum daily temperature at 4-ft level (°F)
- mean daily relative humidity (%)
- mean daily wind velocity (MPH)
- average cloud cover (scale 1-10)
- daily precipitation (inches)

Other climatic parameters required by the various methods were estimated by the FAO Program utilizing tabulated average values for various global regions.

The years 1947 and 1948 were chosen because these years were two consecutive years of nearly equal but above average total precipitation (23.5 and 24.1 cm, respectively). They also exhibited entirely different rainfall distribution patterns. This allowed for analysis of rainfall distribution effects on annual drainage losses.

Figures 6 and 7 show the cumulative potential evaporation at the Hanford Site in 1947-48 based on four methods. Estimates based on the Blaney-Criddle method were subsequently selected for example simulations since that method relies only on the given climatic data. Moreover, except for the uncorrected Penman method, all other methods yielded nearly the same cumulative potential evaporation. Different distributions of daily evaporation, however, were obtained for the methods. Daily distributions are displayed in Figures 8 and 9.

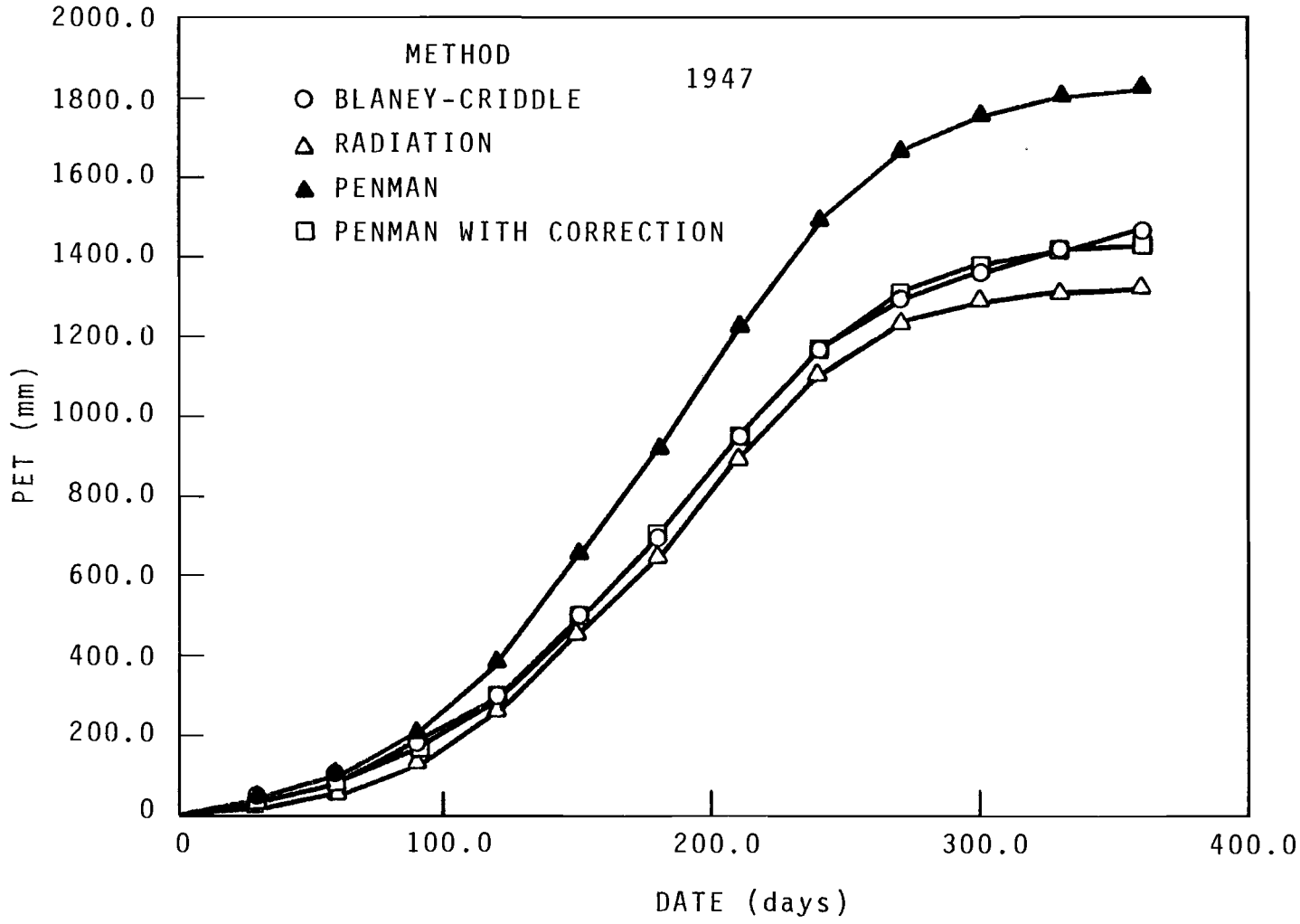

FIGURE 6. Cumulative Potential Evaporation by Four Methods for 1947

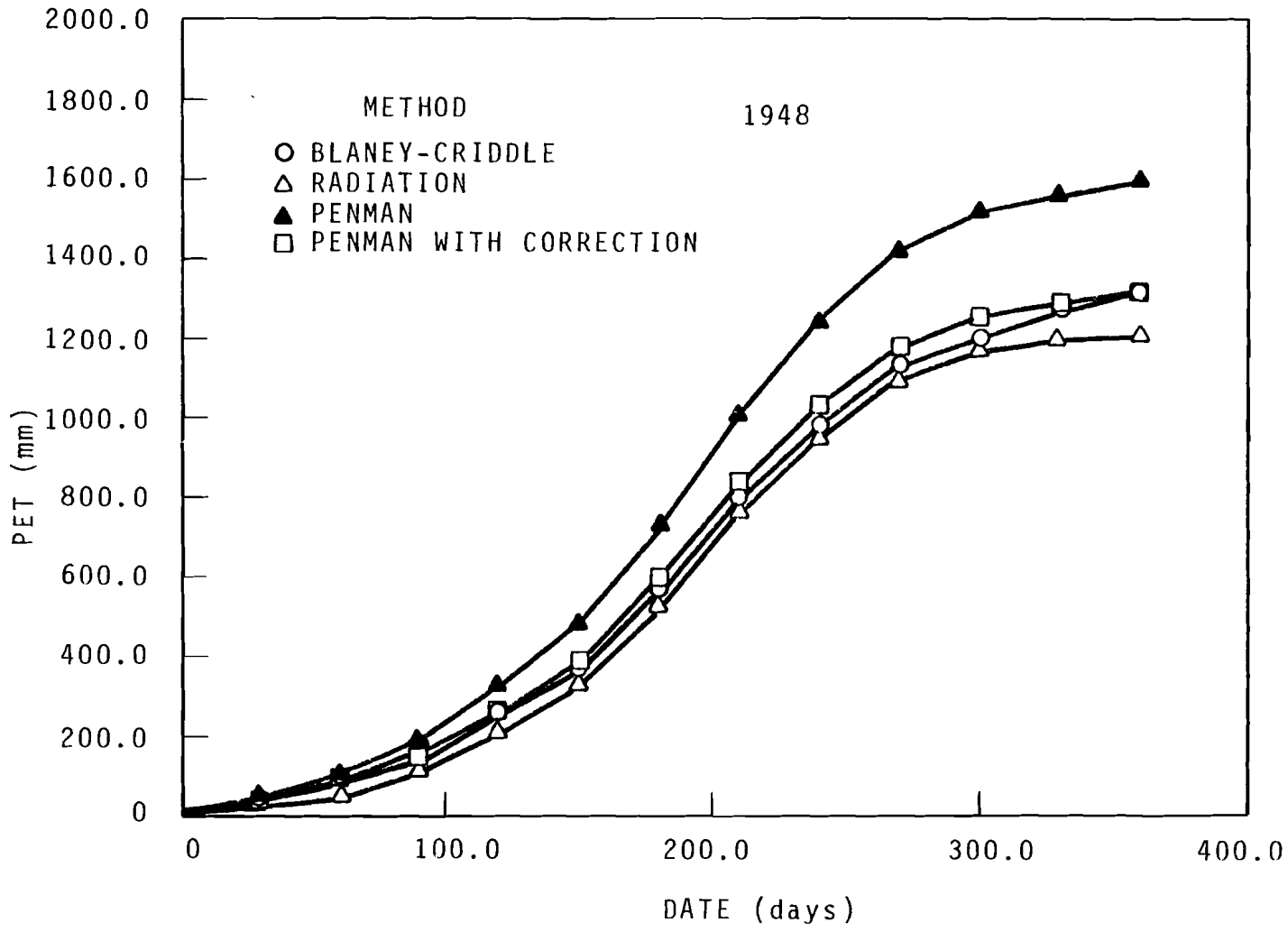

FIGURE 7. Cumulative Potential Evaporation by Four Methods for 1948

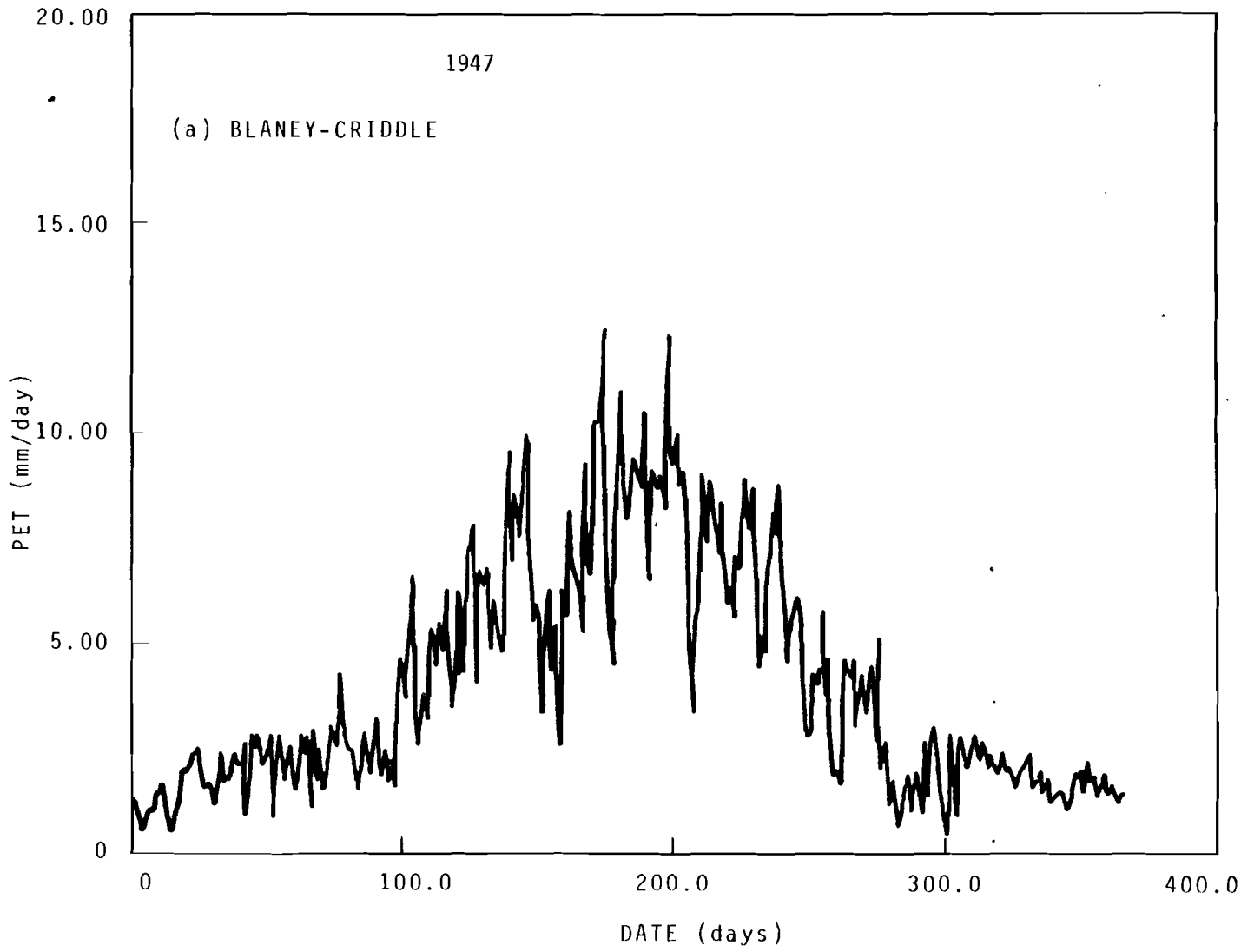

FIGURE 8. Daily Potential Evaporation by Four Methods for 1947: a) Blaney-Criddle, b) Radiation, c) Penman, and d) Penman with Correction Factor

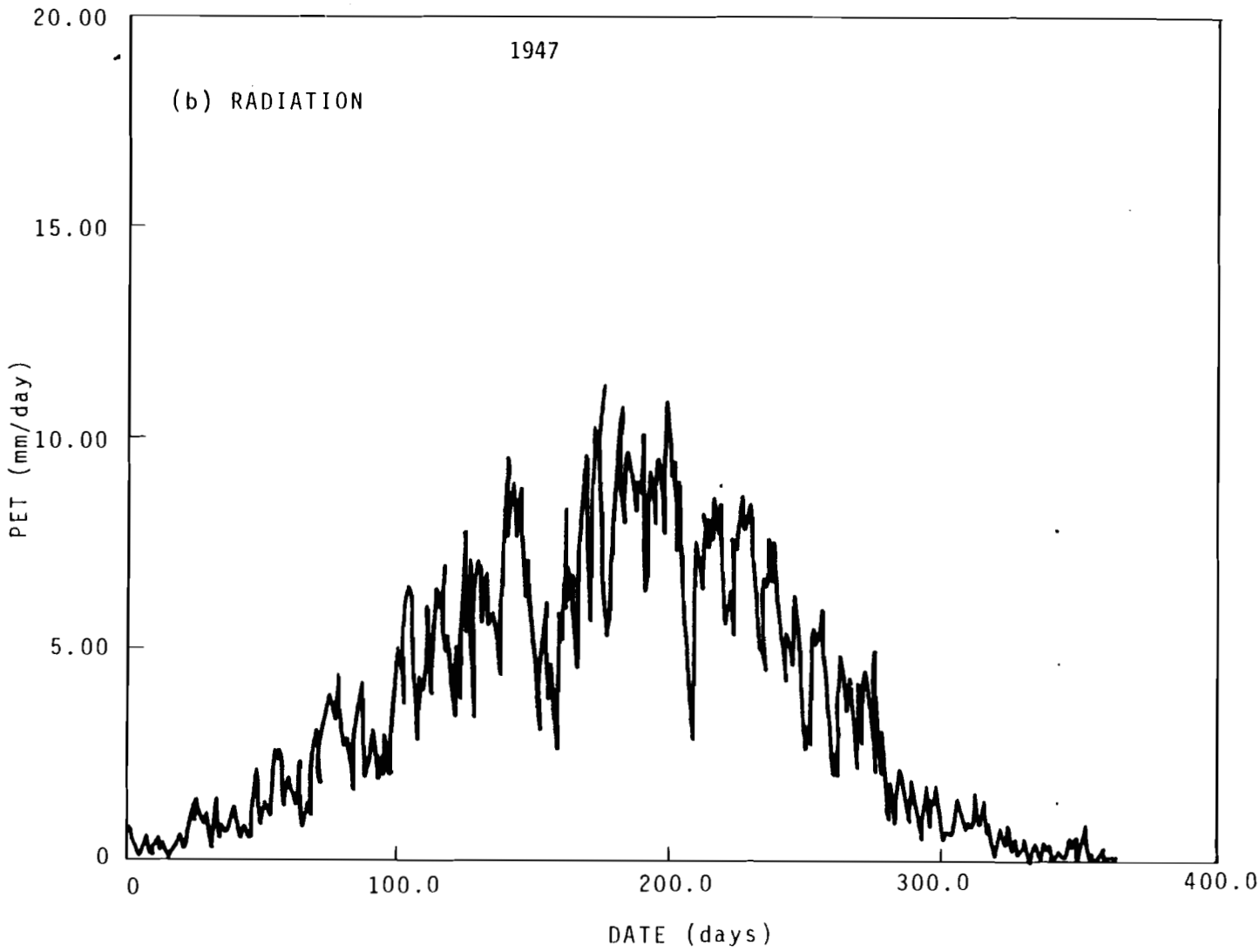

FIGURE 8. (contd)

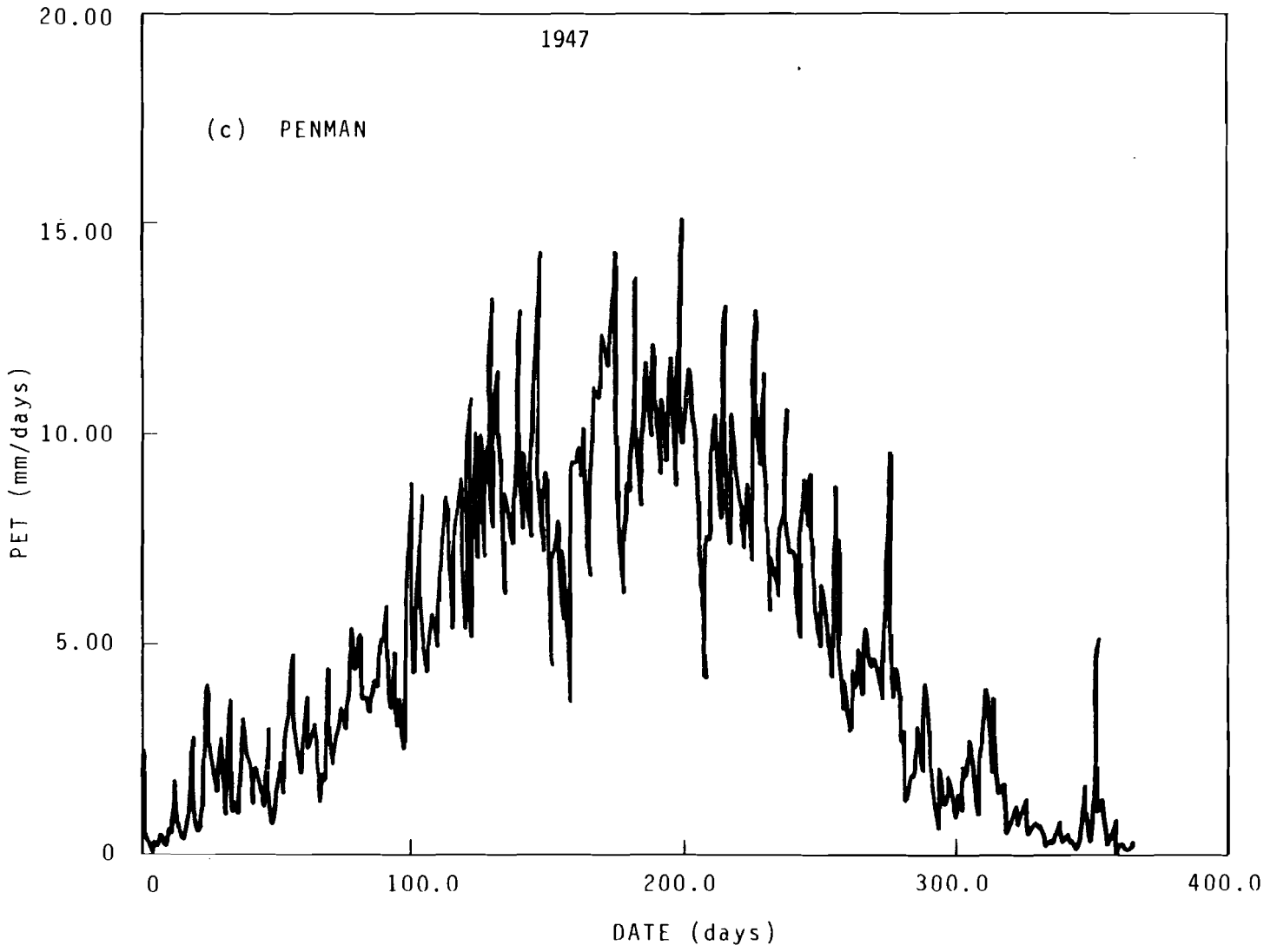

FIGURE 8. (contd)

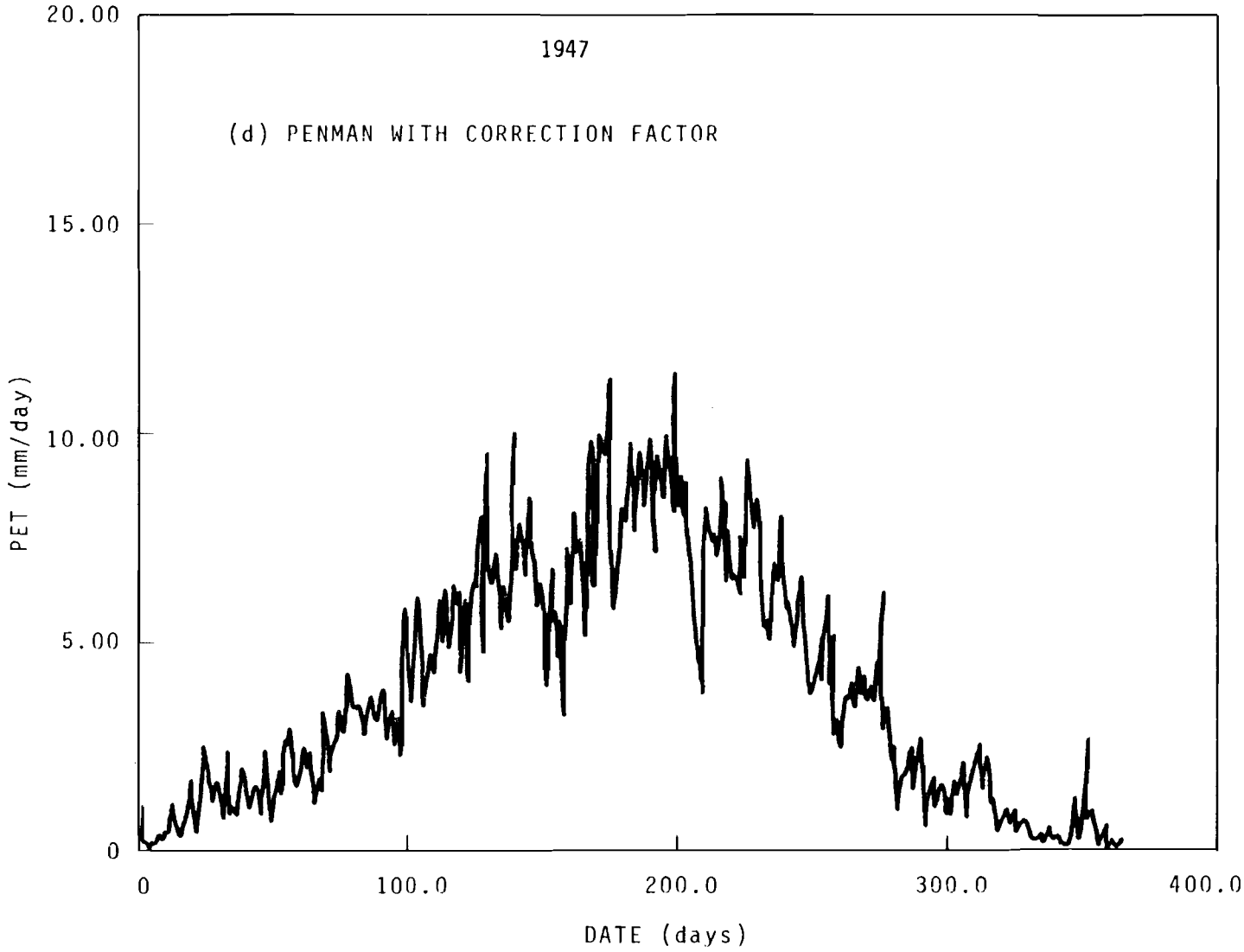

FIGURE 8. (contd)

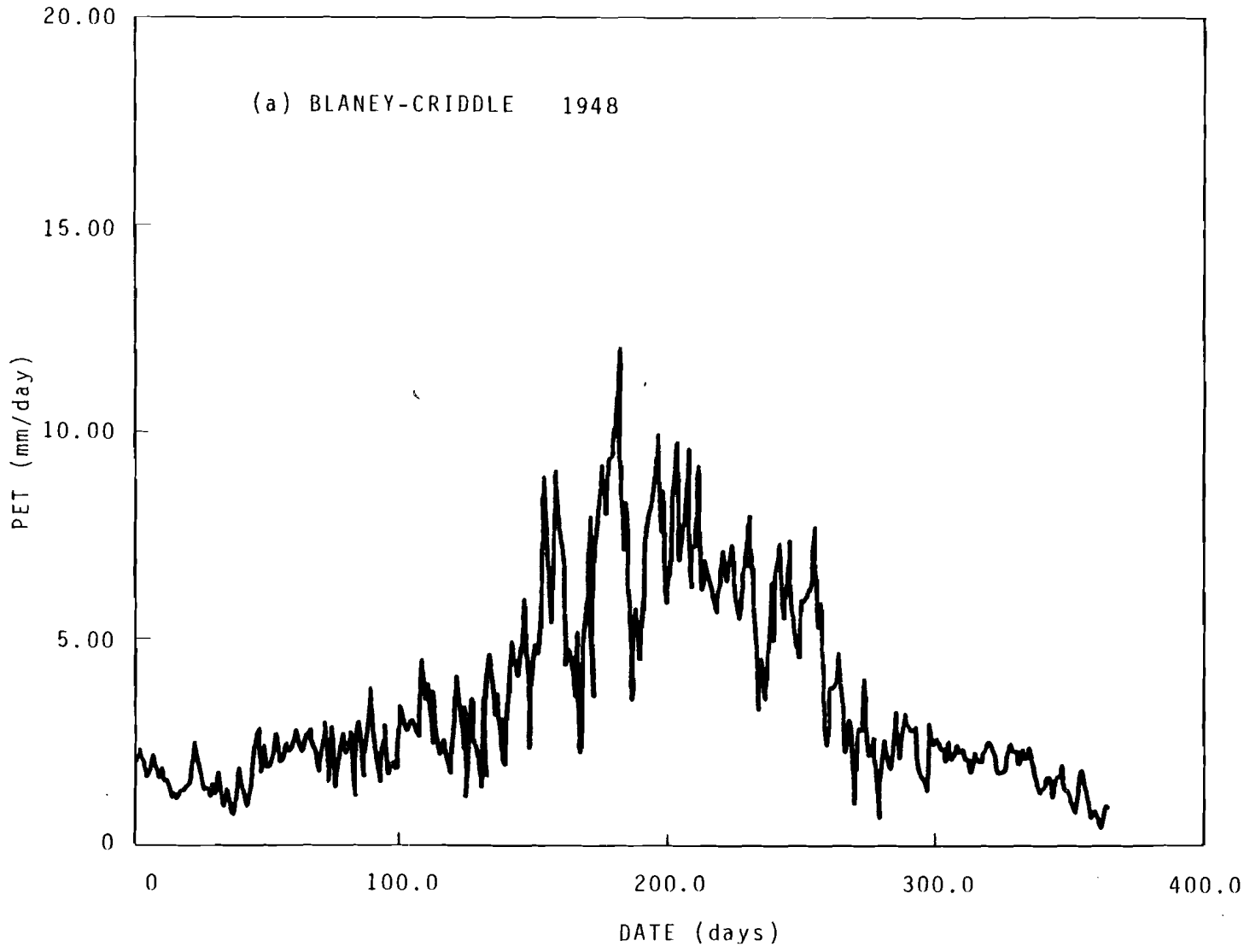

FIGURE 9. Daily Potential Evaporation by Four Methods as in Figure 8 but for 1948

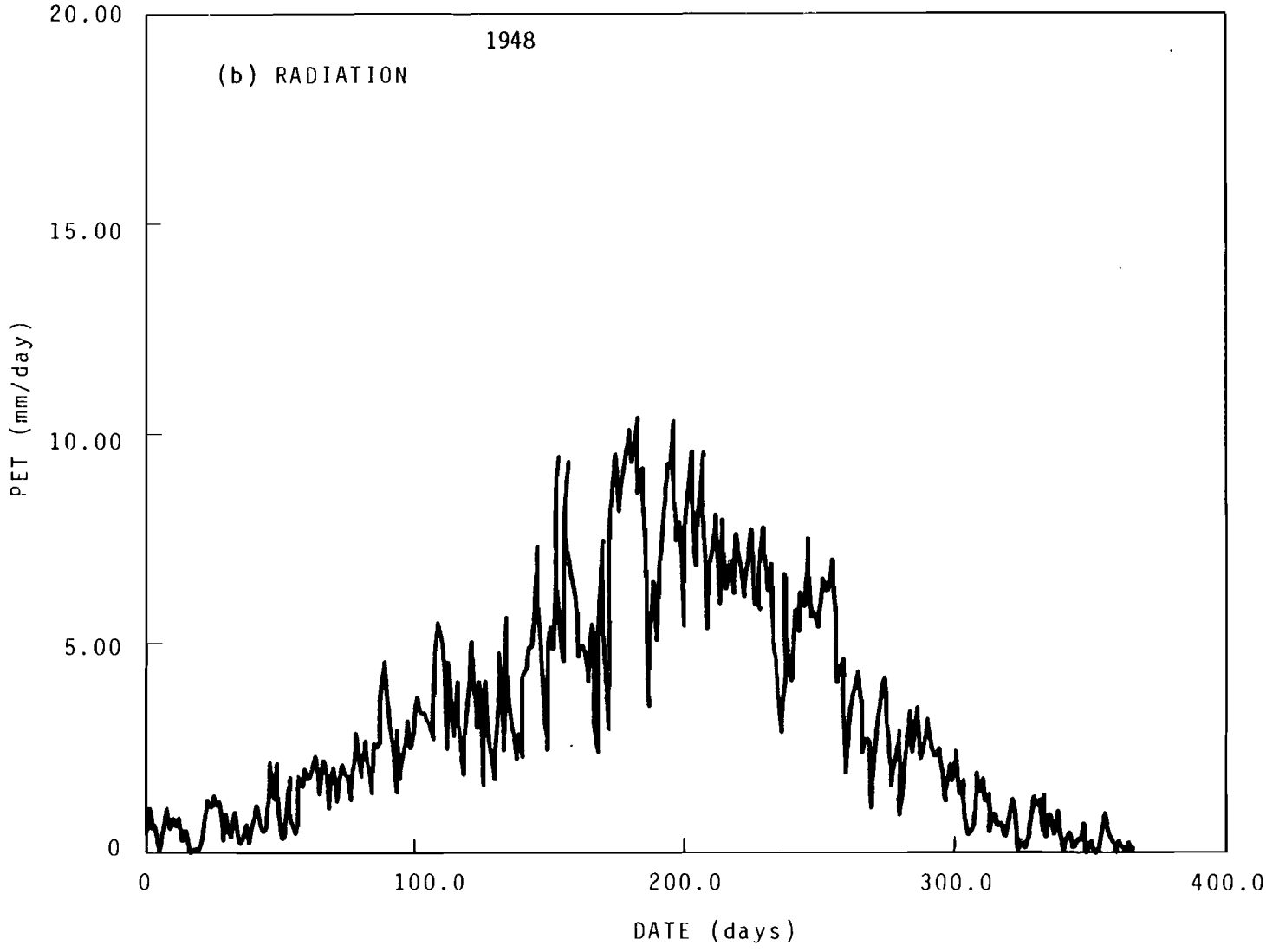

FIGURE 9. (contd)

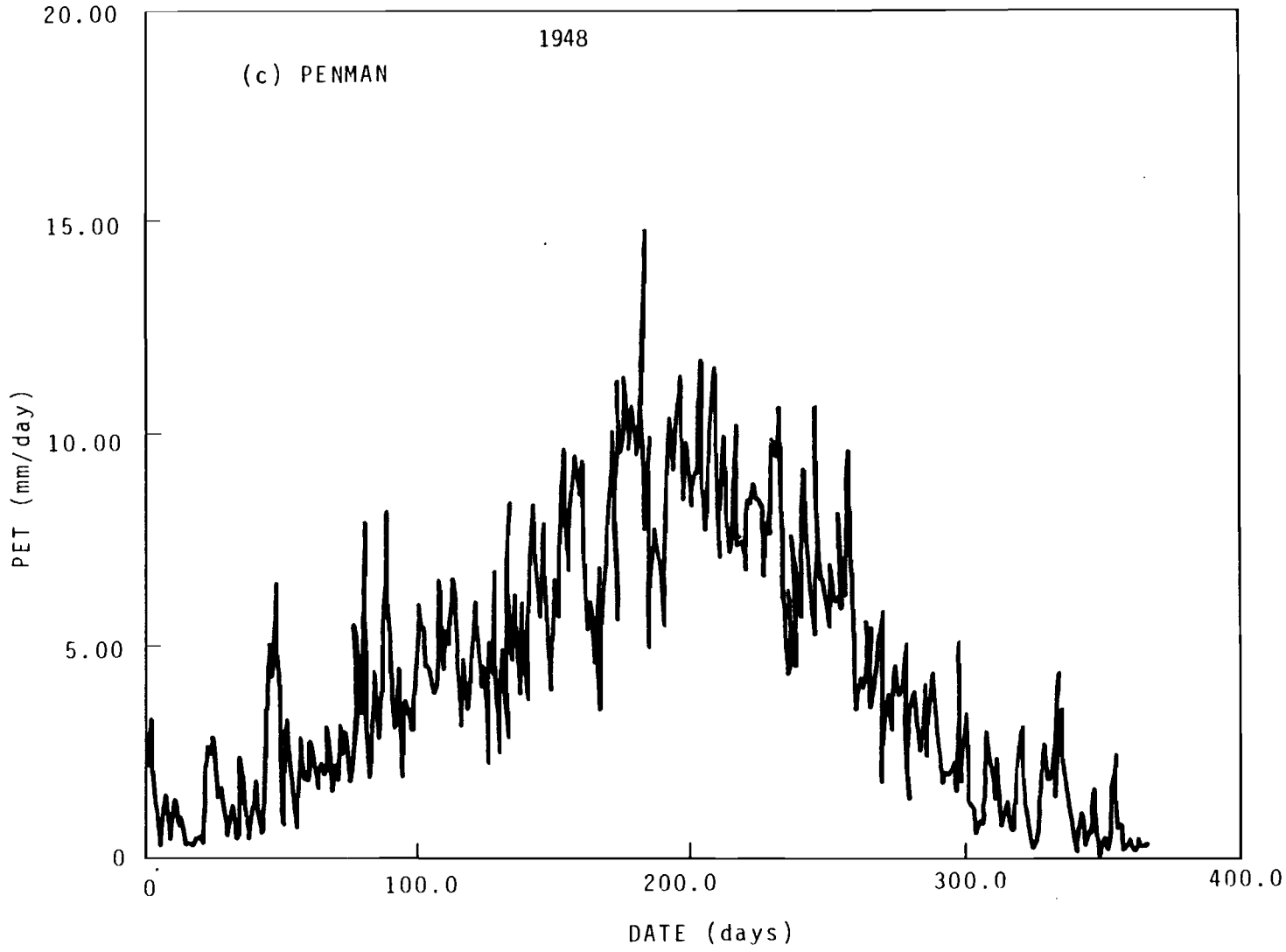

FIGURE 9. (contd)

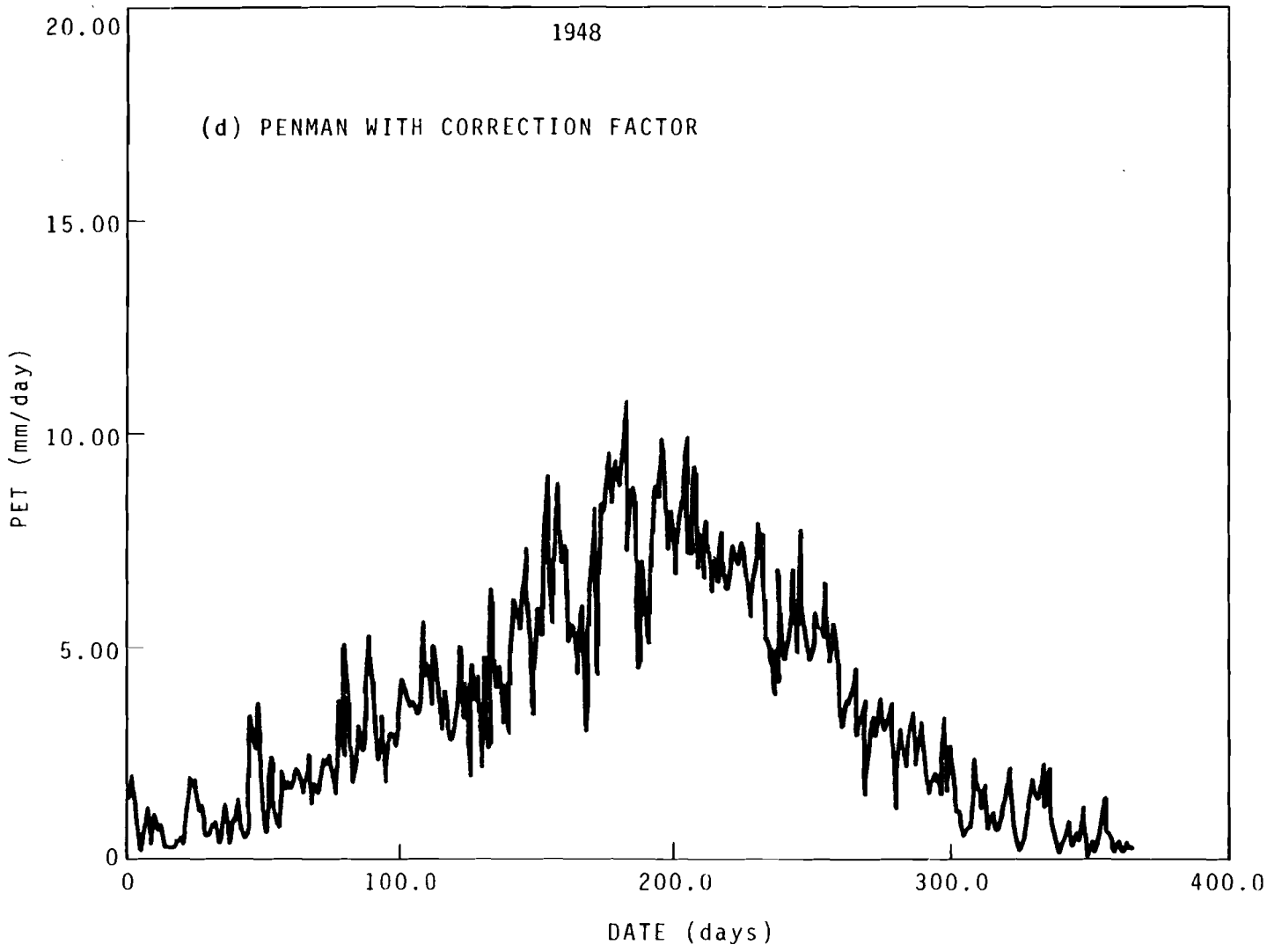

FIGURE 9. (contd)

The pattern of diurnal variation in daily potential evaporation was unknown and therefore taken as uniform. Hourly rainfall rates were also unknown for 1947-48 and were described as uniform over the 8- to 16-hr period of each day whenever rain occurred. For small rainfall quantities at Hanford, this likely constituted an underestimate of possible intensity. Cumulative rainfall over days, however, was exact. In addition, evaporation was considered negligible during rainfall.

BOUNDARY CONDITIONS

Since a water table was assumed present at the 800-cm depth, the soil there was held saturated with the pressure head equal 5 cm. At the surface the dry limit h_d equaled 15,000 cm and the hydrophobic layer's head limit h_1 equaled 5000 cm, corresponding to a water content of 0.03 (cm^3/cm^3) in the fine sand. The surface layer's vapor transport rate q_1 was taken as 0.001 cm/day and constant. Lysimeter measurements indicate a rate of 0.004 cm/day with water content 0.025 (cm^3/cm^3) just below the soil surface.

INITIAL CONDITIONS

Most uncertain of the model's required input data were the initial conditions of water content throughout the profile. When simulating past climatic periods, initial water content can be measured directly only for some future unknown climate. This uncertainty, however, can be resolved partially by allowing the simulation model to approach a steady-state condition controlled by the dynamics of typical climatic conditions. The disturbed initial soil conditions will not matter because a final condition consistent with climatic influences will eventually be reached.

This approach was taken to generate standard initial profile conditions for use in subsequent simulation examples. Table 3 gives the standard initial conditions obtained by simulating 1948 climate using only the dry limit head control and no surface layer. The disturbed initial conditions used represented excessive soil-water storage which rapidly drained during the year. Figures 10 through 12 depict the approach to the standard initial conditions.

Simulated water content profiles for days 1, 50, 200, and 365 shown in Figure 9 display a continual decrease. Seepage, which is the integral of flux, is shown in Figure 11 for some selected depths. Figure 12 contains the difference in water storage from its initial value for depths 200 and 800 cm. These figures demonstrate that the majority of the influence of rainfall and evaporation is on the first 200 cm of soil profile. Drainage of existing soil-water accounts for the behavior at the deeper depths.

TABLE 3. Standard Initial Conditions Derived from Simulation of a Transient State Using 1948 Climate

	Disturbed Initial Conditions		Standard Initial Conditions	
Depth (cm)	Head (cm)	Water Content (cm/cm)	Head (cm)	Water Content (cm/cm)
0	947	0.048	15000	0.023
20	461	0.056	4197	0.032
40	302	0.059	2253	0.038
60	230	0.061	1599	0.042
80	189	0.062	1282	0.045
100	164	0.063	1100	0.046
150	122	0.065	899	0.049
200	122	0.065	758	0.051
250	122	0.065	668	0.052
300	122	0.065	595	0.053
350	122	0.065	525	0.054
400	122	0.065	461	0.056
450	113	0.066	425	0.056
500	113	0.066	424	0.056
550	87	0.069	442	0.056
600	46	0.019	390	0.006
625	41	0.023	212	0.007
650	54	0.015	155	0.007
700	77	0.070	105	0.067
750	56	0.076	55	0.076
800	5	0.308	5	0.308

Initial Storage = 53.9 cm
Final Storage = 44.6 cm
Infiltration = 24.1 cm
Evaporation = 29.2 cm
Drainage = 5.1 cm

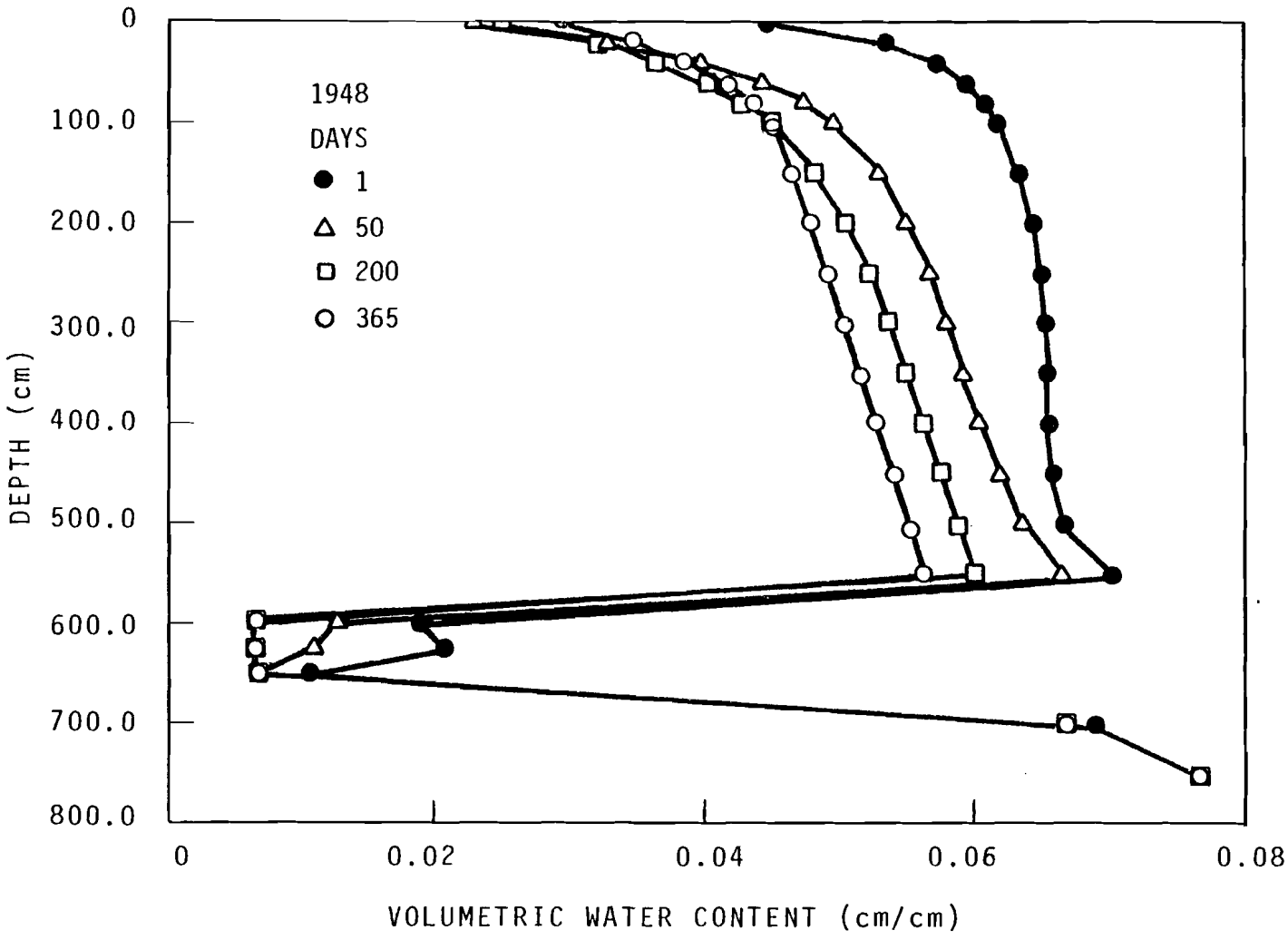

FIGURE 10. Water Content Profiles for Days 1, 50, 200, and 365 During Simulation of a Transient State Using 1948 Climate

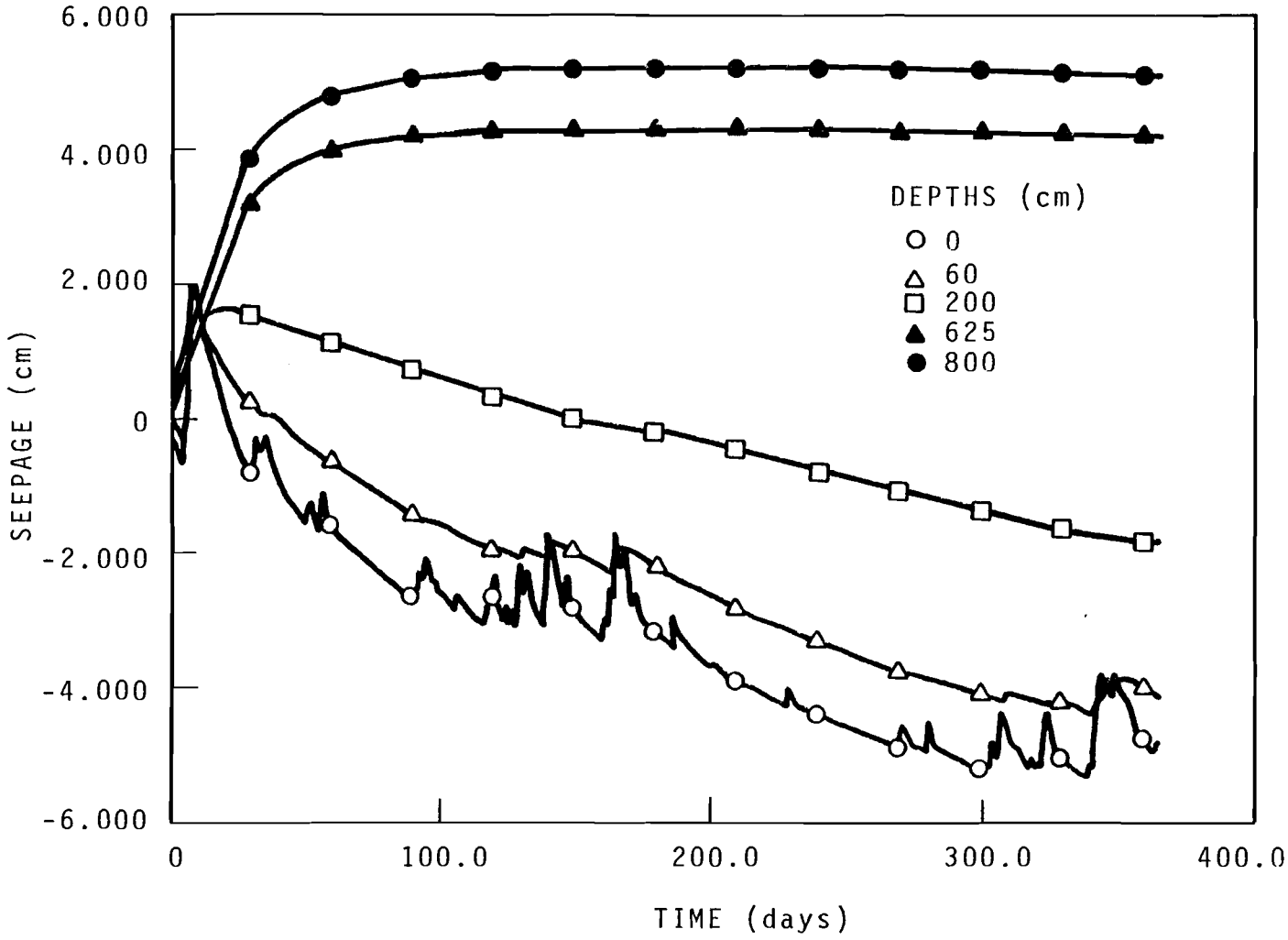

FIGURE 11. Cumulative Seepage at Selected Depths During Simulation of a Transient State Using 1948 Climate

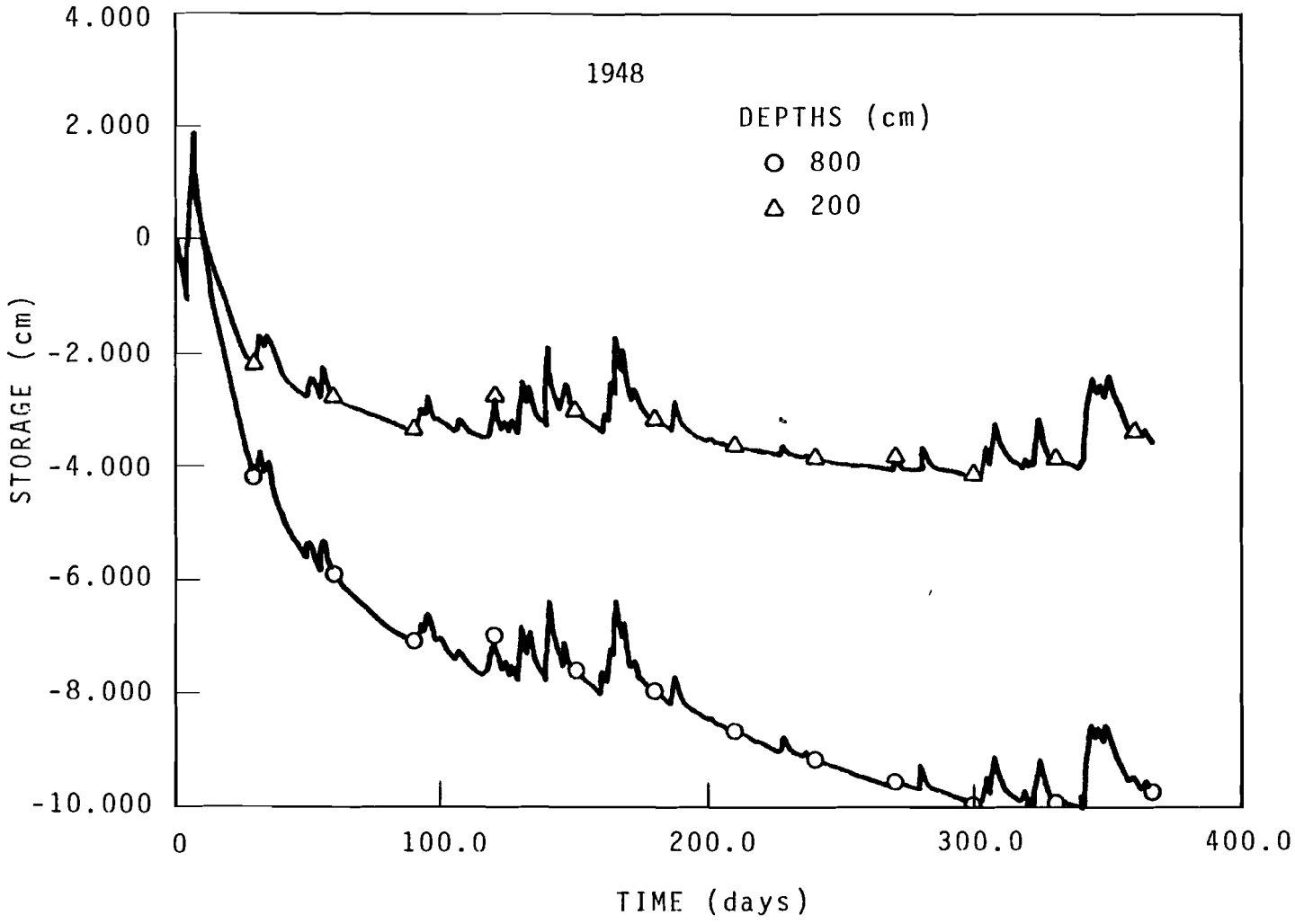

FIGURE 12. Soil-Water Storage Difference from Initial Values During Simulation of a Transient State Using 1948 Climate

The following simulations were performed using a 6-hr maximum time step with a 0.5-hr time step during infiltration. Mass balance was maintained at a maximum error of 0.1 cm/year. Under ideal conditions, the UNSAT model (Gupta et al., 1978) was efficient with 15 min of CPU time on a PDP 11/70 computer required to simulate 1 year. Simulation times, however, will vary considerably depending on the mass balance error constraint. Water content and flux were output at daily intervals to disk files for subsequent plotting.

HYDROPHOBIC SURFACE LAYER SENSITIVITY

Sensitivity simulations were performed using only the 1948 climatological data and standard initial conditions of Table 3. The effect of a hydrophobic surface layer is summarized in Table 4. About 1 cm of water is retained by the profile with a hydrophobic surface layer in comparison to 2 cm lost

TABLE 4. Simulation of 1948 Climate with and without a Hydrophobic Surface Layer. Blaney-Criddle PET and standard initial conditions of Table 2 are assumed.

	Infiltration (cm)	Evaporation (cm)	Drainage (cm)	Storage (cm)
Without Layer:	24.09	26.28	-0.40	42.57
With Layer:	24.51	23.41	-0.25	45.90

Initial Storage	=	44.62 cm
Potential Evaporation	=	131.2 cm
Dry Limit Suction Head	=	15000 cm
Layer Suction Head Limit	=	5000 cm
Layer Evaporation Rate	=	0.001 cm/day

without it for the 24-cm rainfall. Figures 13 through 16 display the behavior of water content profiles for selected days. Retardation of drying below the surface layer is seen in Figure 16. Seepage at various depths is compared in Figures 17 and 18. Considerable difference occurs near the surface, whereas little difference occurs at the water table (positive seepage indicates downward movement, and negative is upward).

A phenomenon of wetting redistribution beneath the surface layer is displayed in Figures 19 and 20. After the soil has dried and the surface layer formed, moisture moves upward to again wet the soil beneath. The degree of wetting beneath the layer depends on the characteristic vapor transport rate, with greater rates producing less wetting beneath.

It is important to note that with or without a hydrophobic surface layer effect the evaporation approximates the rainfall, and calculated evaporation is substantially less than its potential value (Table 4). This balance of estimated evaporation and rainfall is controlled primarily by the limiting dryness, h_d, of the soil surface.

HYDRAULIC CONDUCTIVITY SENSITIVITY

To evaluate the dependence on hydraulic conductivity, simulations were run with reductions of $K(\theta)$ by factors of 1/10 and 1/100. Only the fine sand conductivity was reduced, however. These simulations did not include a hydrophobic surface layer formation either. Reduction of K caused the soil-water flow rate to be reduced so that infiltrated water remained near the surface. Furthermore, infiltrated water showed reduced evaporation, and was not as easily removed by the same potential evaporation conditions. Water content profiles for selected days shown in Figures 21 through 24 show the effect of reduced conductivity.

Figures 25 and 26 for the seepage at various depths indicate reduced water penetration with reduced conductivity, especially at 60 cm. Storage differences compared with that for unit factor conductivity of Figure 17 indicate that little change in storage occurs below 200 cm for 1/10 and 1/100 of K. Results are summarized in Table 5.

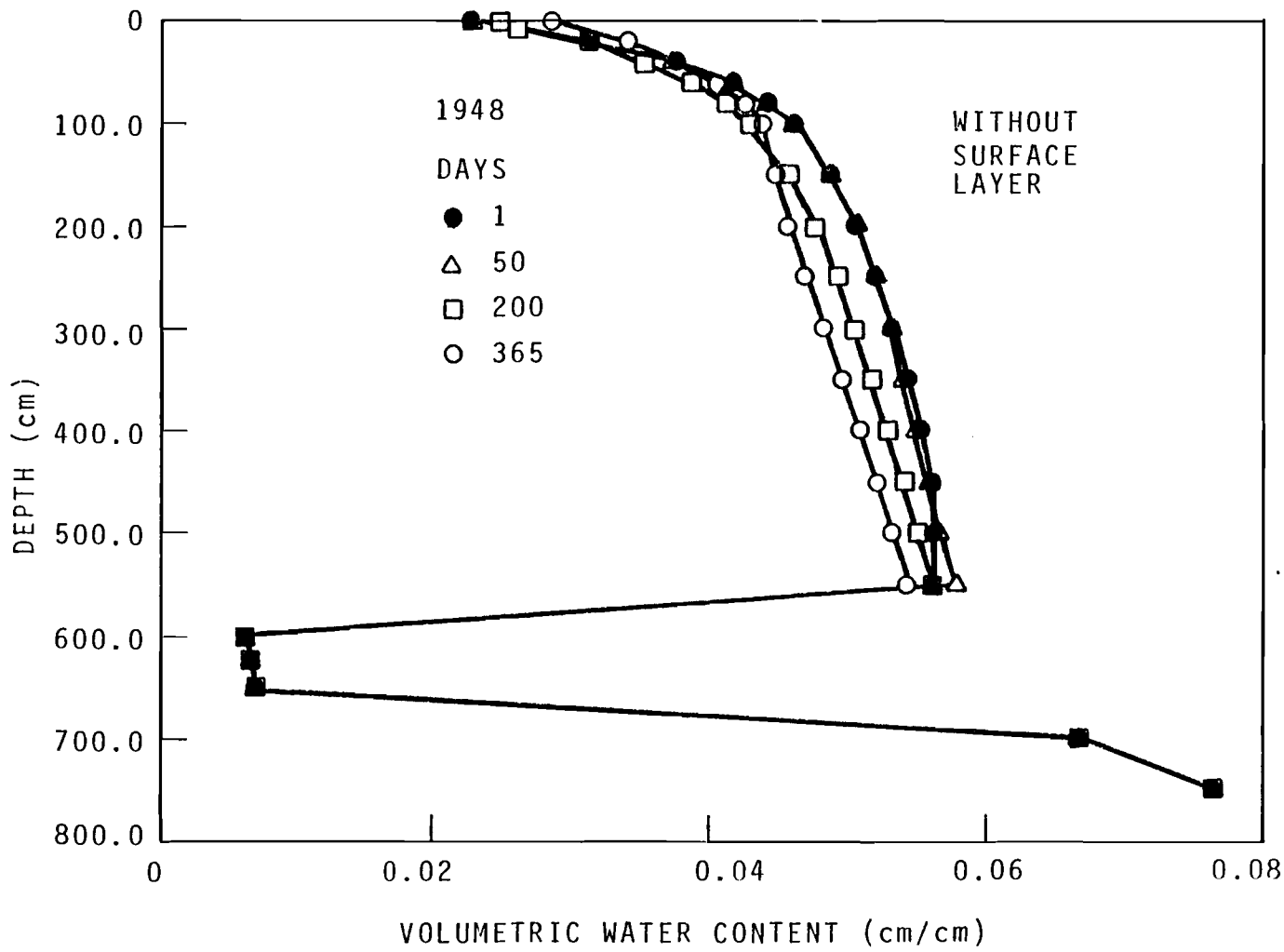

FIGURE 13. Water Content Profiles for Selected Days for Simulation without a Hydrophobic Surface Layer

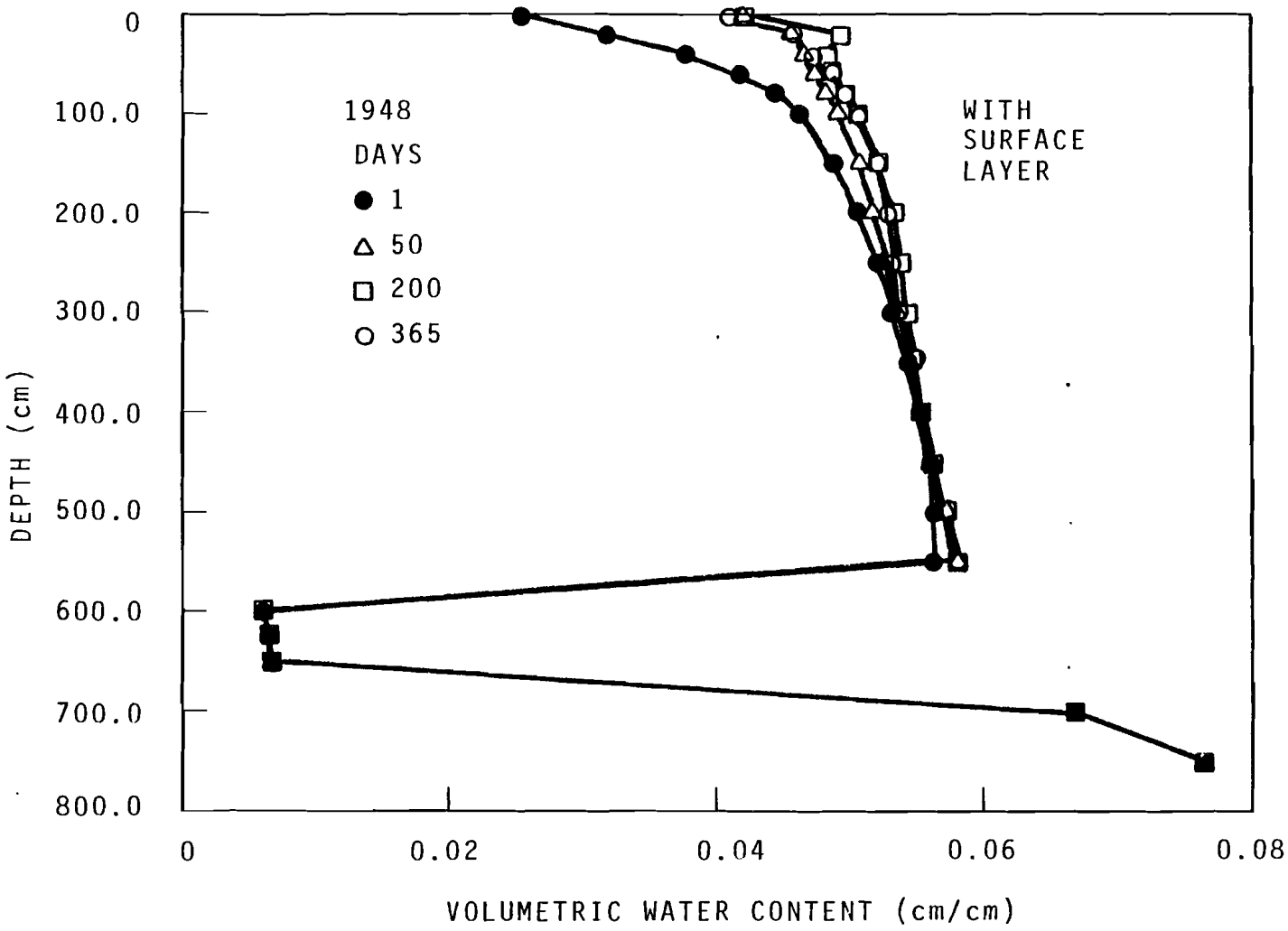

FIGURE 14. Water Content Profiles for Selected Days for Simulation with a Hydrophobic Surface Layer

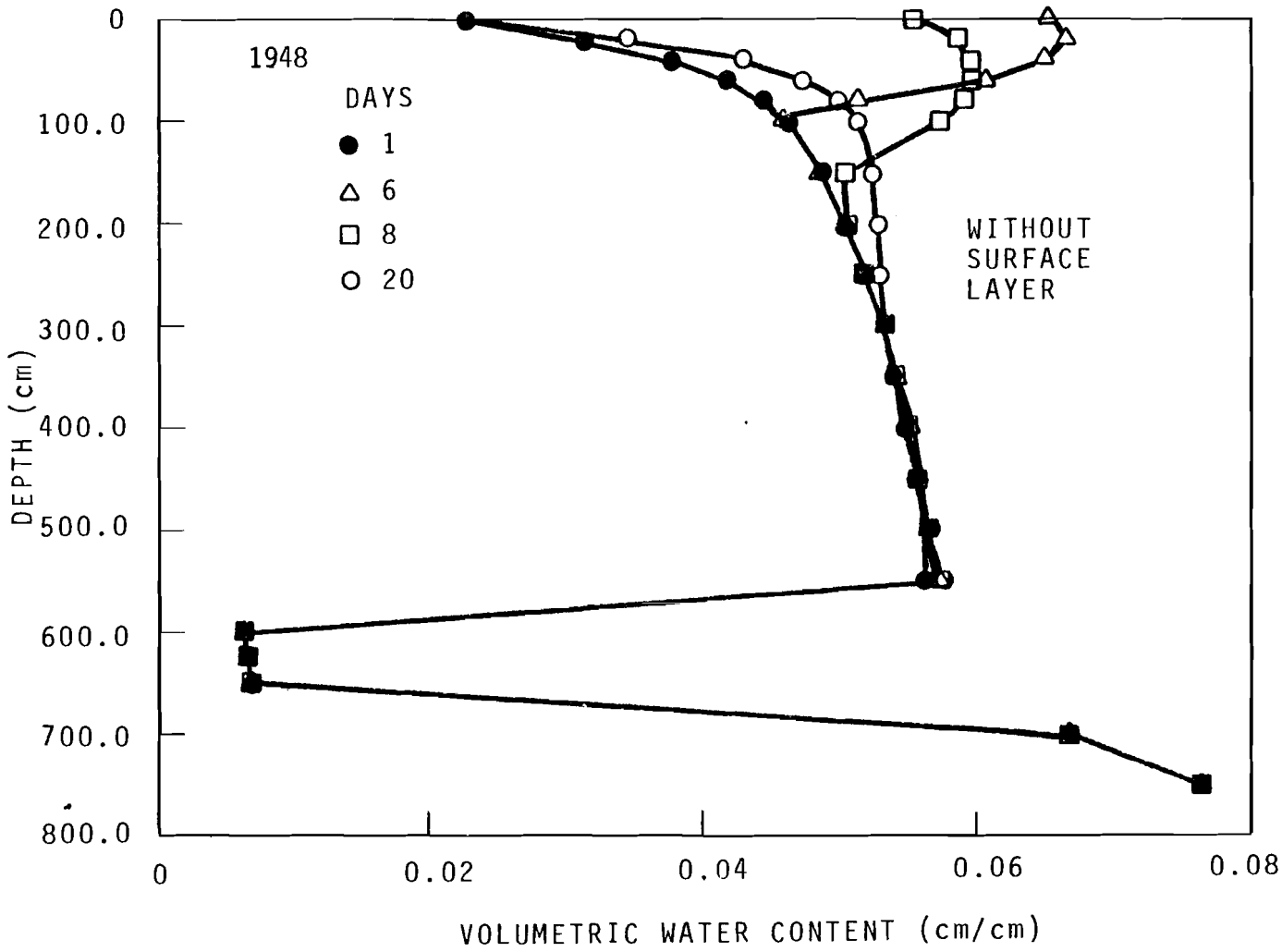

FIGURE 15. Water Content Profiles for Selected Days Following Rainfall--without Surface Layer

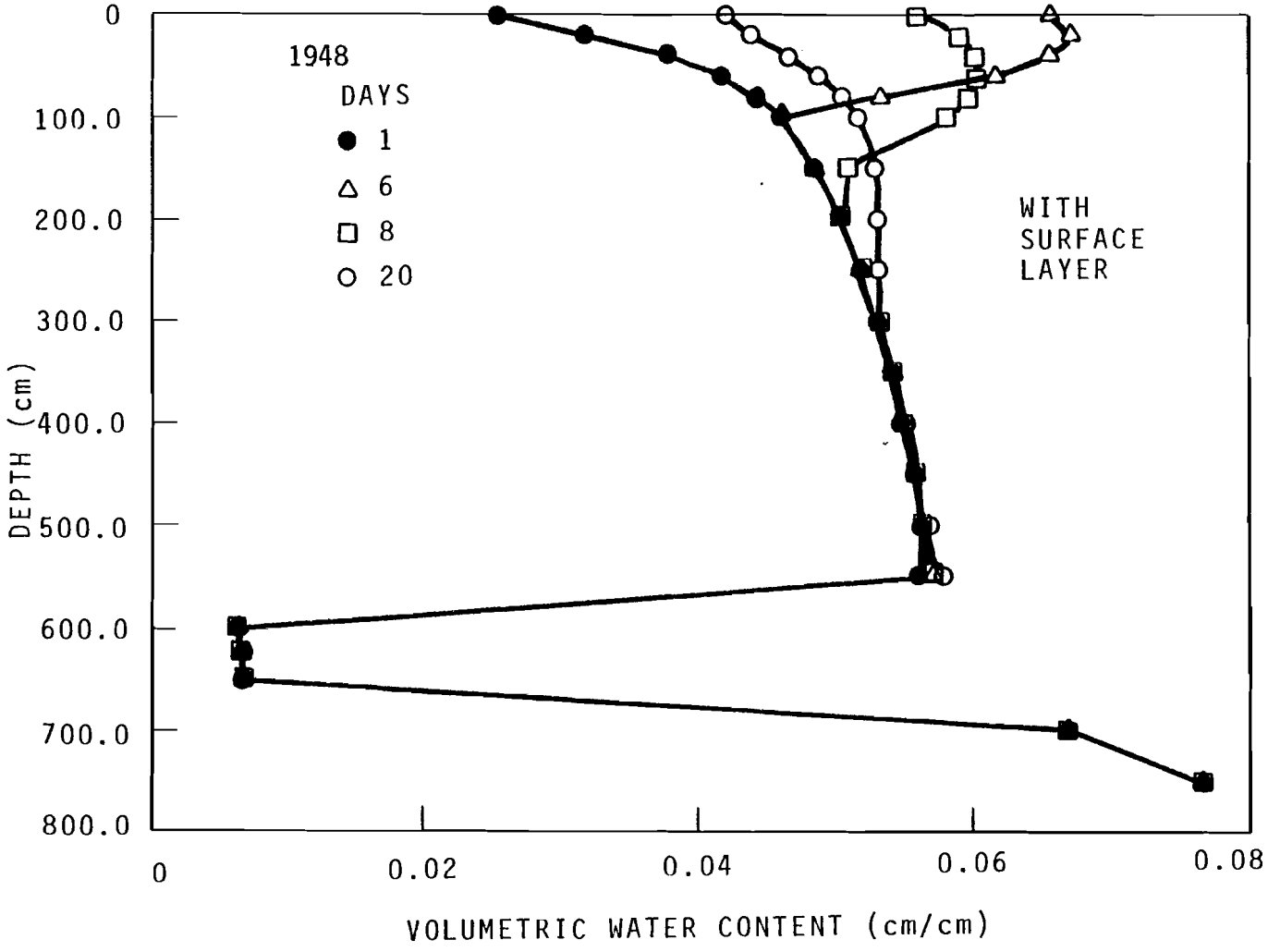

FIGURE 16. Water Content Profiles for Selected Days Following a Rainfall--with Surface Layer

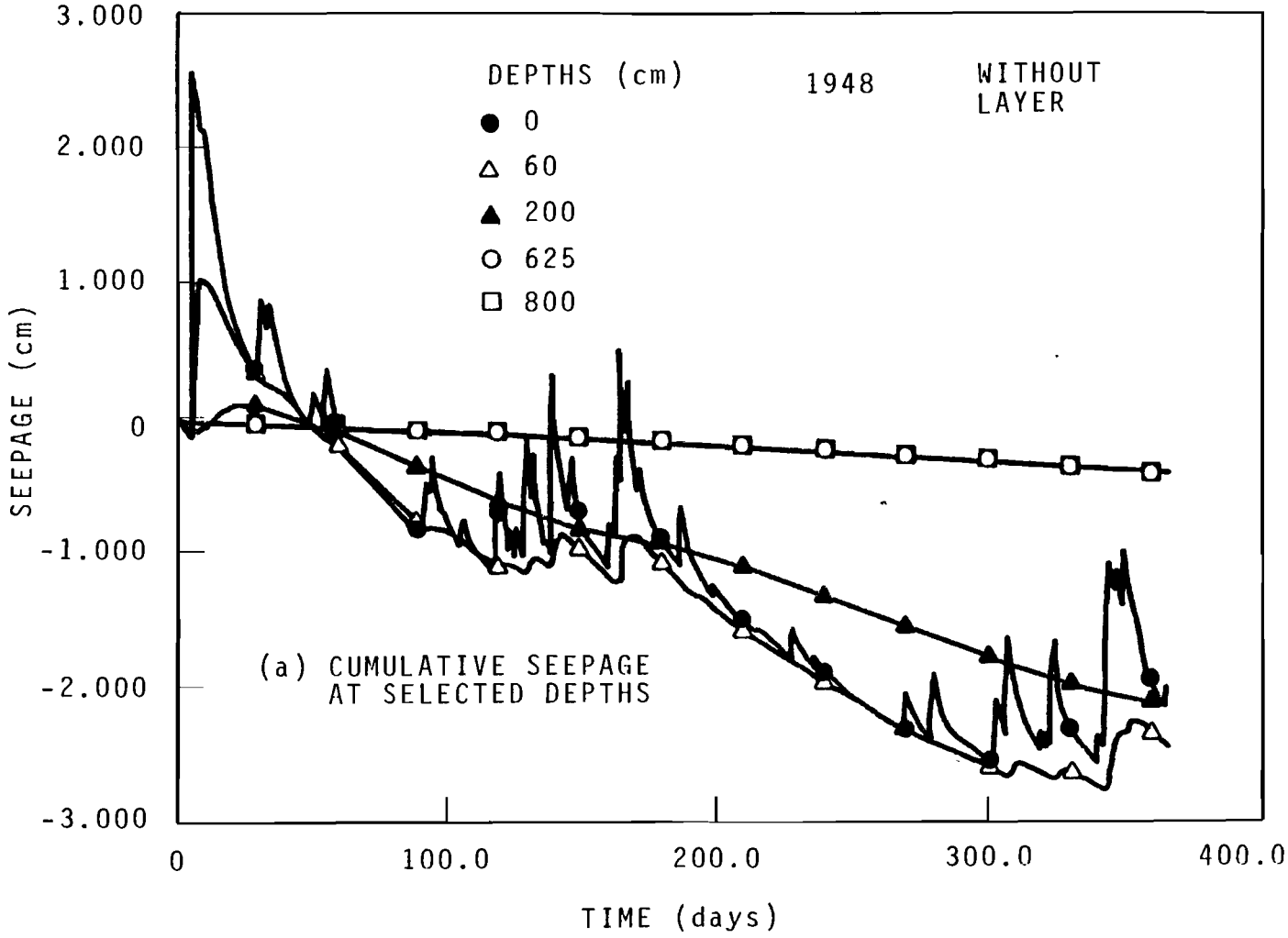

FIGURE 17. Simulation of Water Movement without Surface Layer: a) Cumulative Seepage at Selected Depths, b) Soil-Water Storage Difference in the Profile

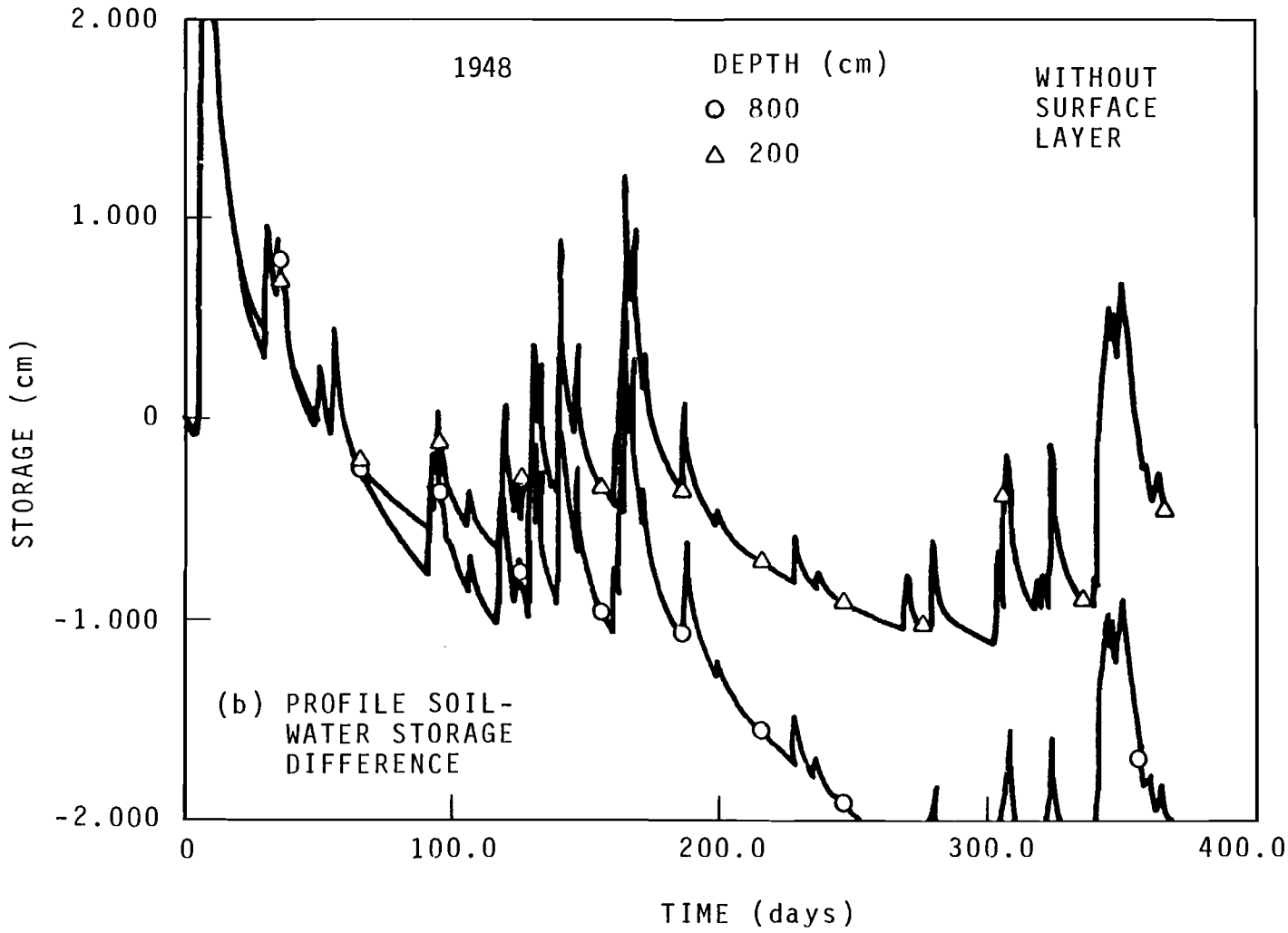

FIGURE 17. (contd)

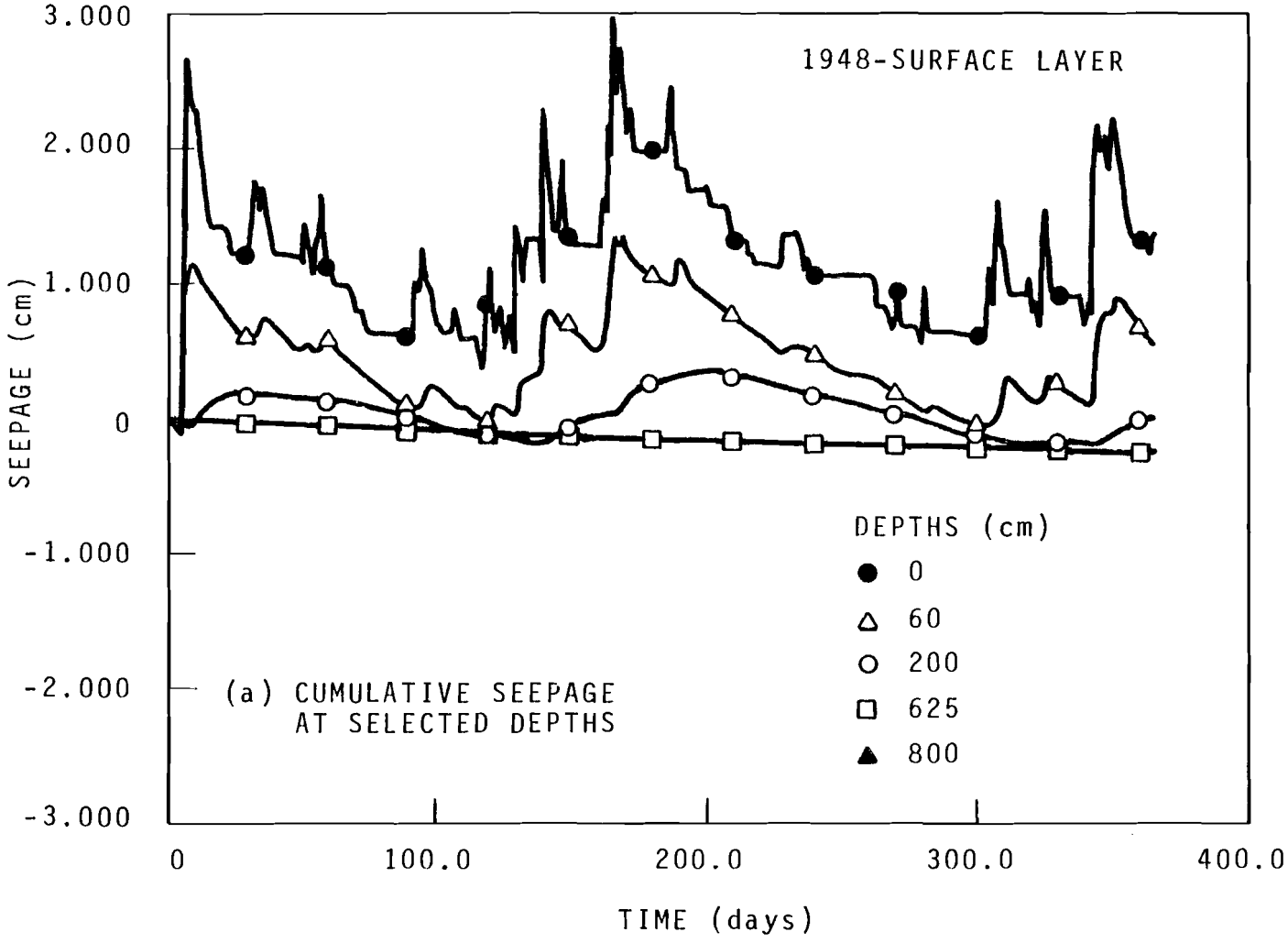

FIGURE 18. Simulation of Water Movement with a Surface Layer: a) Cumulative Seepage at Selected Depths, b) Soil-Water Storage Difference in the Profile

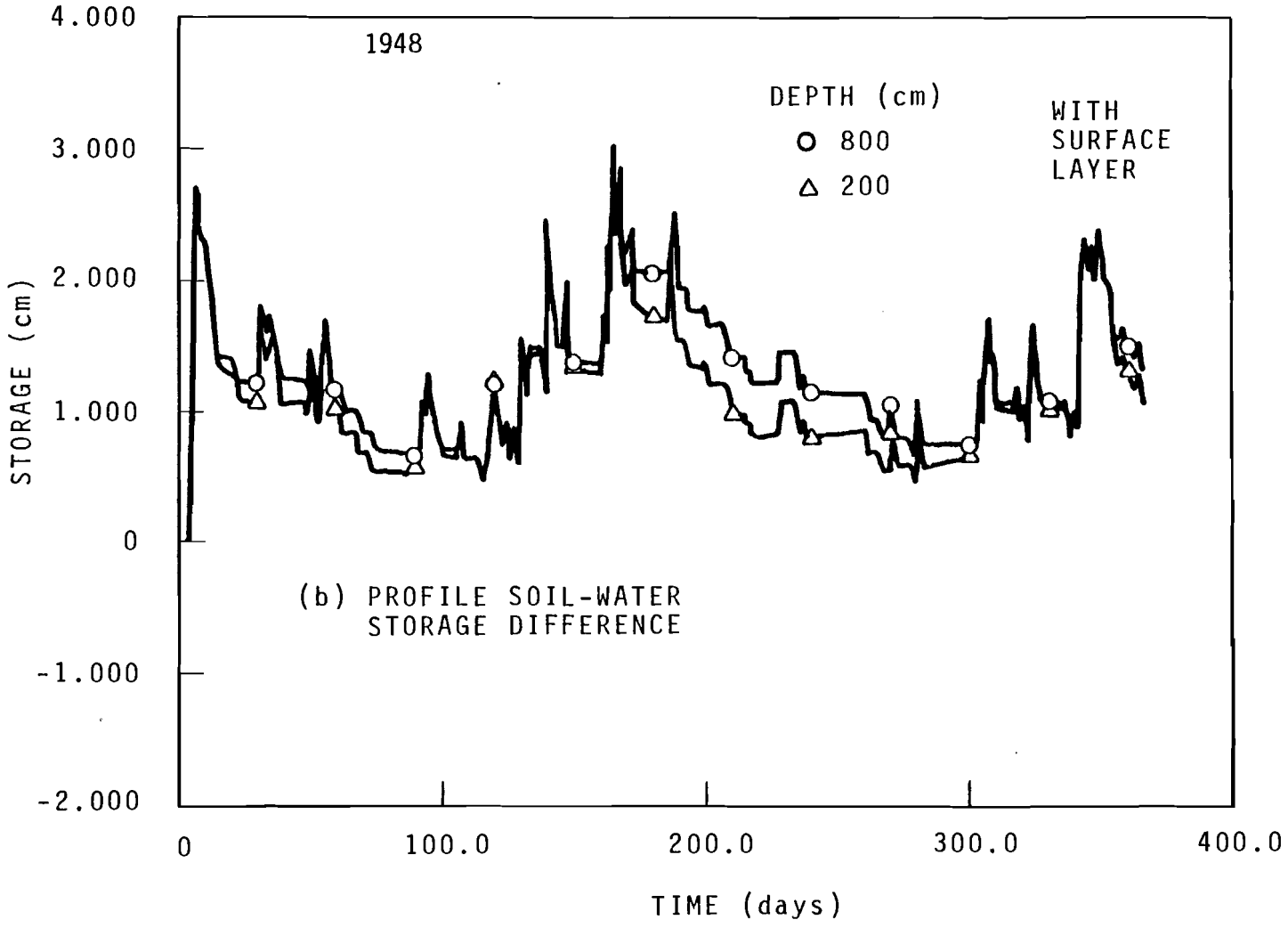

FIGURE 18. (contd)

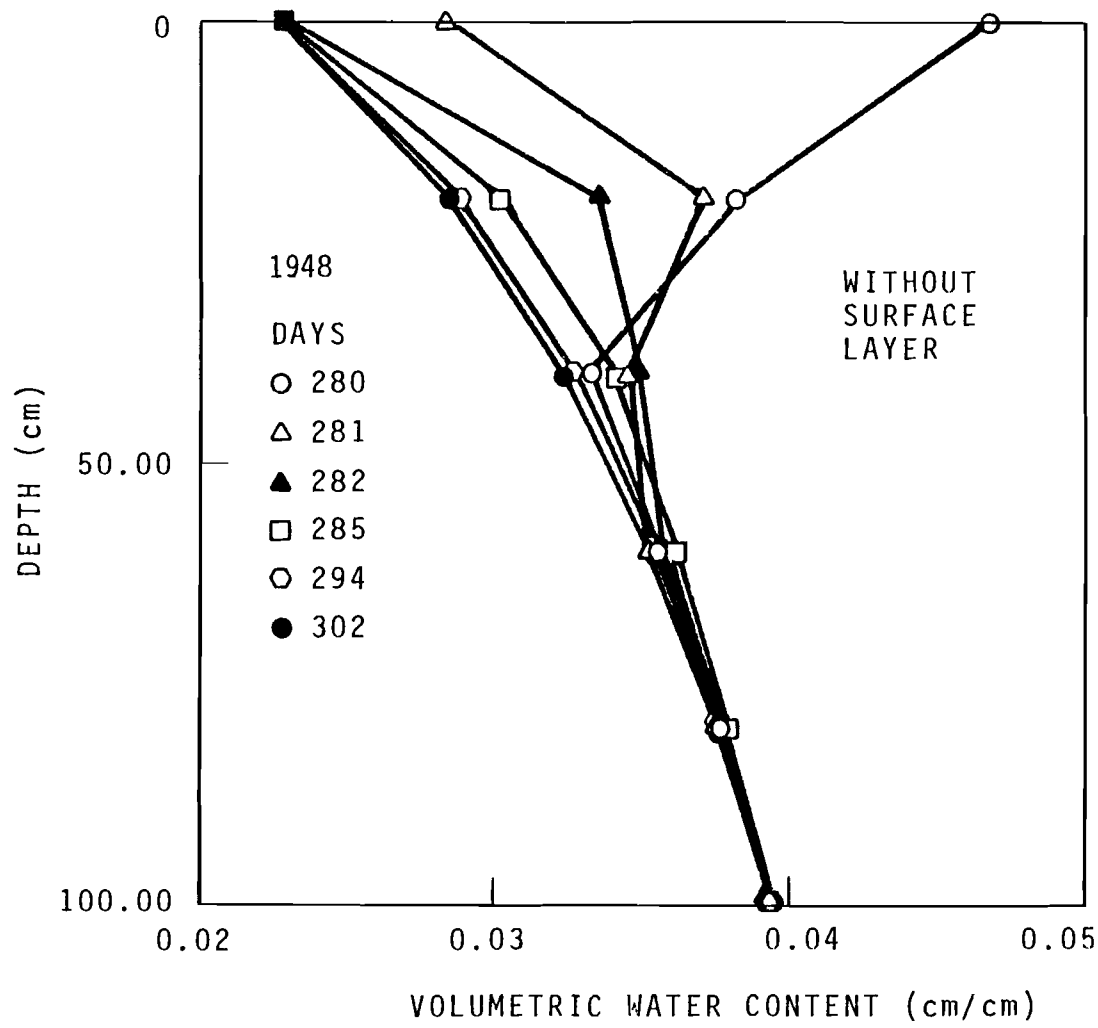

FIGURE 19. Water Content Profiles near the Surface without Surface Layer During Drying

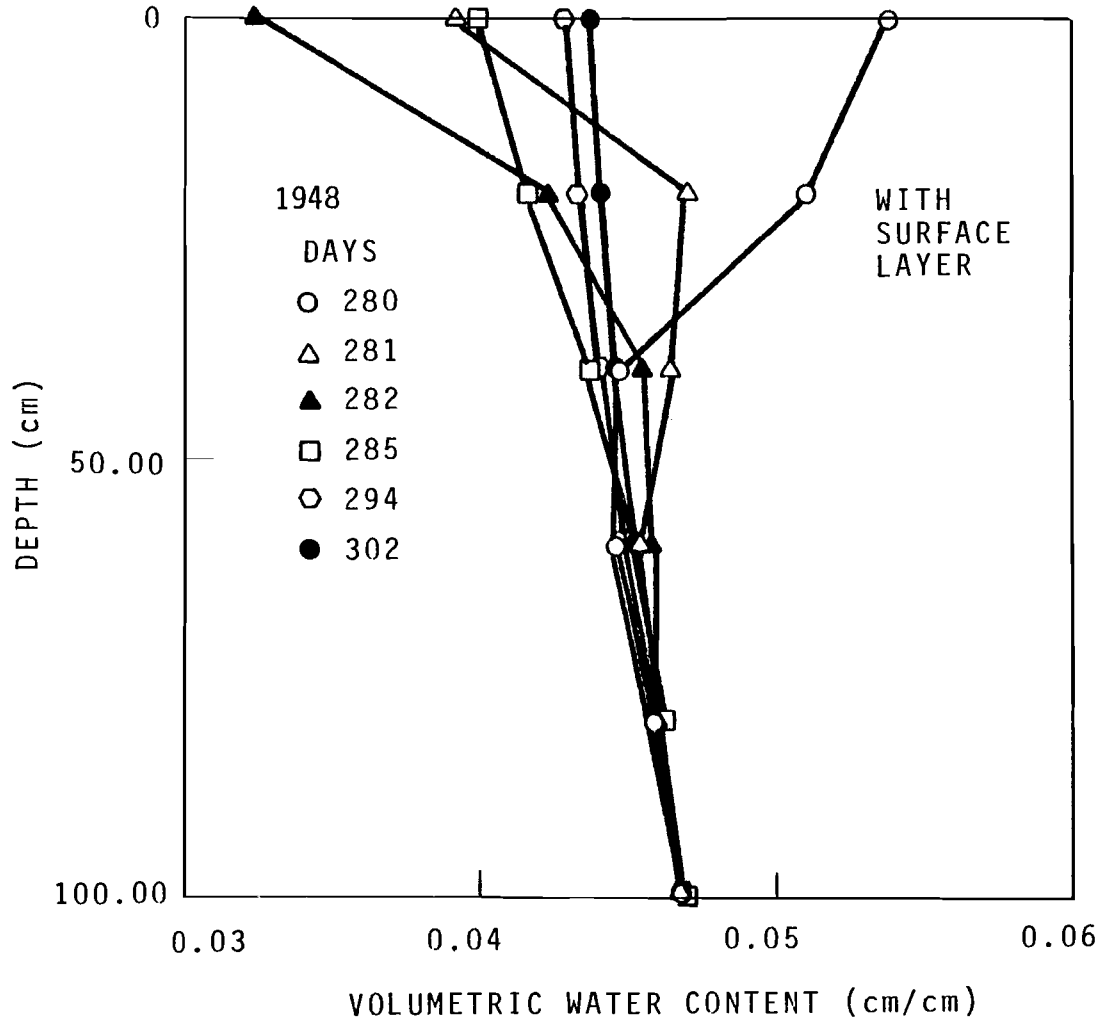

FIGURE 20. Water Content Profiles beneath a Hydrophobic Surface Layer During Drying

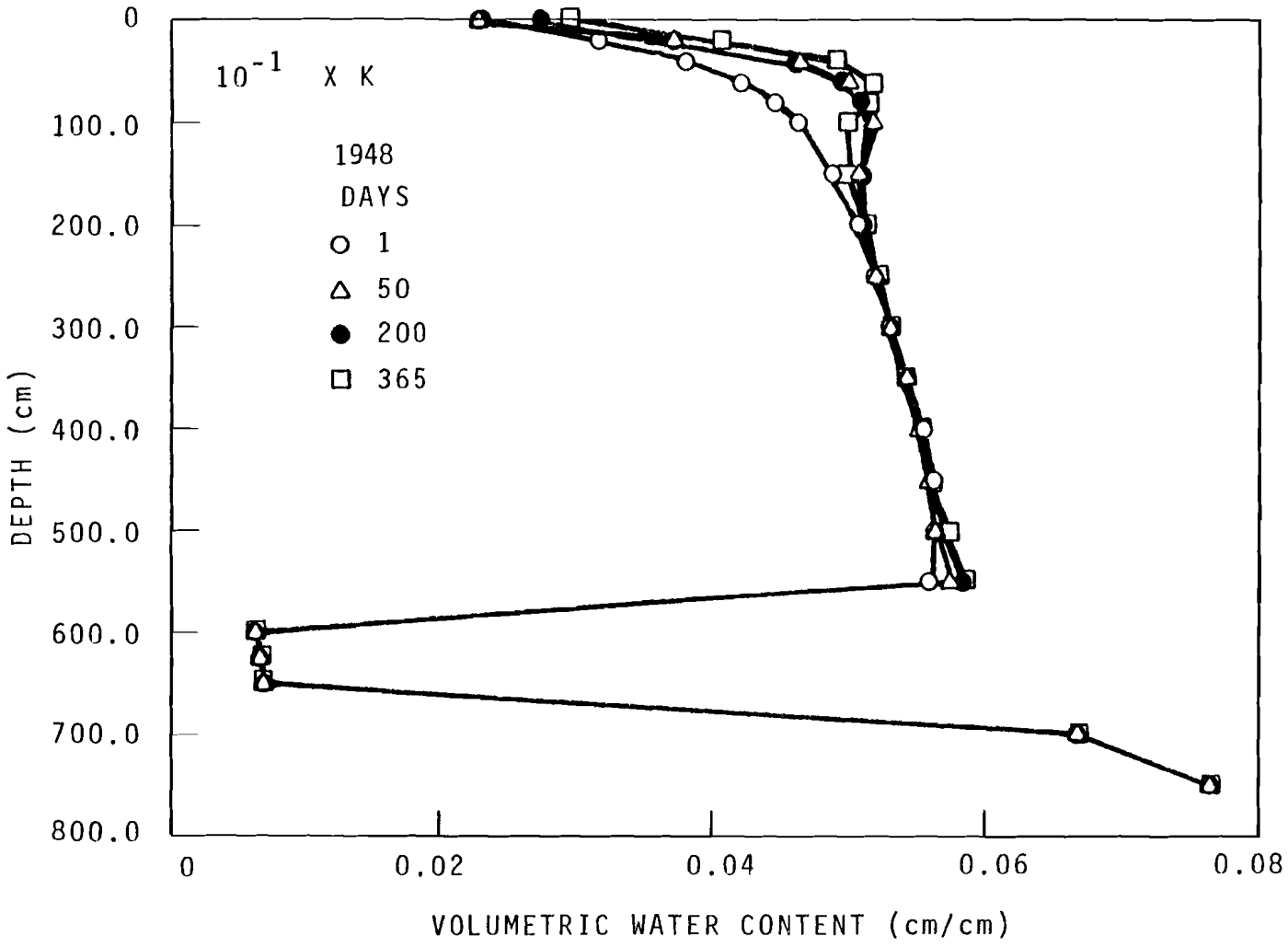

FIGURE 21. Water Content Profiles for 1, 50, 200, 365 Days Using 1/10 Conductivity

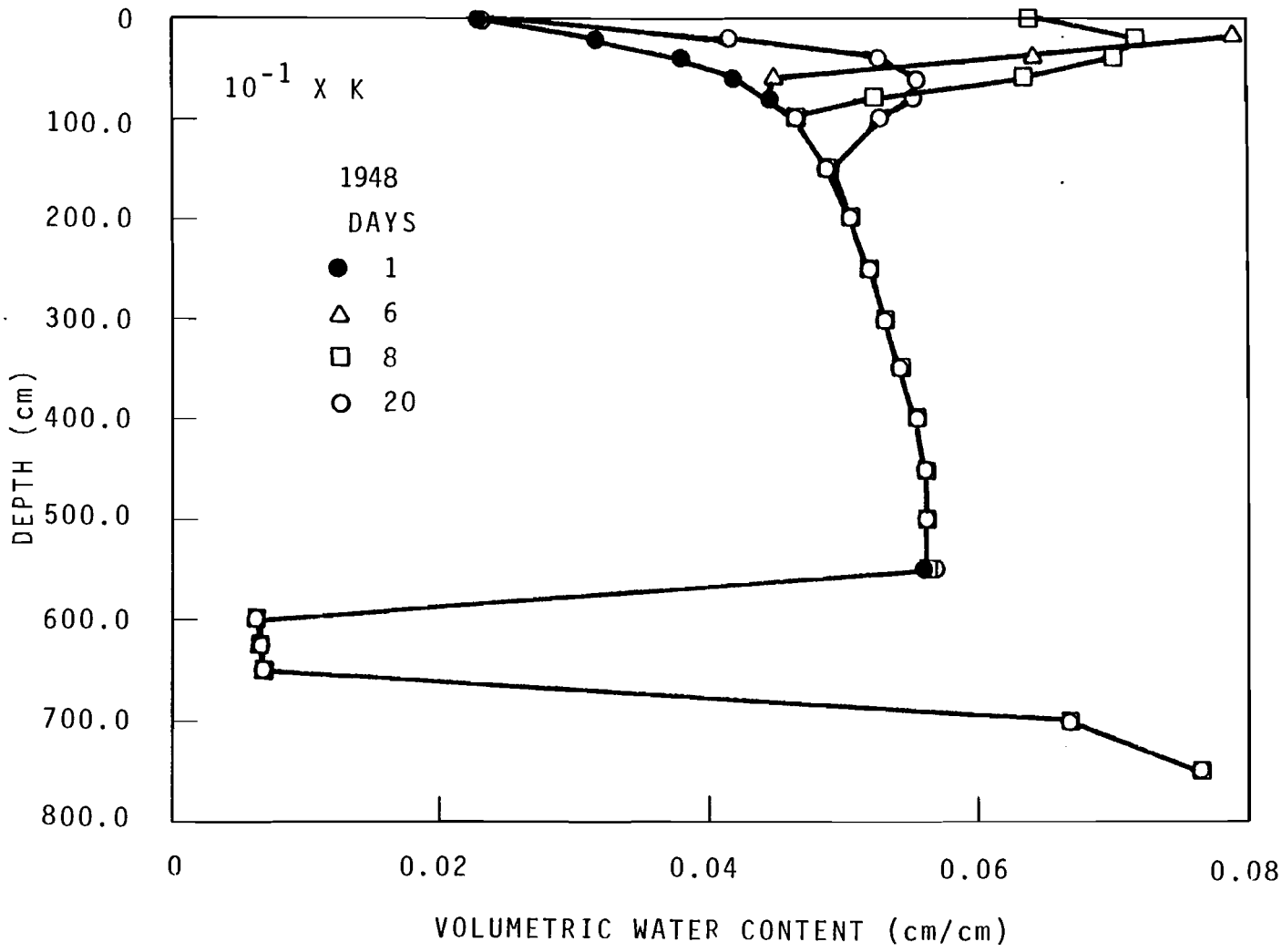

FIGURE 22. Water Content Profiles for 1, 6, 8, 20 Days Using 1/10 Conductivity

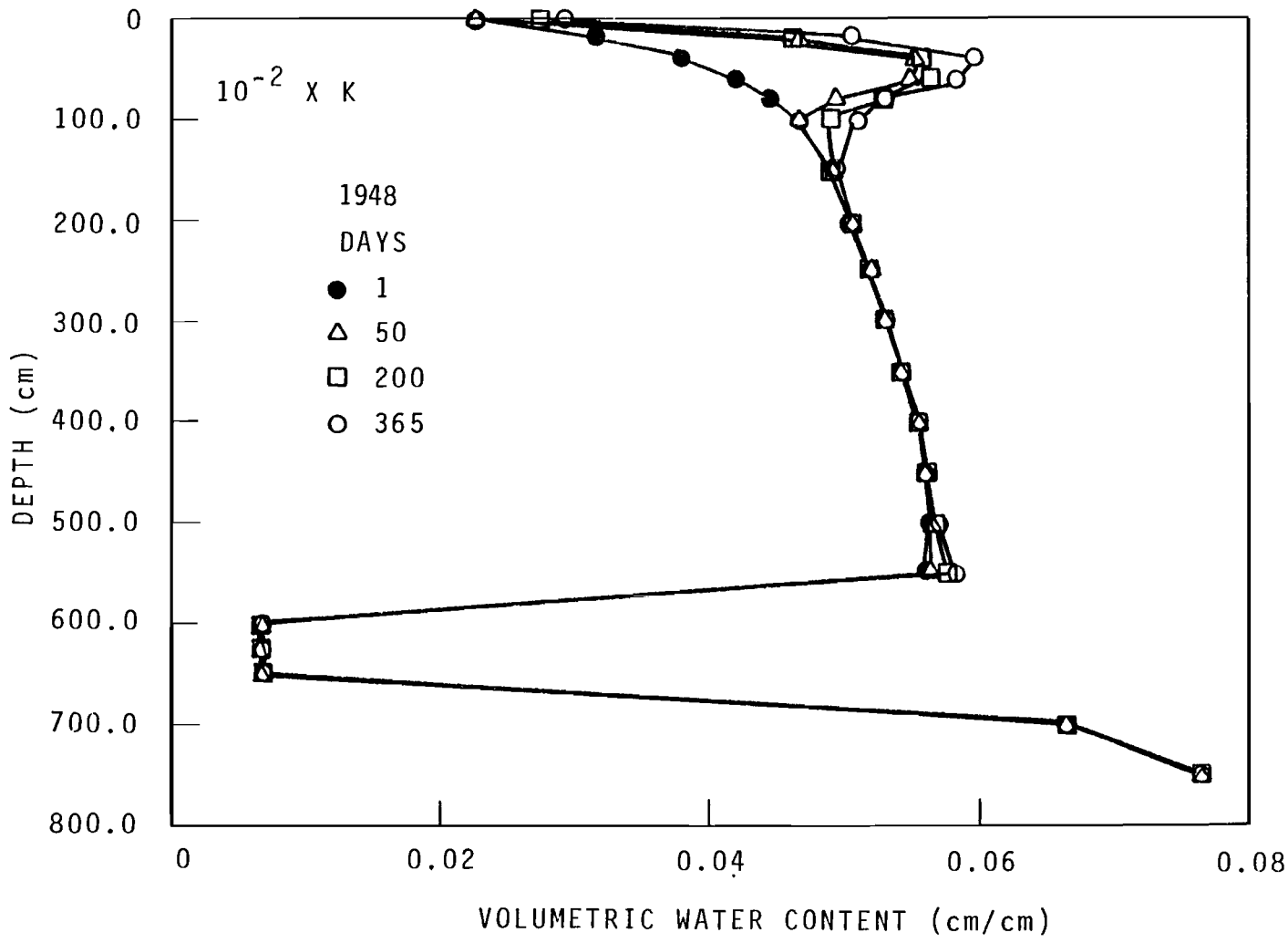

FIGURE 23. Water Content Profiles for 1, 50, 200, and 365 Days Using 1/100 Conductivity

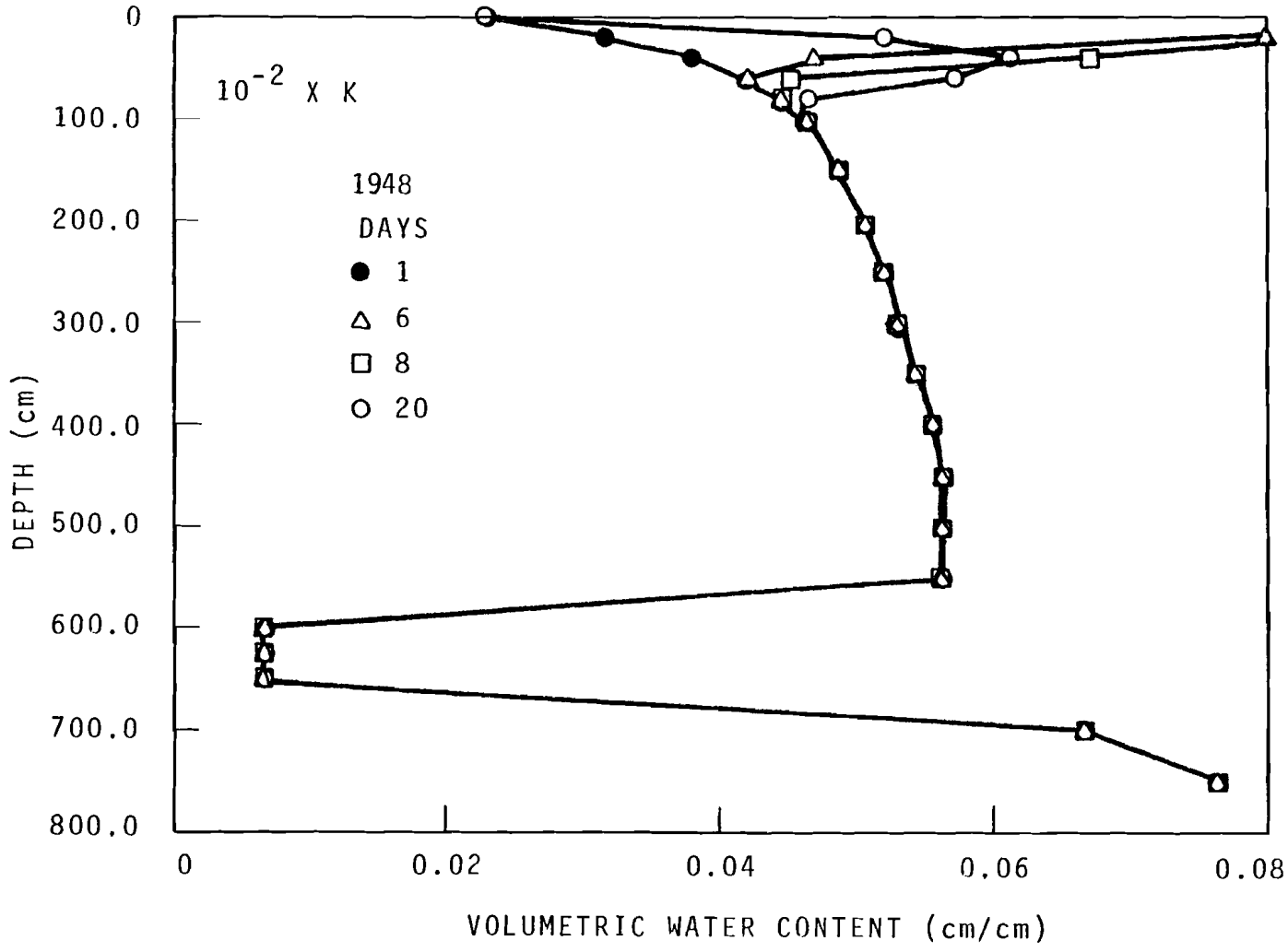

FIGURE 24. Water Content Profiles for 1, 6, 8, and 20 Days Using 1/100 Conductivity

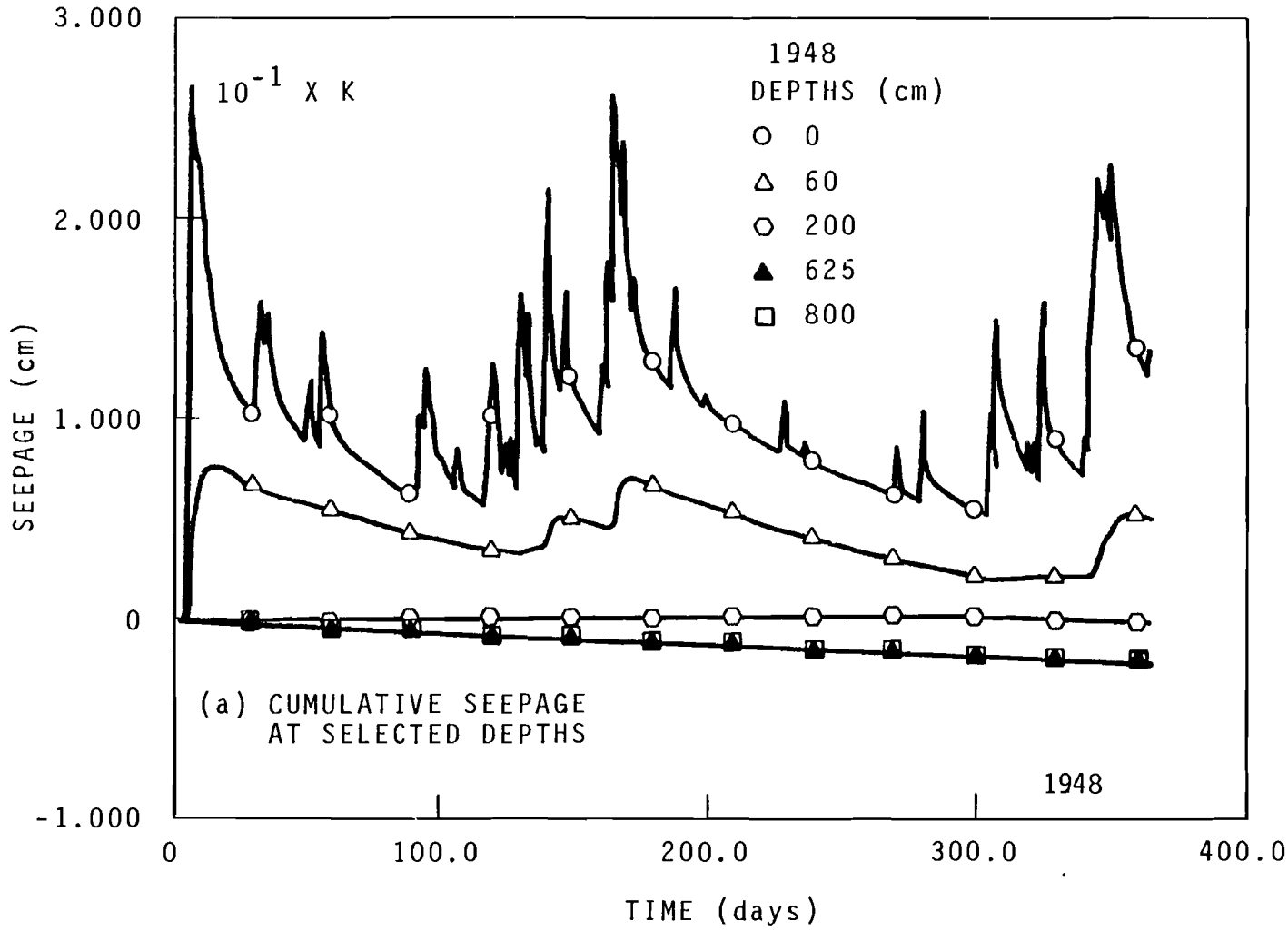

FIGURE 25. Simulated Soil-Water Movement Using 1/100 Conductivity and 1948 Climate: a) Cumulative Seepage at Selected Depths, b) Profile Soil-Water Storage Difference

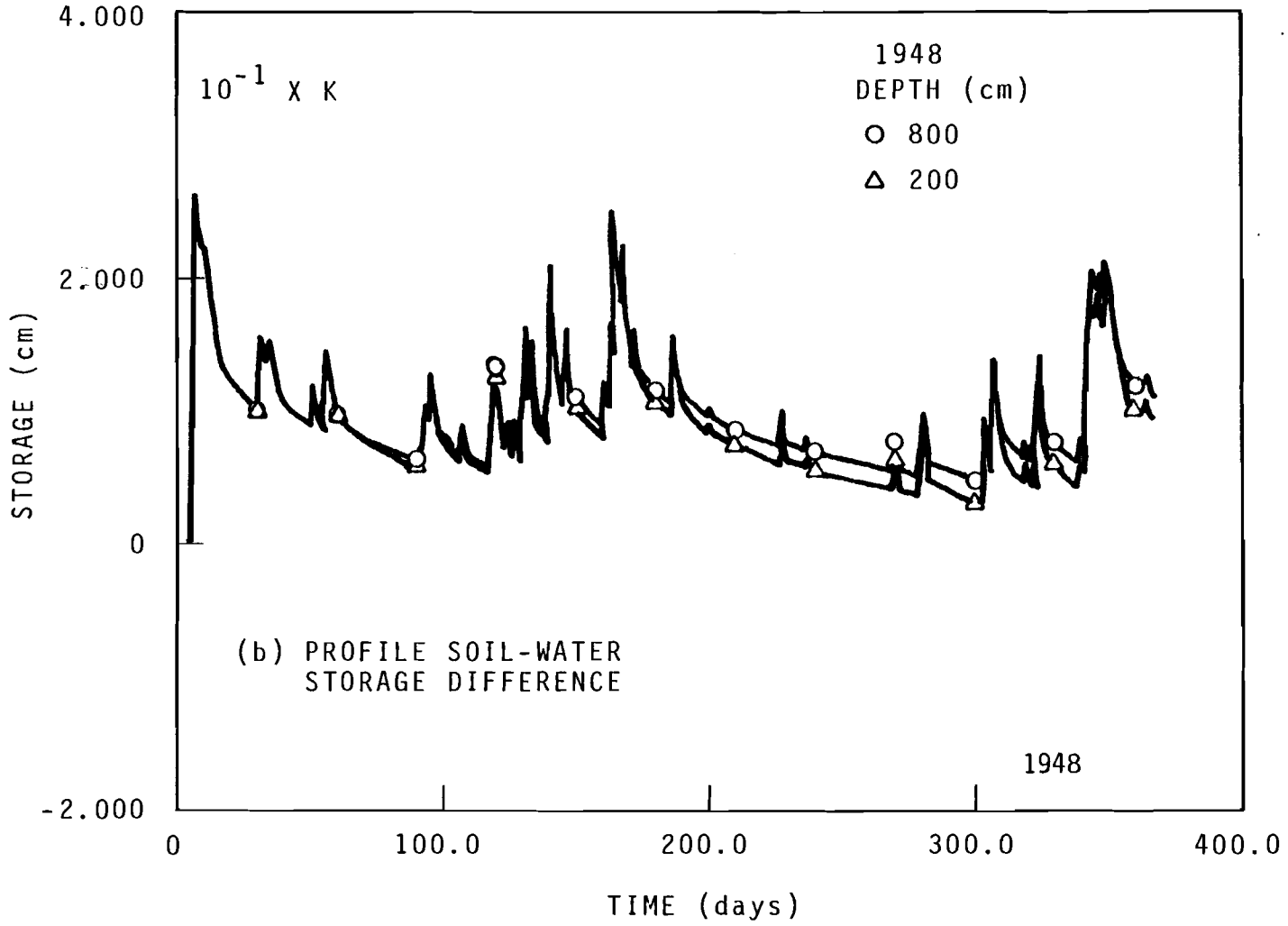

FIGURE 25. (contd)

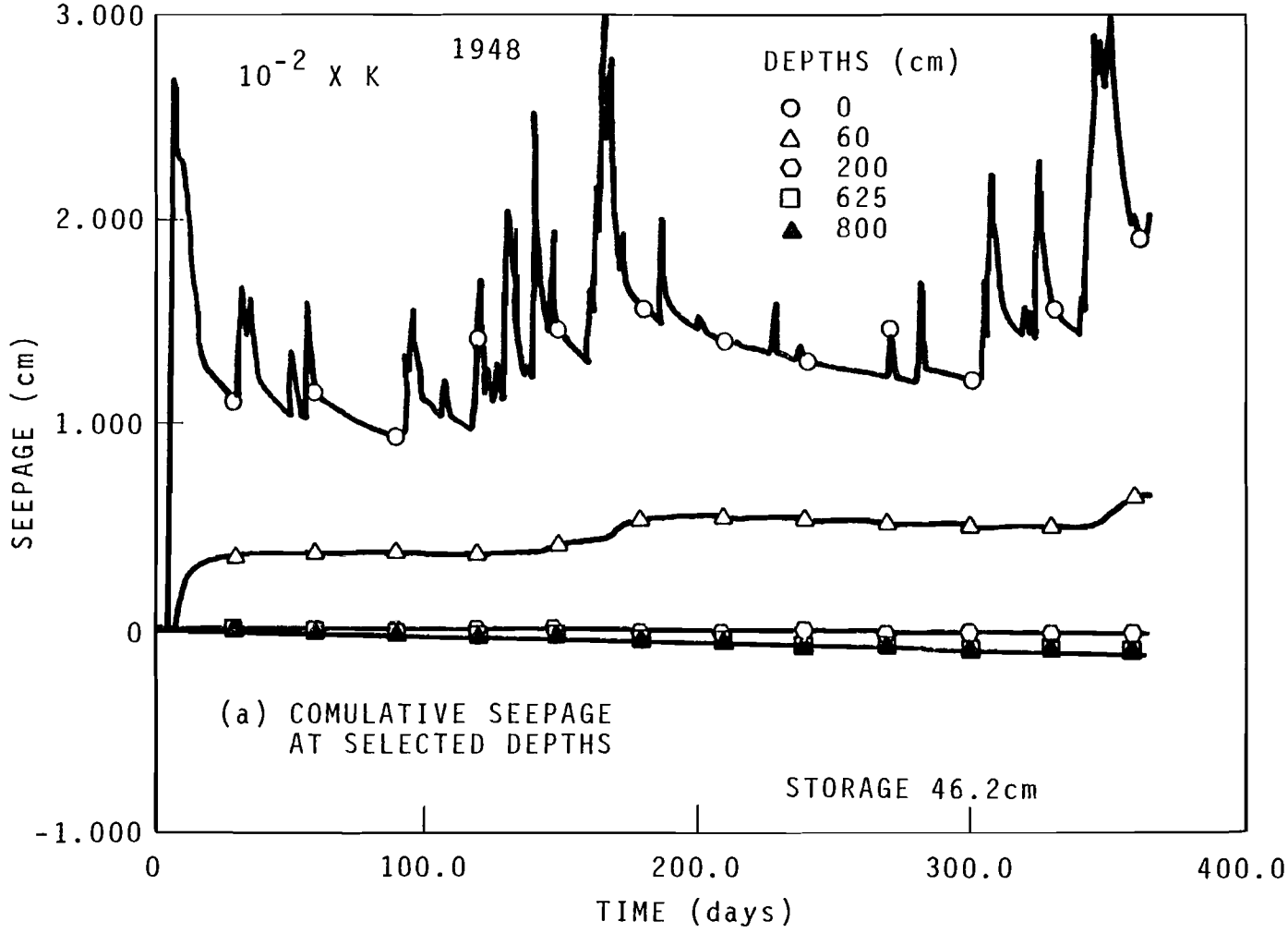

FIGURE 26. Simulated Soil-Water Movement Using 1/100 Conductivity and 1948 Climate: a) Cumulative Seepage at Selected Depths, b) Profile Soil-Water Storage Difference

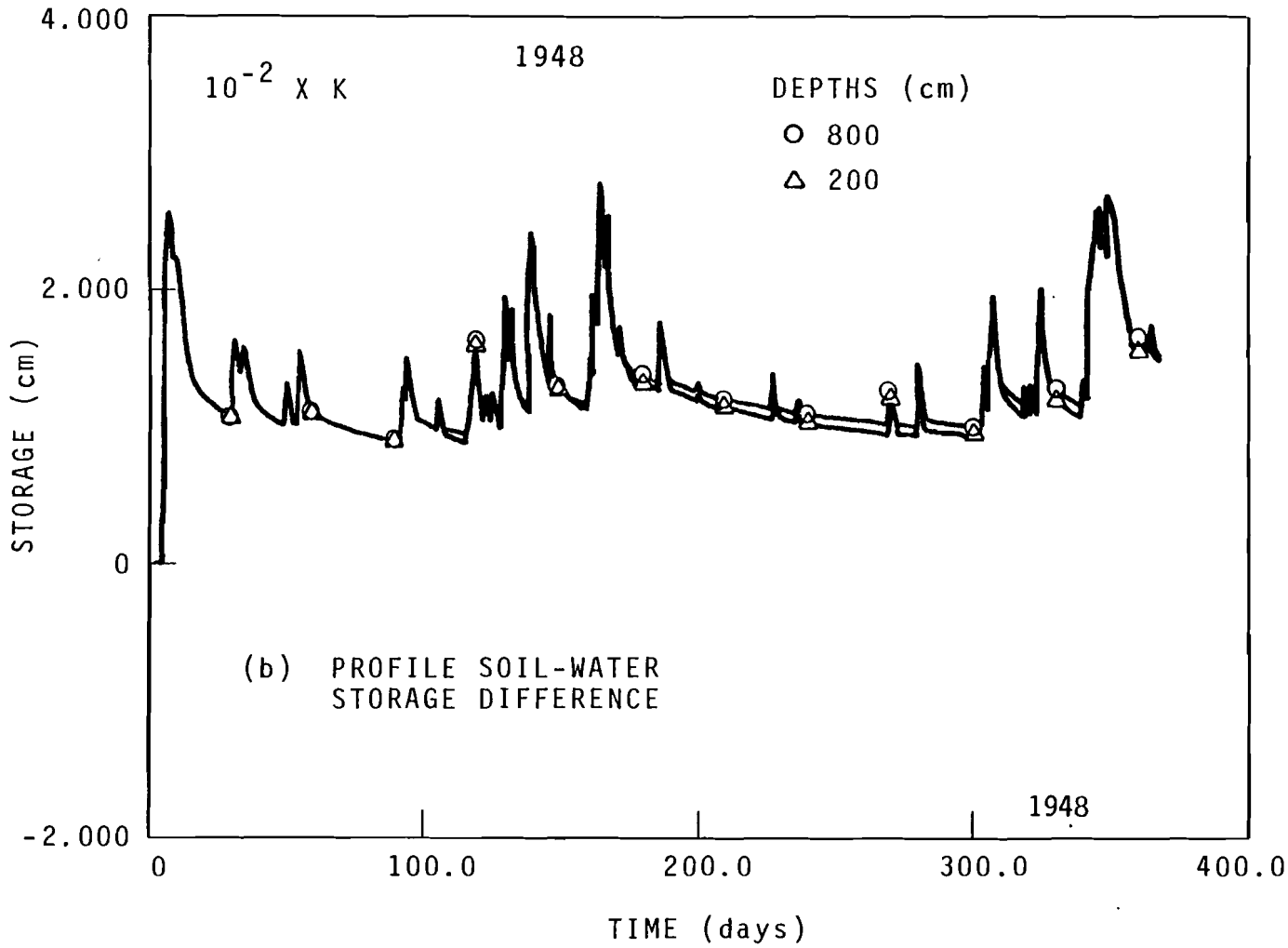

FIGURE 26. (contd)

TABLE 5. Simulations Based on 1948 Climate, without Hydrophobic Surface Layer. Standard initial conditions used for each simulation.

Method	Infiltration (cm)	Evaporation (cm)	Drainage (cm)	Storage (cm)
Blaney-Criddle PET[a]	24.09	26.28	-0.40	42.57
Blaney-Criddle PET[b]	24.46	23.29	-0.21	45.70
Blaney-Criddle PET[c]	24.51	22.66	-0.12	46.19
Penman PET[d]	24.48	25.42	-0.38	43.85

Blaney-Criddle PET = 131.2 cm

Penman without correction PET = 159.0 cm

Initial storage 44.62 cm

(a) Conductivity = K
(b) Conductivity = K/10
(c) Conductivity = K/100
(d) Conductivity = K

POTENTIAL EVAPORATION SENSITIVITY

The modified Penman method for estimating potential evaporation was used to test the model's sensitivity, since this method gave the greatest cumulative evaporation. Also, this PET method differed most in daily distribution of evaporation. Figure 27 gives the corresponding simulation shown in Figure 17 for the Blaney-Criddle method. The summary of results for both PET methods given in Table 5 indicates that soil surface dryness controls actual evaporation, not the level of cumulative potential evaporation. Differences that are observed are mainly a consequence of the daily pattern of PET - not of the magnitudes.

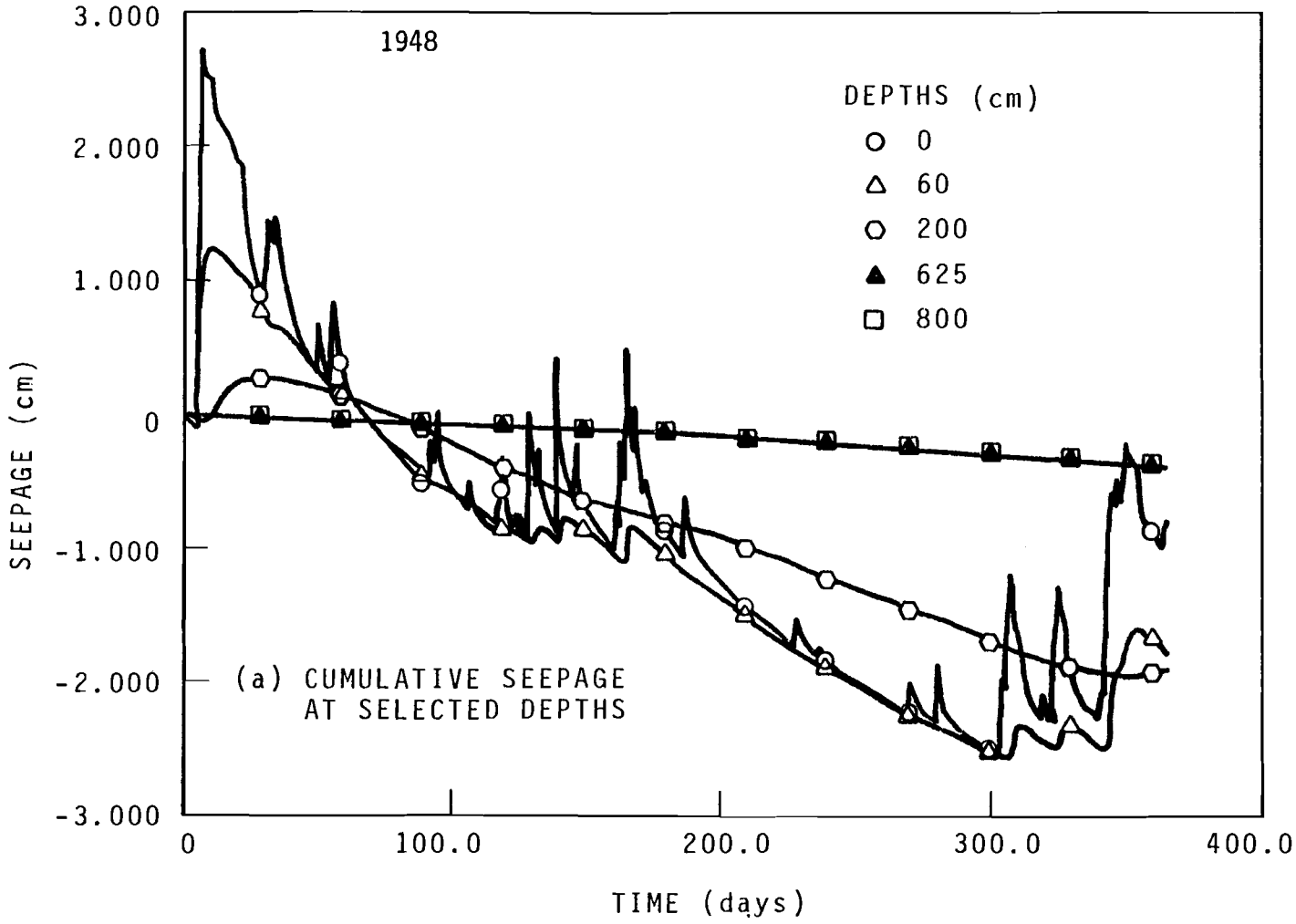

FIGURE 27. Simulated Soil-Water Movement Using Penman PET and 1948 Climate: a) Cumulative Seepages at Selected Depths, b) Profile Soil-Water Storage Difference

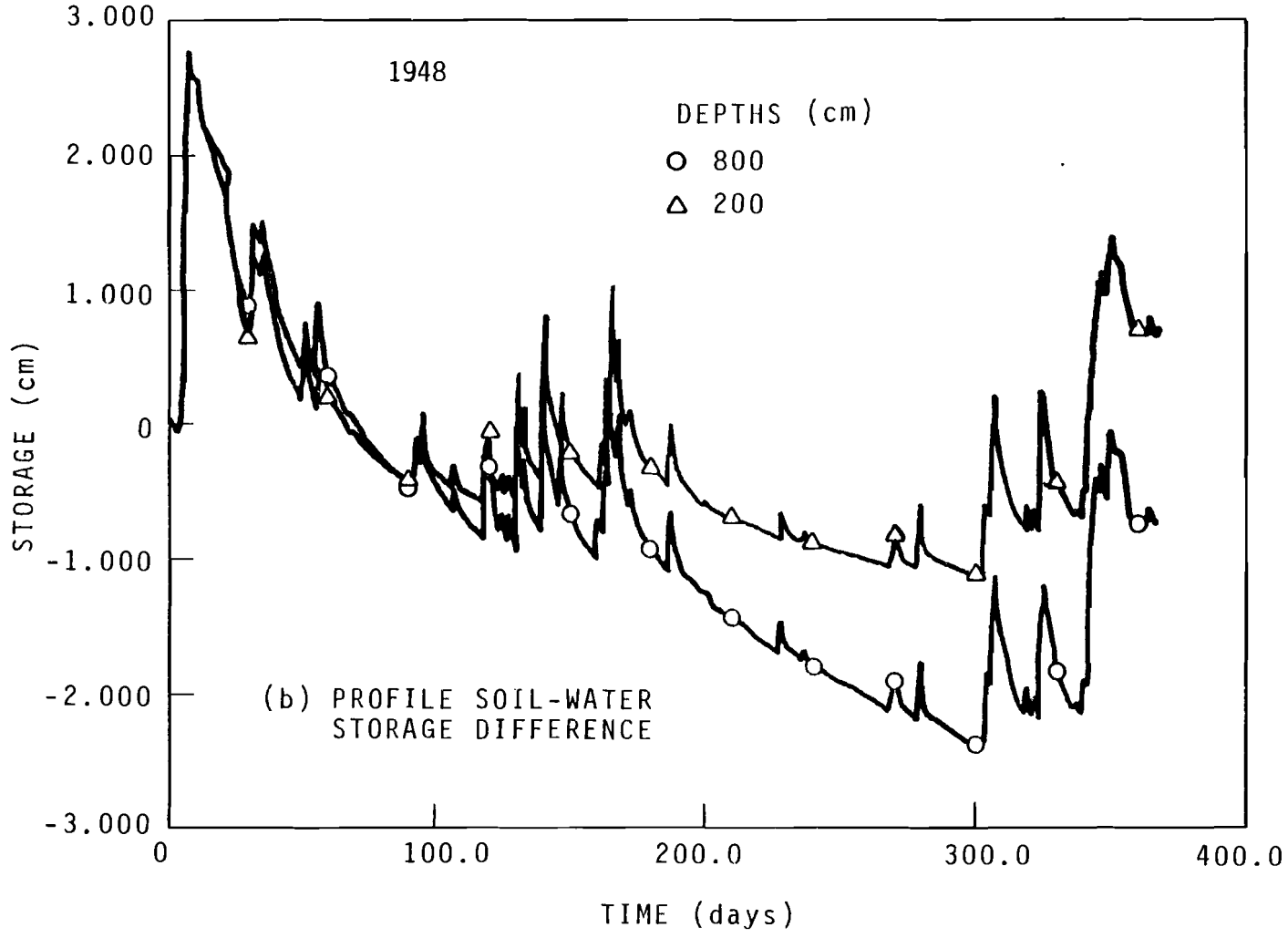

FIGURE 27. (contd)

TOTAL RAINFALL SENSITIVITY

It is expected that increased rainfall amounts can increase the amounts of water draining into the water table. Moreover, the likelihood of net drainage into the water table can depend on the previous rainfall history. To study effects of rainfall amount, six consecutive years with rainfall equal to various multiples of 1948 rainfall were simulated. Each year the same pattern of potential evaporation and rainfall was repeated, but the rainfall was multiplied by a common factor each year. Each year's simulation used as initial conditions the final conditions of the previous year, except in the first year where the standard intial conditions were applied. Based on prior sensitivity tests, the Blaney-Criddle PET method and a hydrophobic surface layer were employed. A summary of results for the end of each year is given in Table 6.

TABLE 6. Simulation of Six Consecutive Years Based on Multiples of Rainfall in 1948. Blaney-Criddle PET method and hydrophobic surface layer assumed.

Year	Infiltration (cm)	Evaporation (cm)	Drainage (cm)	Storage (cm)
1	49.07 (2.0 x)	34.87	7.49	51.04
2	36.81 (1.5 x)	31.51	6.81	49.35
3	8.14 (0.33 x)	13.08	0.57	43.90
4	24.51 (1.0 x)	23.22	-0.34	45.48
5	36.78 (1.5 x)	30.87	1.87	49.33
6	18.46 (0.75 x)	21.14	0.99	45.61

Initial Storage: 44.62 cm

Potential Evaporation: 131.2 cm

h_d = 15,000 cm

h_1 = 5,000 cm

q_1 = 0.001 cm/day

The 6-year rainfall sequence begins with two times rainfall of 1948. Water content profiles for selected days are provided in Figures 28 and 29, and are to be compared with Figures 14 and 15. Flow restriction by the coarse sand layer is evident in Figure 29. The same sequence of days is repeated in Figures 30 and 31 for the next 2 years. The water content in the layer remains high due to continued drainage from the previous year's storage increase.

Figures 32 through 37 for cumulative flux at various nodes and storage over the profile describe the consequences of the 6-year rainfall sequence. Most years show continued drainage from previous years because rainfall exceeds the average of 16 cm observed at Hanford.

EFFECT OF RAINFALL DISTRIBUTION

Climatological years 1947 and 1948 proved to be particularly interesting because they had nearly the same cumulative rainfall and potential evaporation. The patterns of rainfall, however, were distinctly different. In 1947, the majority of rain occurred in the fall, whereas rainfall was distributed over spring and winter of 1948. Beginning with the chosen standard initial conditions, the natural climate sequence for 1947-48 was used to simulate a 3-year period by repeating the 1948 climate. The third year used final profile conditions of 1948 as initial conditions. A summary of results is given in Table 7. Results for 1947 should be compared to those for 1948 given in Table 4 based on the same initial conditions. Again a surface layer was assumed present each year. Drainage observed in 1948 and in the repeated 1948 climate year originates as excess storage of 1947. Details of seepage and storage within the profile are shown in Figures 38 through 40. The simulation of a repeated 1948 appears to approach that shown in Figure 18. Differences remaining are a consequence of the soil profile's past water history.

To further demonstrate importance of the rainfall distribution, a 3-year sequence based on repeated 1947 climate was simulated, as summarized in Table 8. These simulations manifest an approach to steady-state drainage

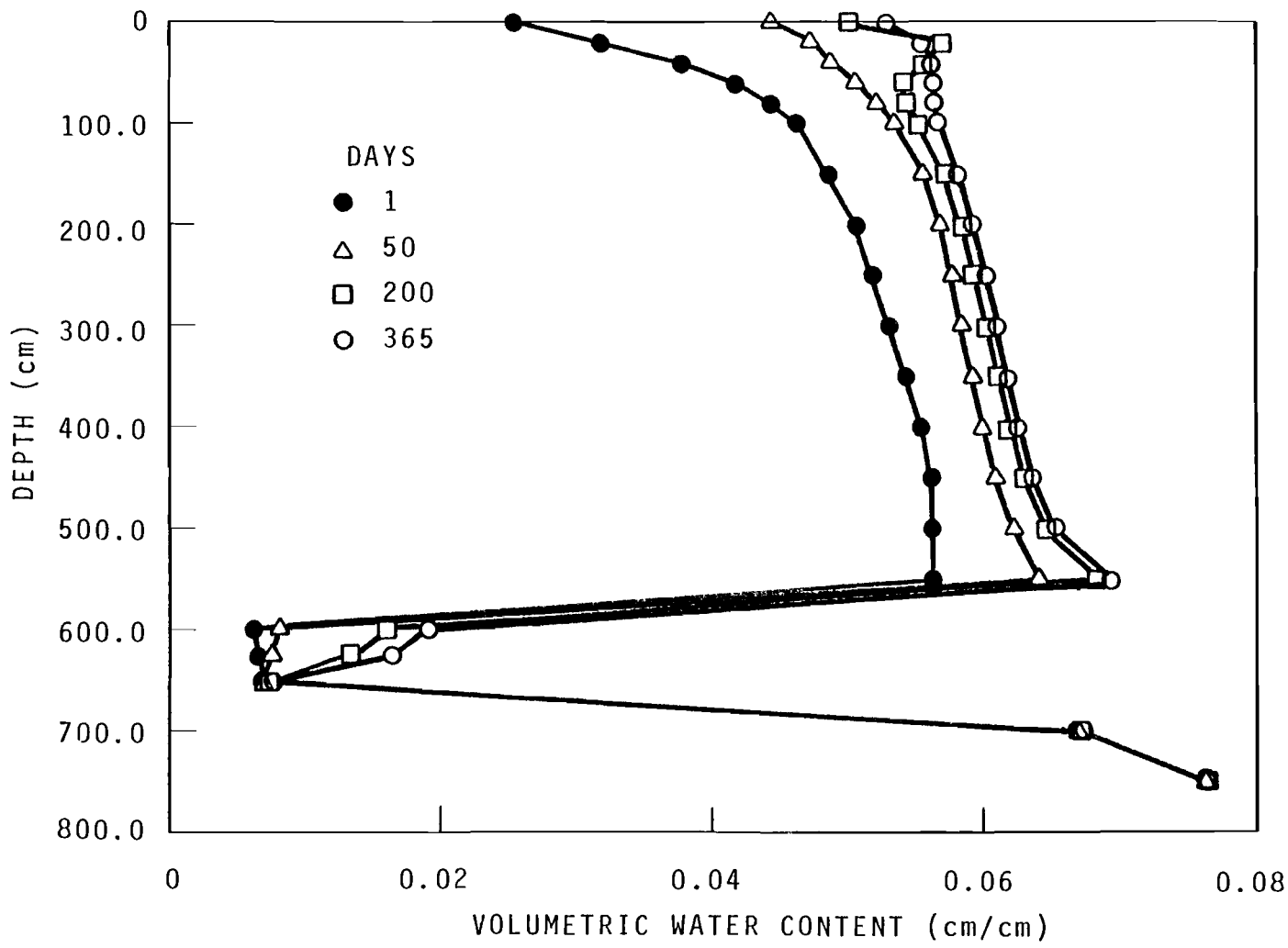

FIGURE 28. Water Content Profiles for 1, 50, 200, 365 Days Using 2X Rainfall of 1948. A hydrophobic surface layer and Blaney-Criddle PET are used.

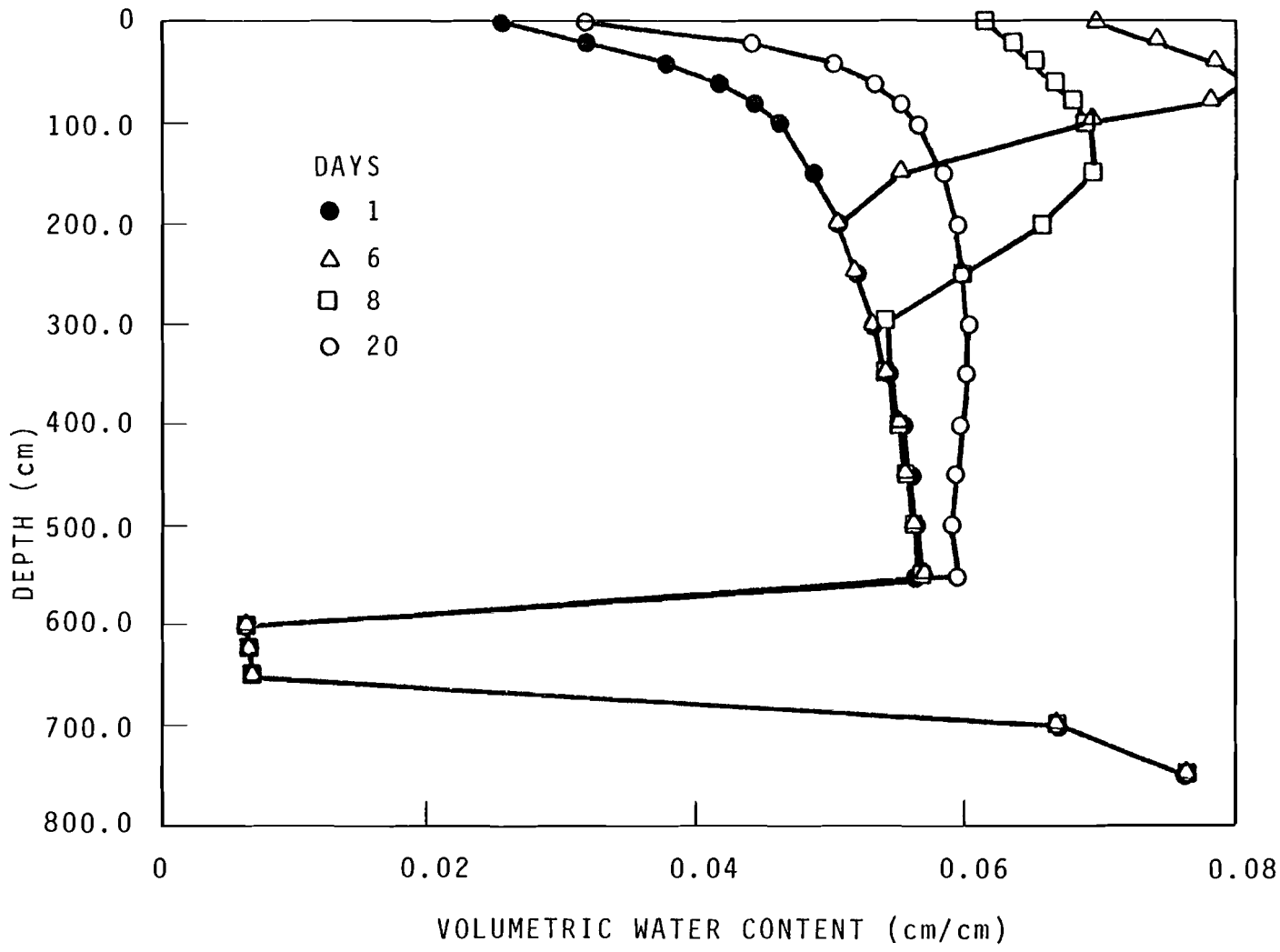

FIGURE 29. Water Content Profiles for 1, 6, 8, 20 Days and Conditions of Figure 28. First year of a 6-year rainfall sequence.

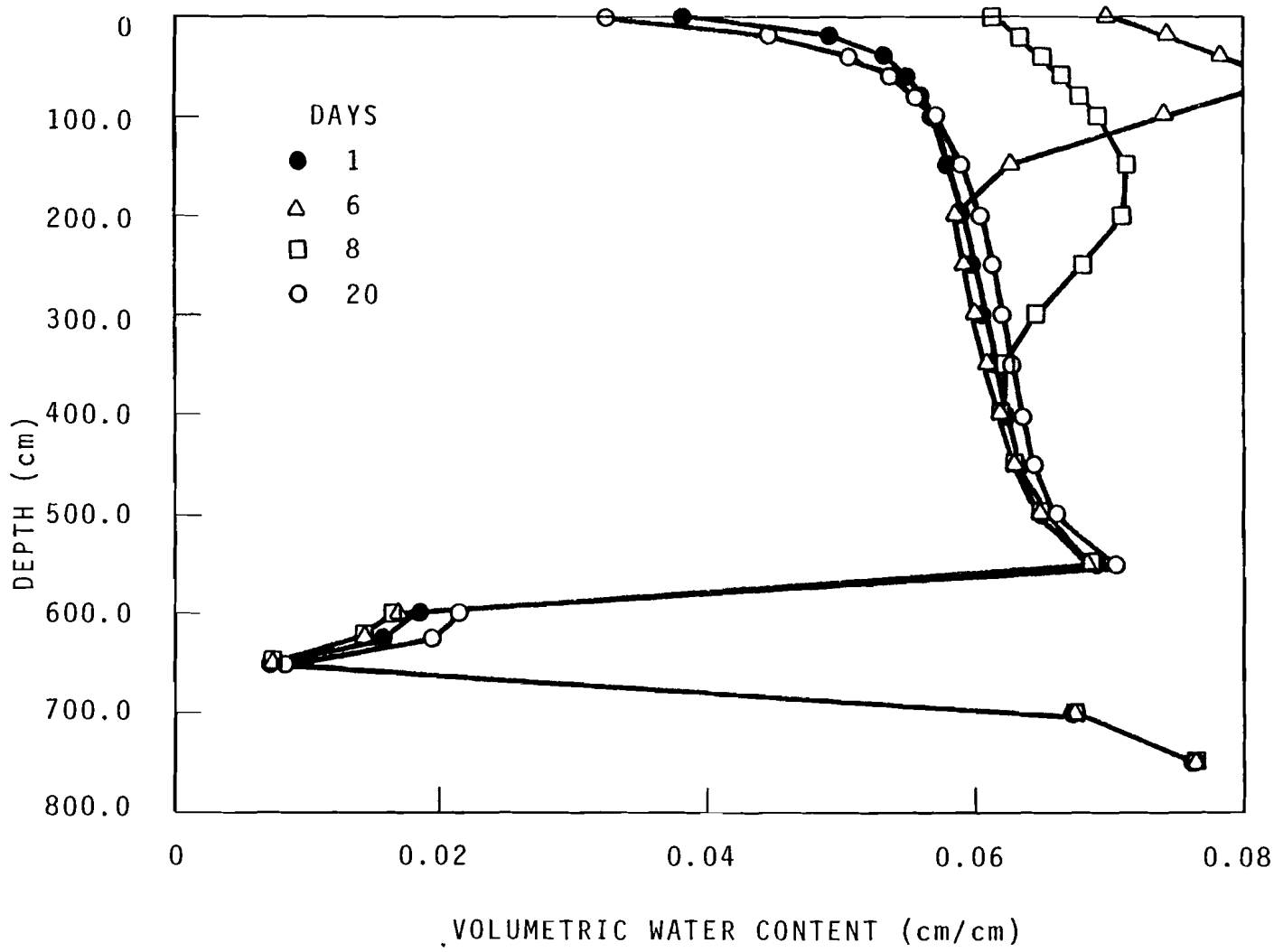

FIGURE 30. Water Content Profiles for 1, 6, 8, 20 Days Using 1.5X Rainfall of 1948. Second year of sequence.

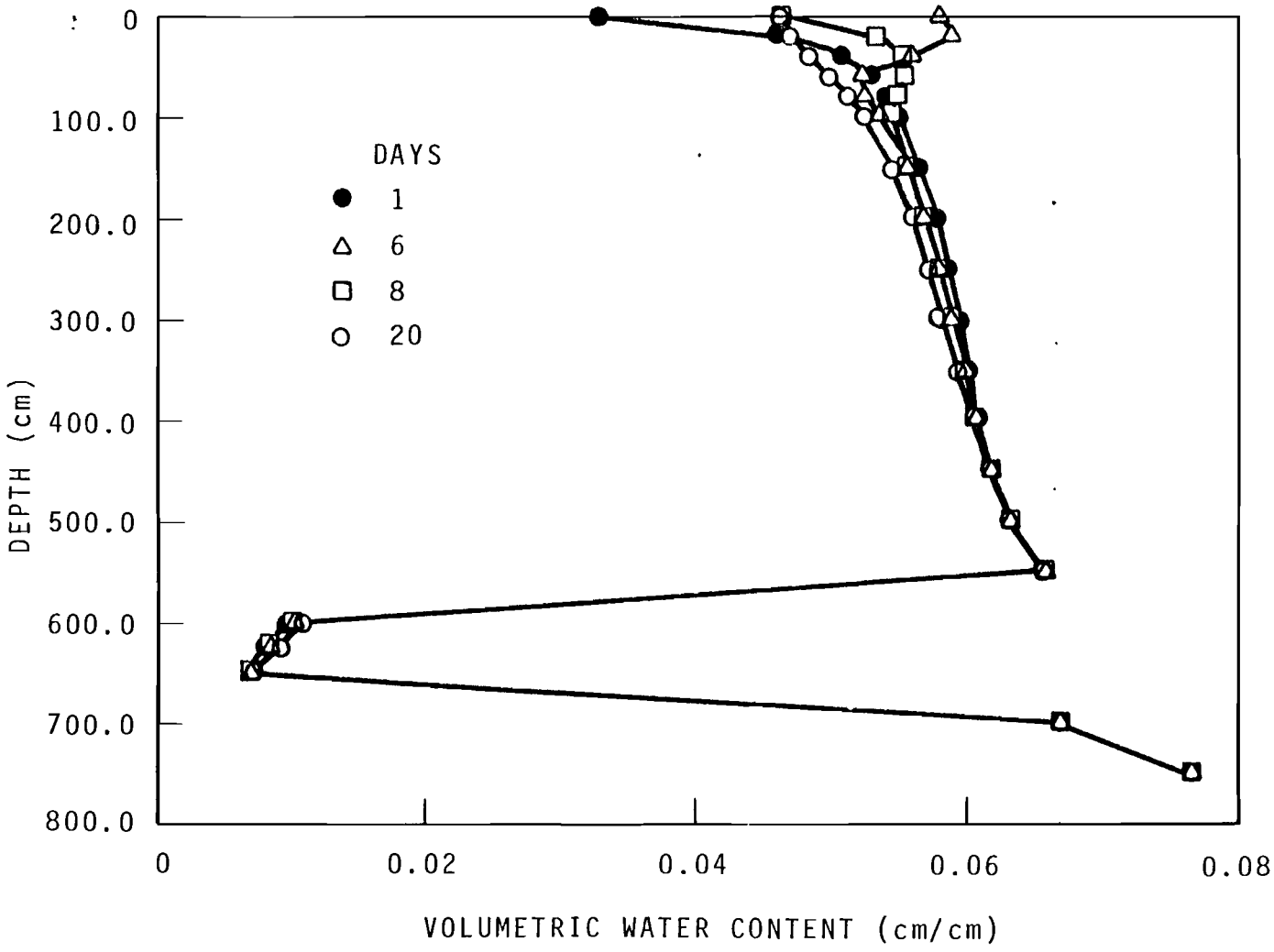

FIGURE 31. Water Content Profiles for 1, 6, 8, 20 Days Using 0.3X Rainfall of 1948. Third year of sequence.

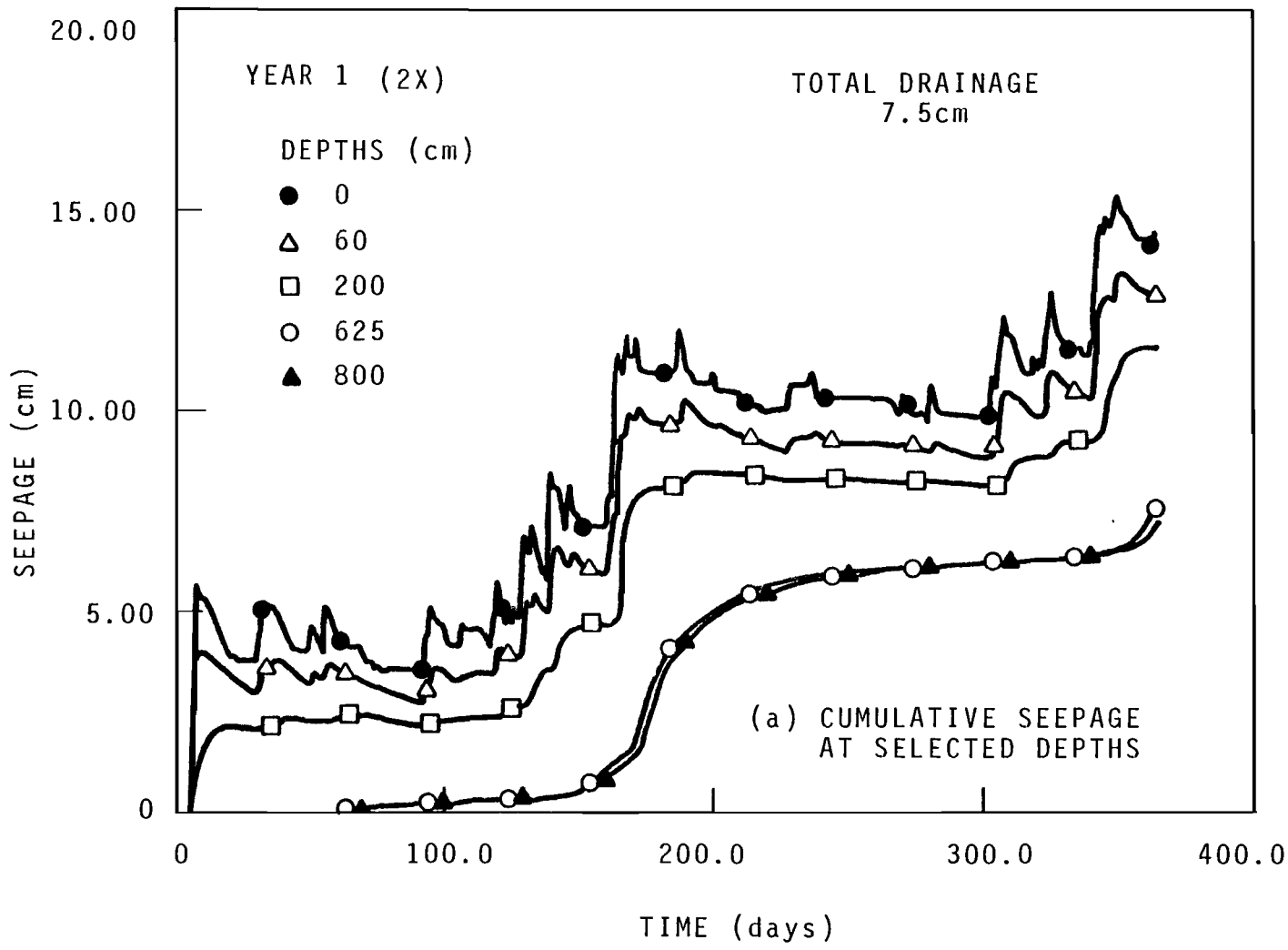

FIGURE 32. Simulated Soil-Water Movement for a 6-year Rainfall Sequence: a) Cumulative Seepage at Selected Depths, b) Soil-Water Storage in the 800-cm Profile. Year 1 with 2X rainfall of 1948. A hydrophobic surface layer and Blaney-Criddle PET are used.

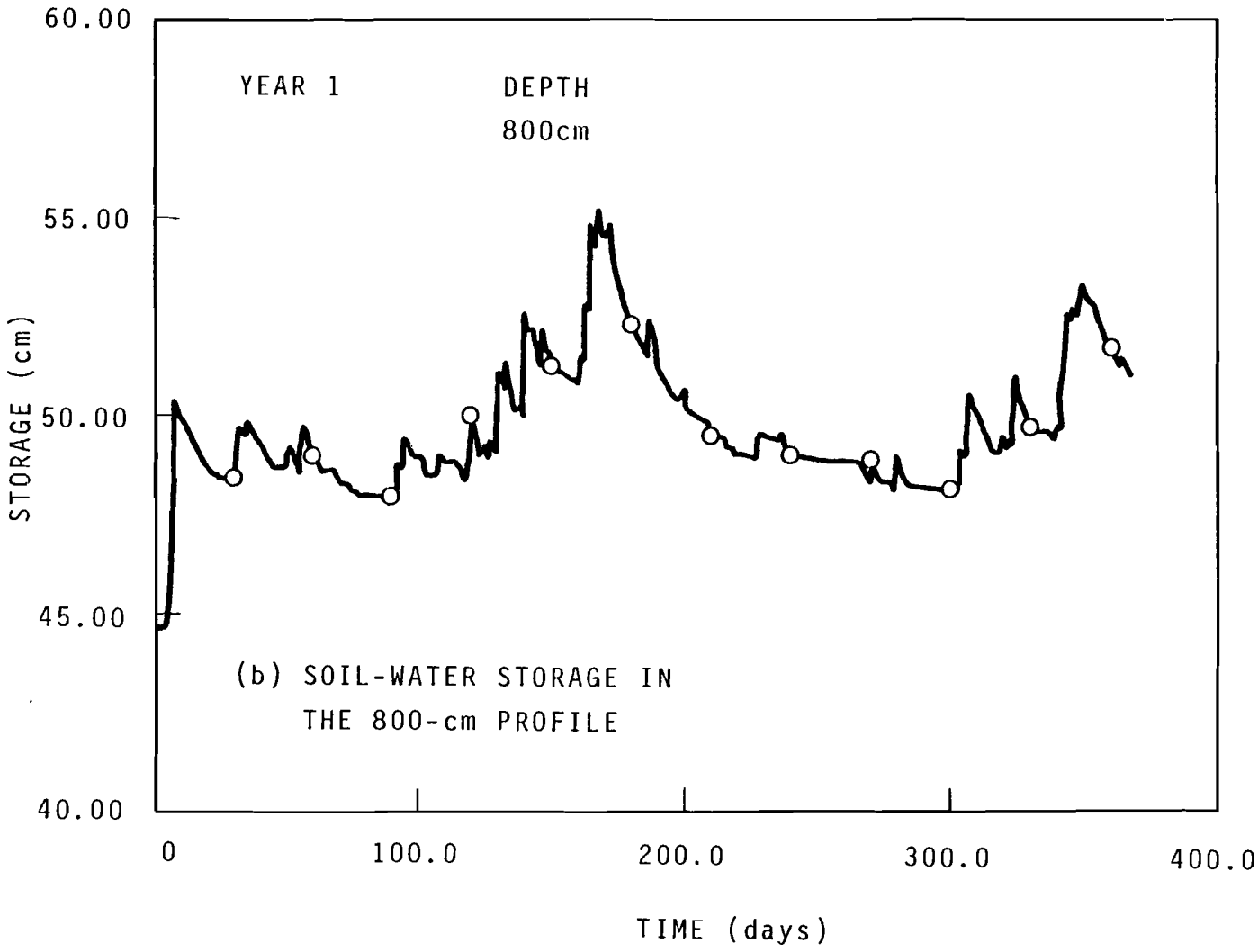

FIGURE 32. (contd)

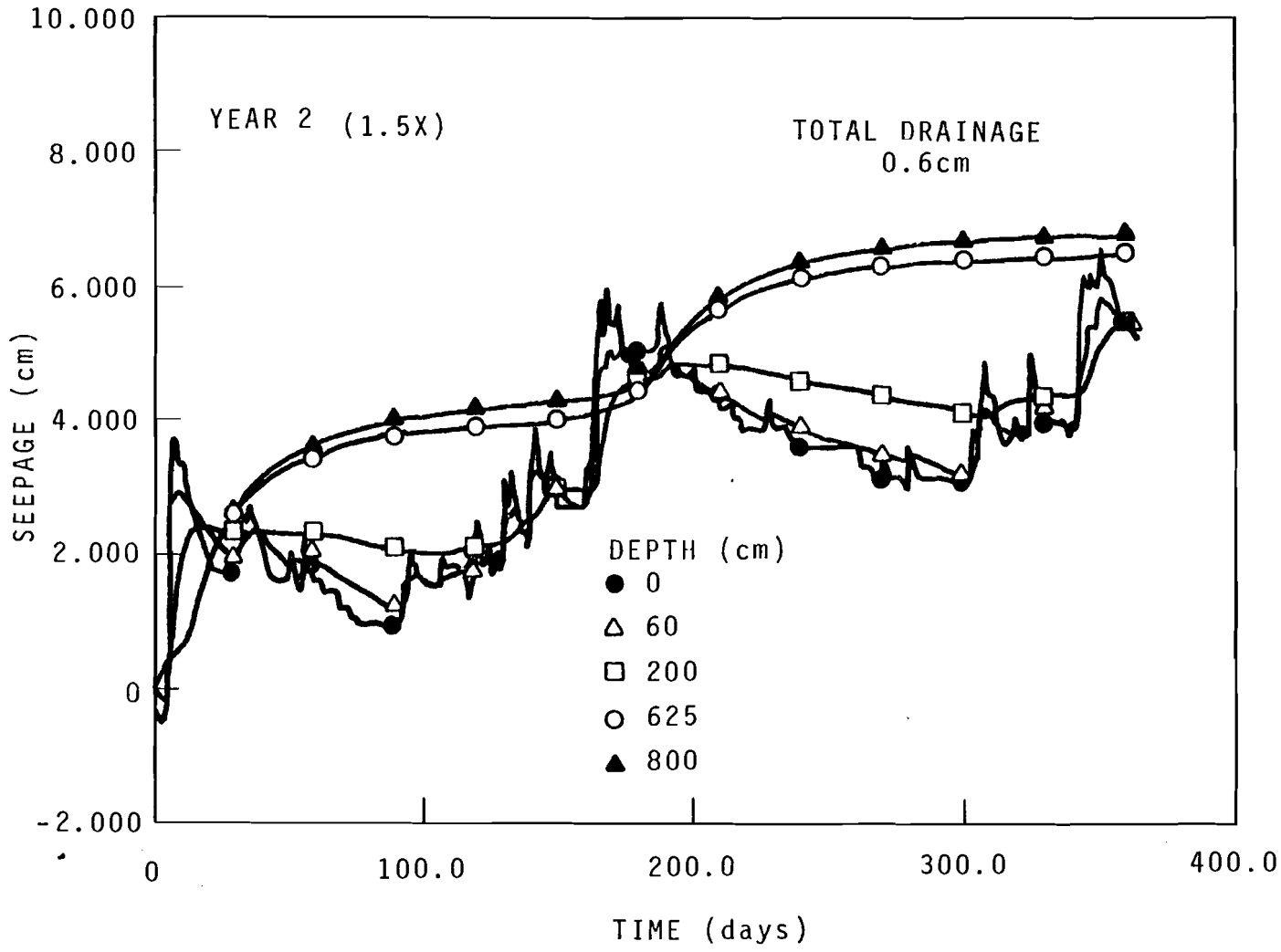

FIGURE 33. Six-year Rainfall Sequence: a) Year 2 with 1.5X Rainfall of 1948, b) Total Water Storage in 800-cm Profile for Year 2

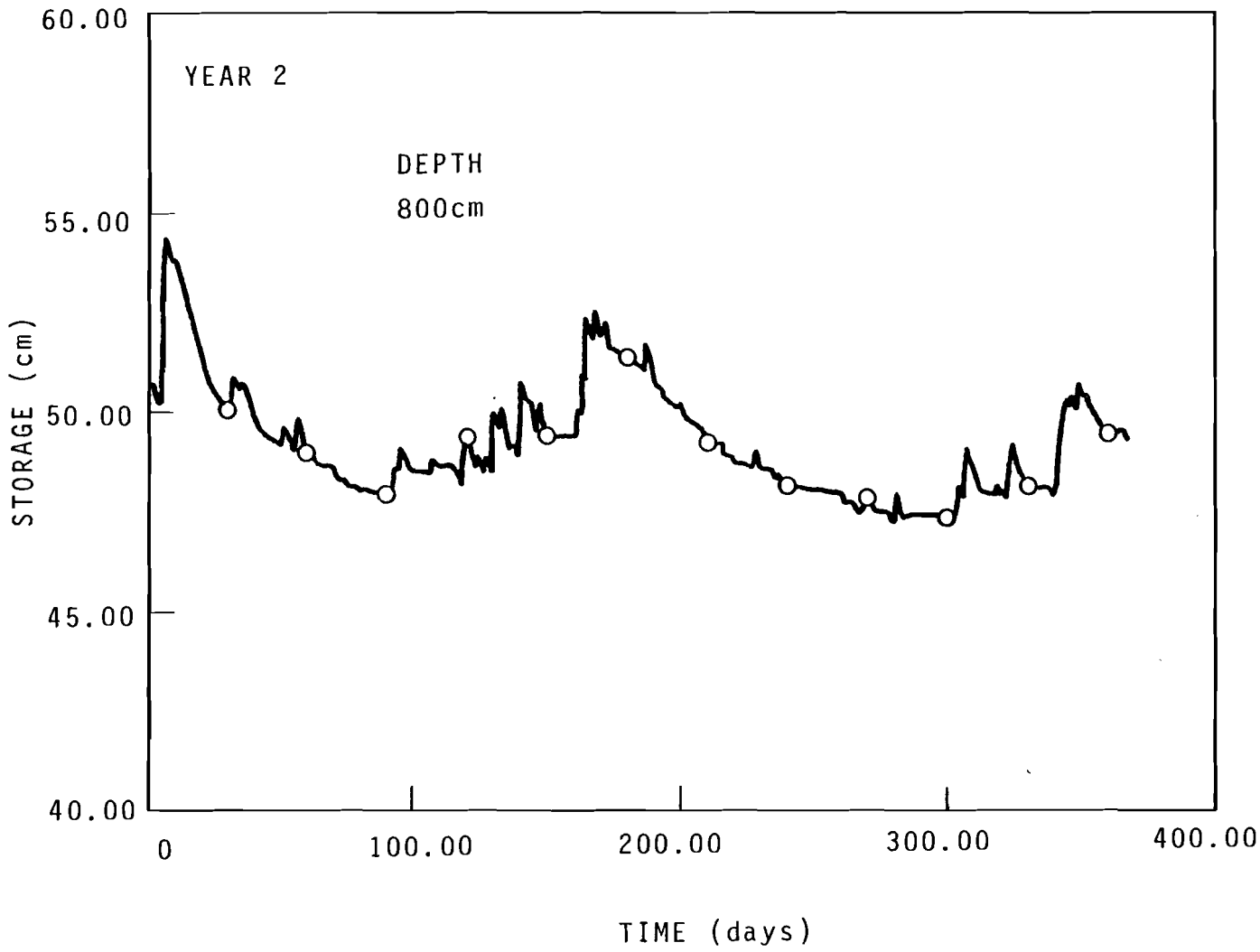

FIGURE 33. (contd)

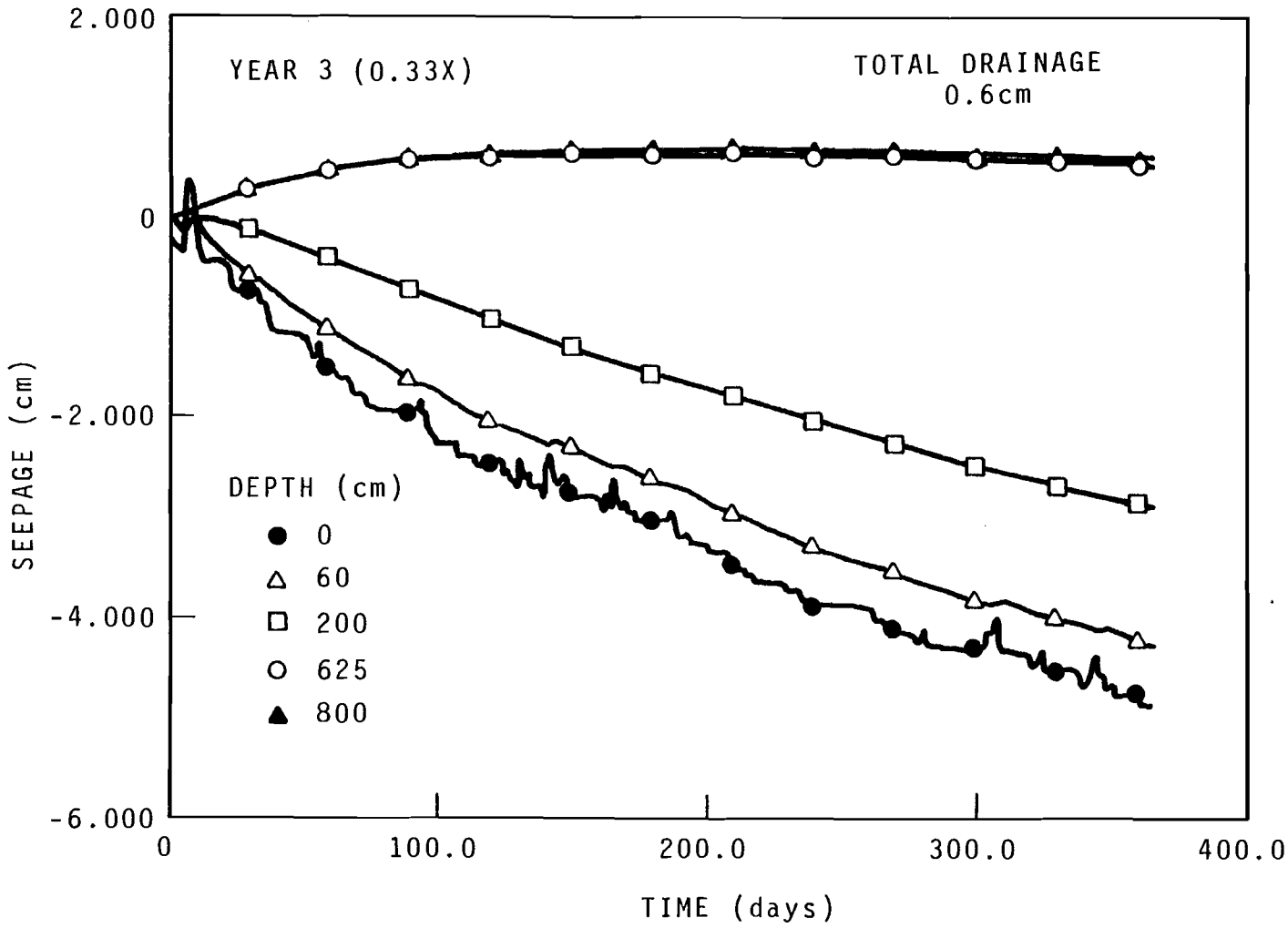

FIGURE 34. Six-year Rainfall Sequence: a) Year 3 with 0.3X Rainfall of 1948, b) Total Water Storage in 800-cm Profile for Year 3

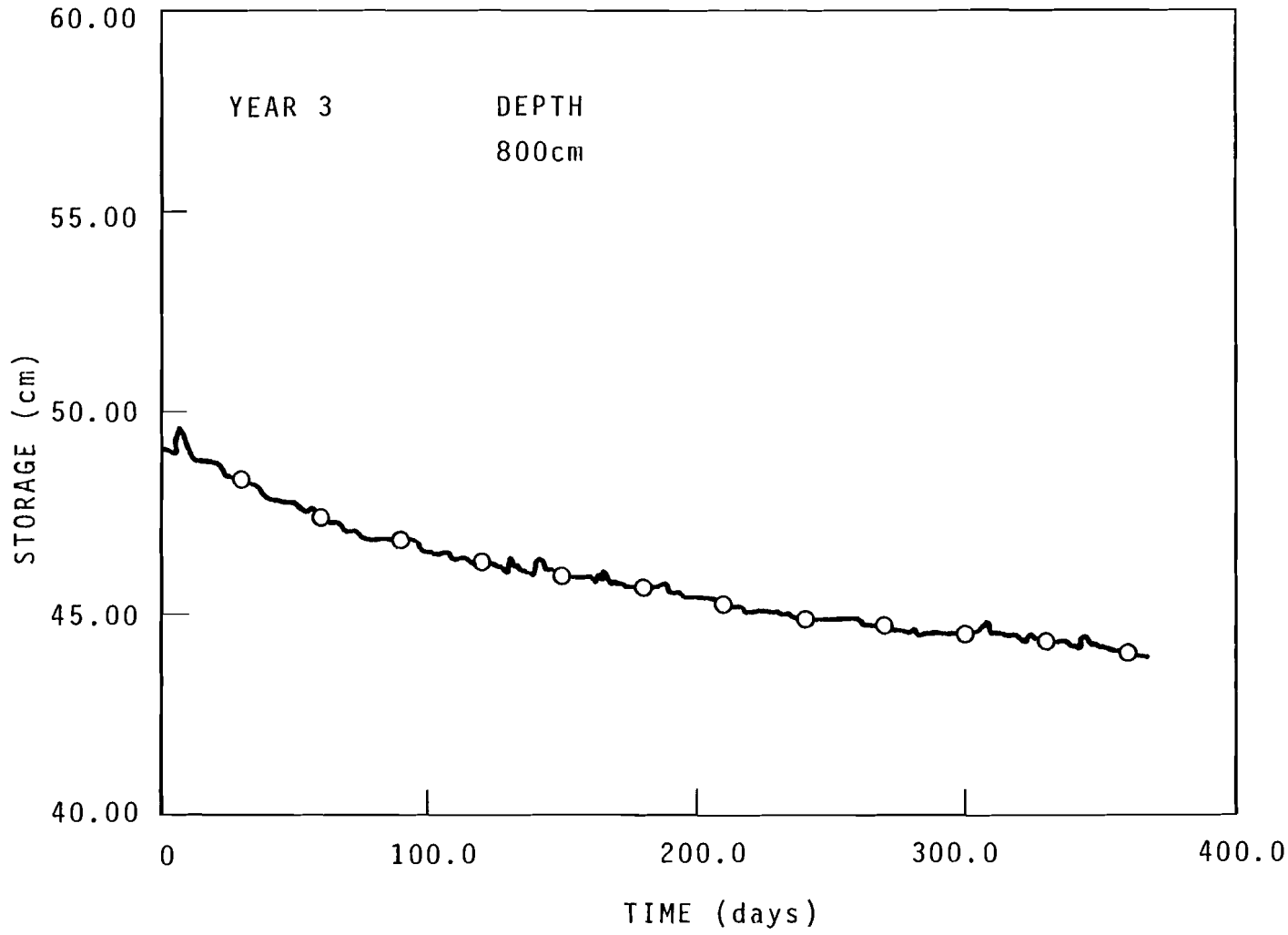

FIGURE 34. (contd)

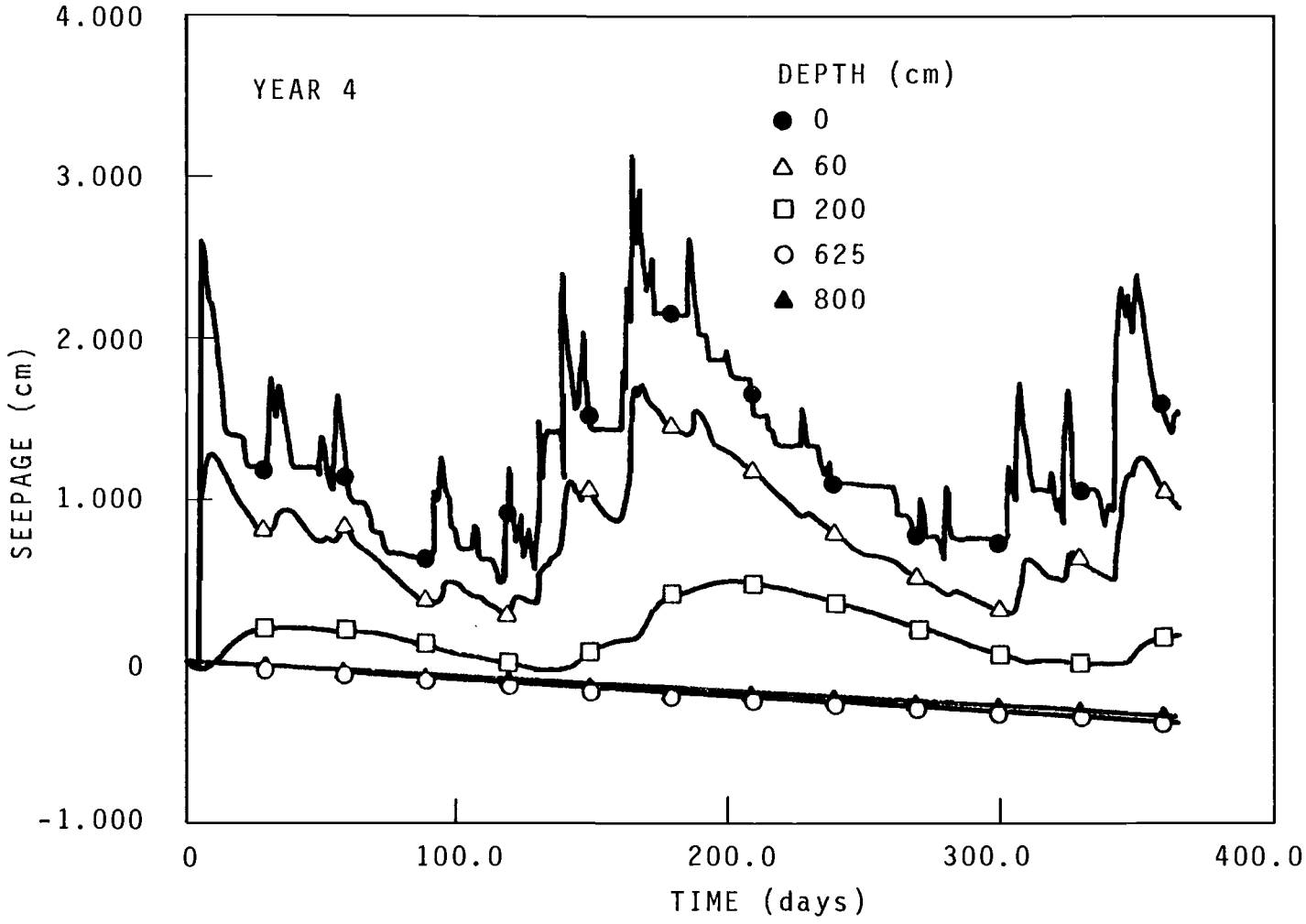

FIGURE 35. Six-year Rainfall Sequence: a) Year 4 with 1.0X Rainfall of 1948, b) Total Water Storage in 800-cm Profile for Year 4

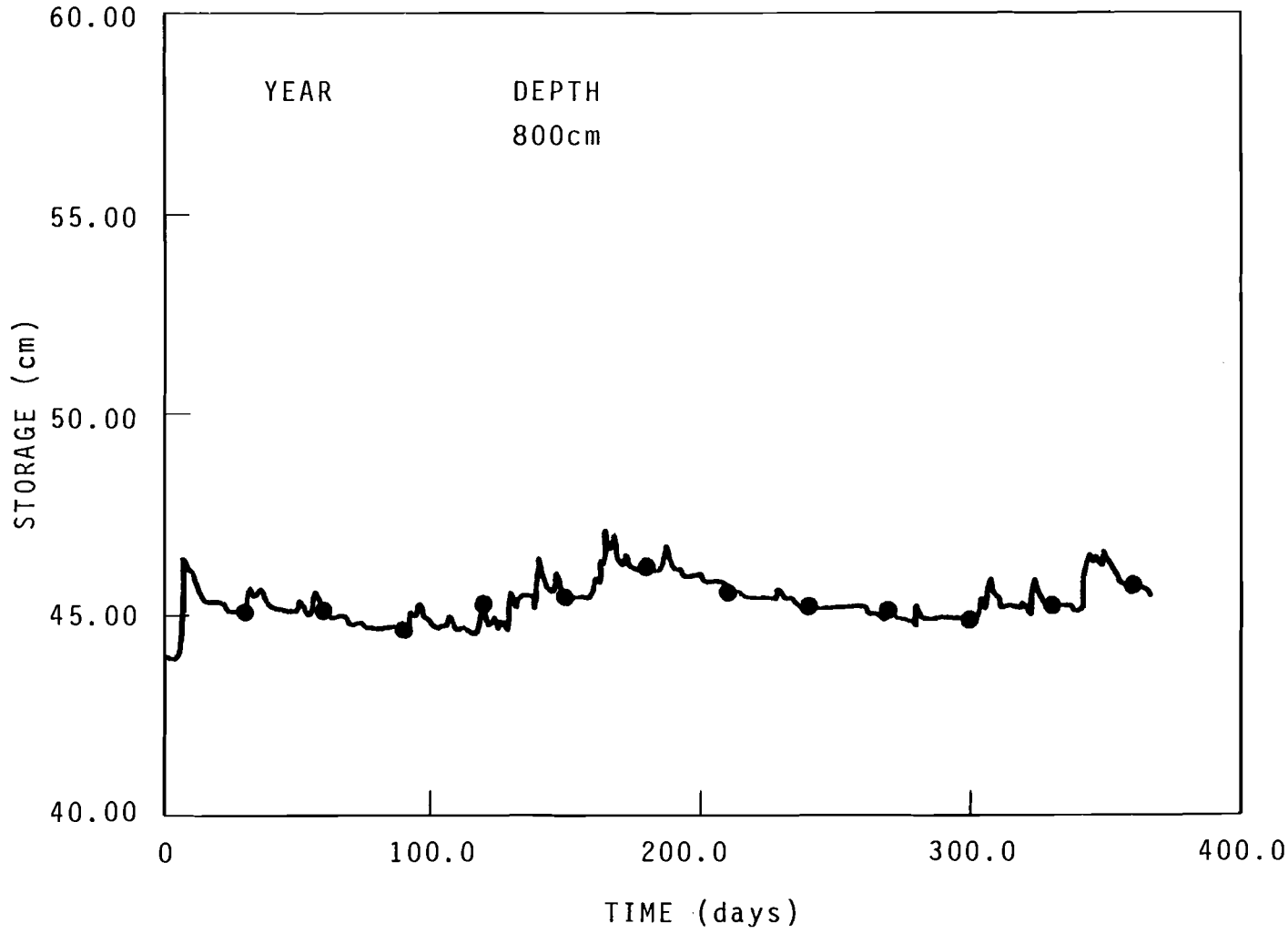

FIGURE 35. (contd)

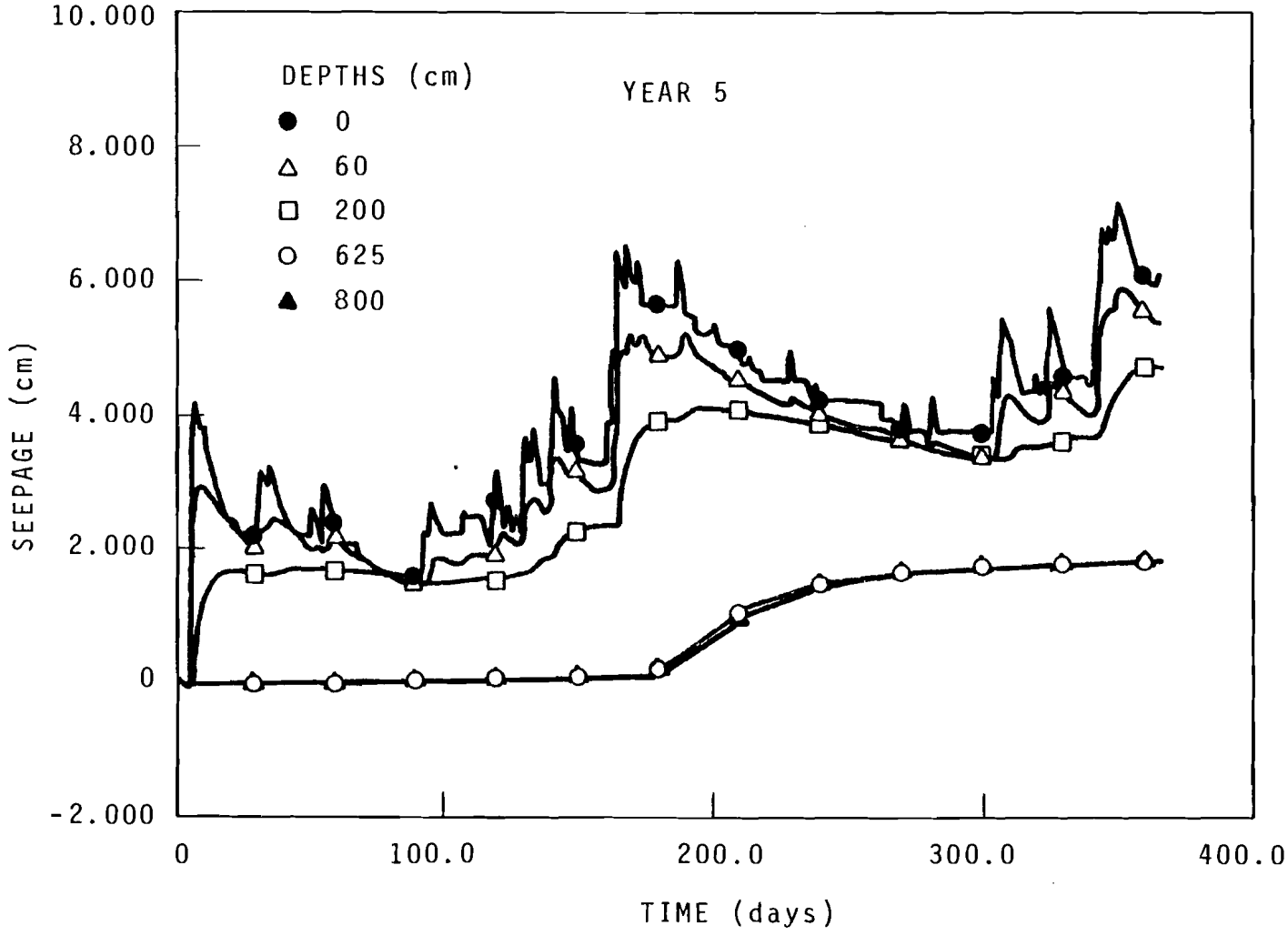

FIGURE 36. Six-year Rainfall Sequence: a) Year 5 with 1.5X Rainfall of 1948, b) Total Water Storage in 800-cm Profile for Year 5

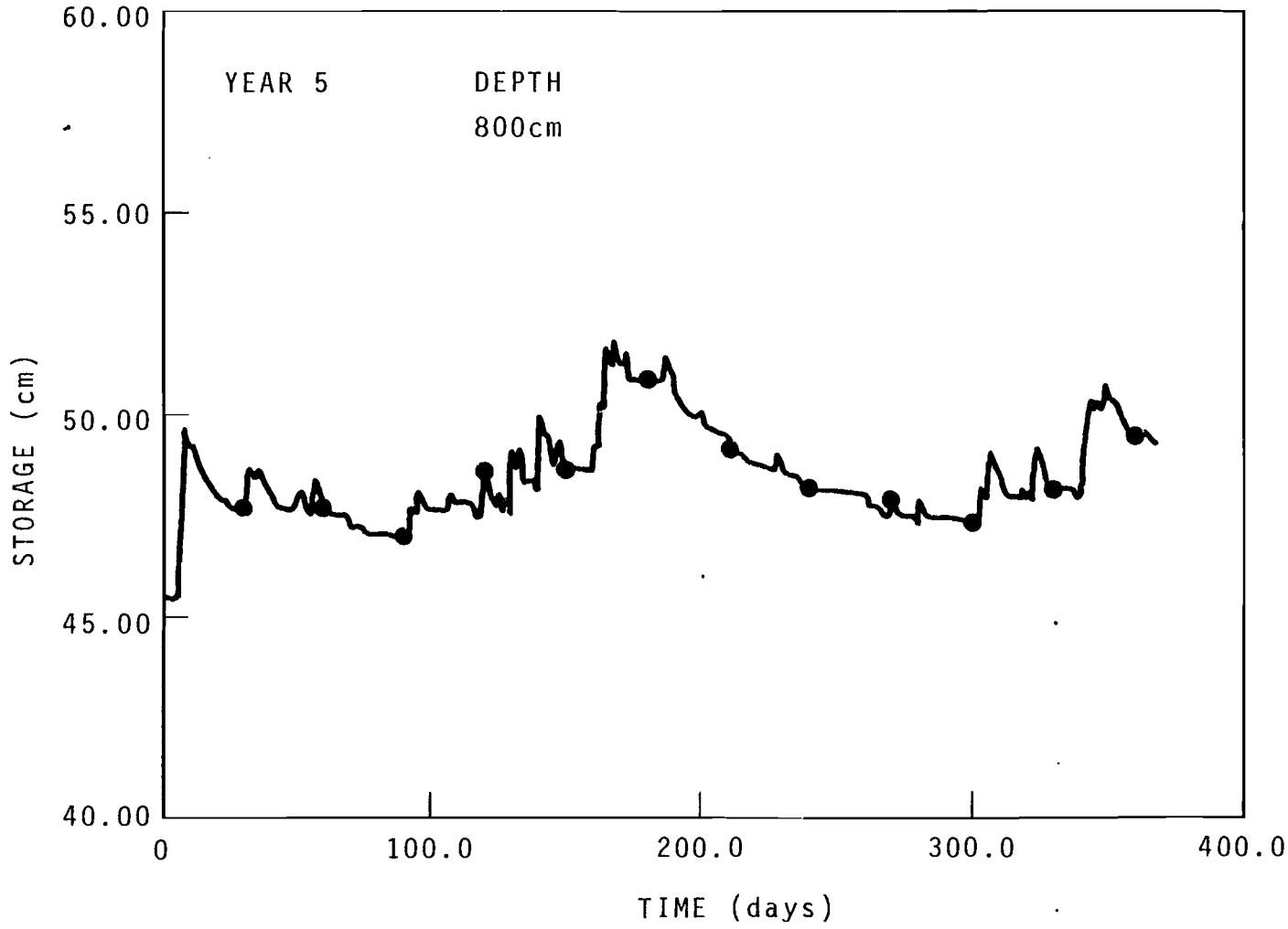

FIGURE 36. (contd)

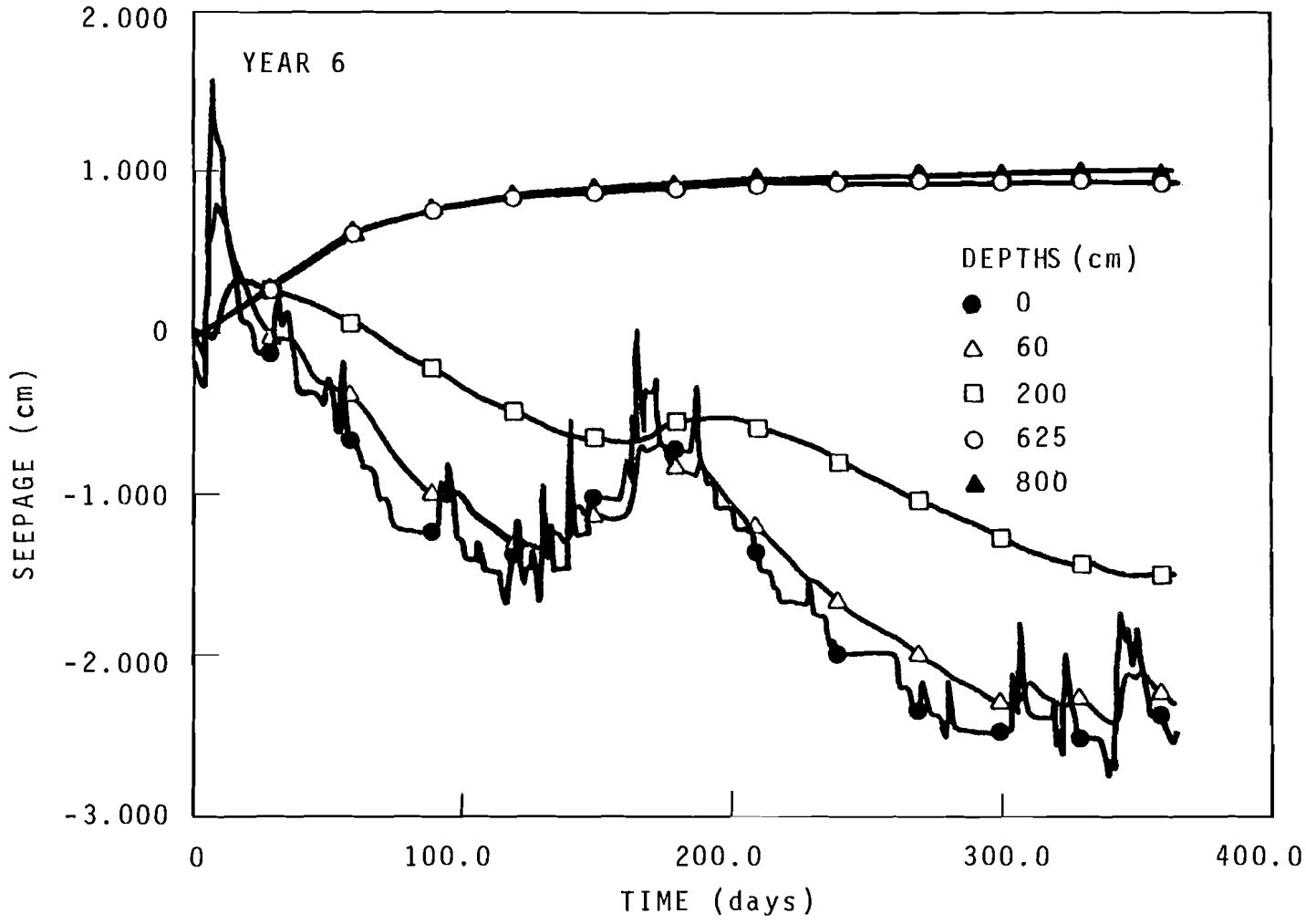

FIGURE 37. Six-year Rainfall Sequence: a) Year 6 with 0.75X Rainfall of 1948, b) Total Water Storage in-800 cm Profile for Year 6

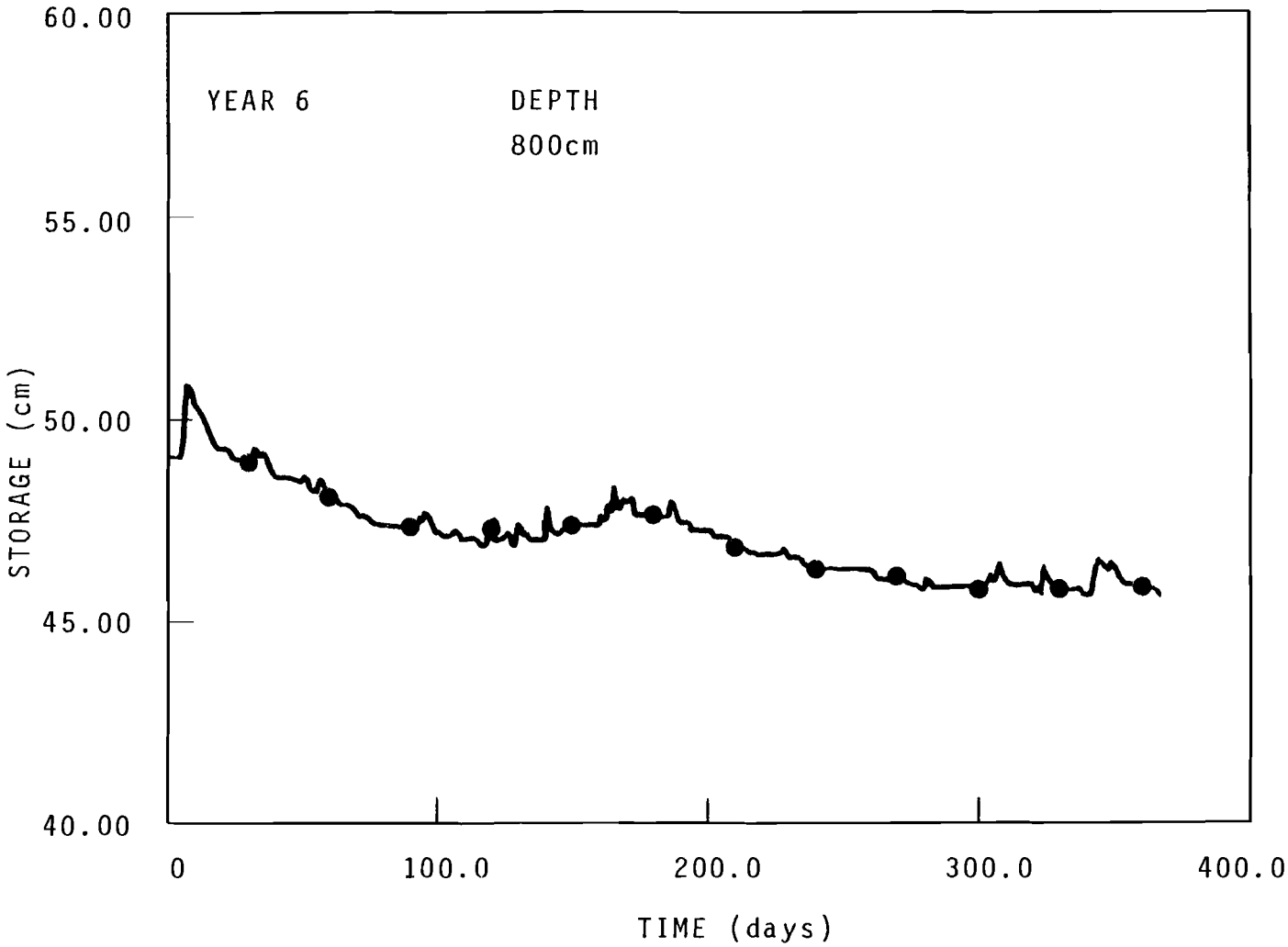

FIGURE 37. (contd)

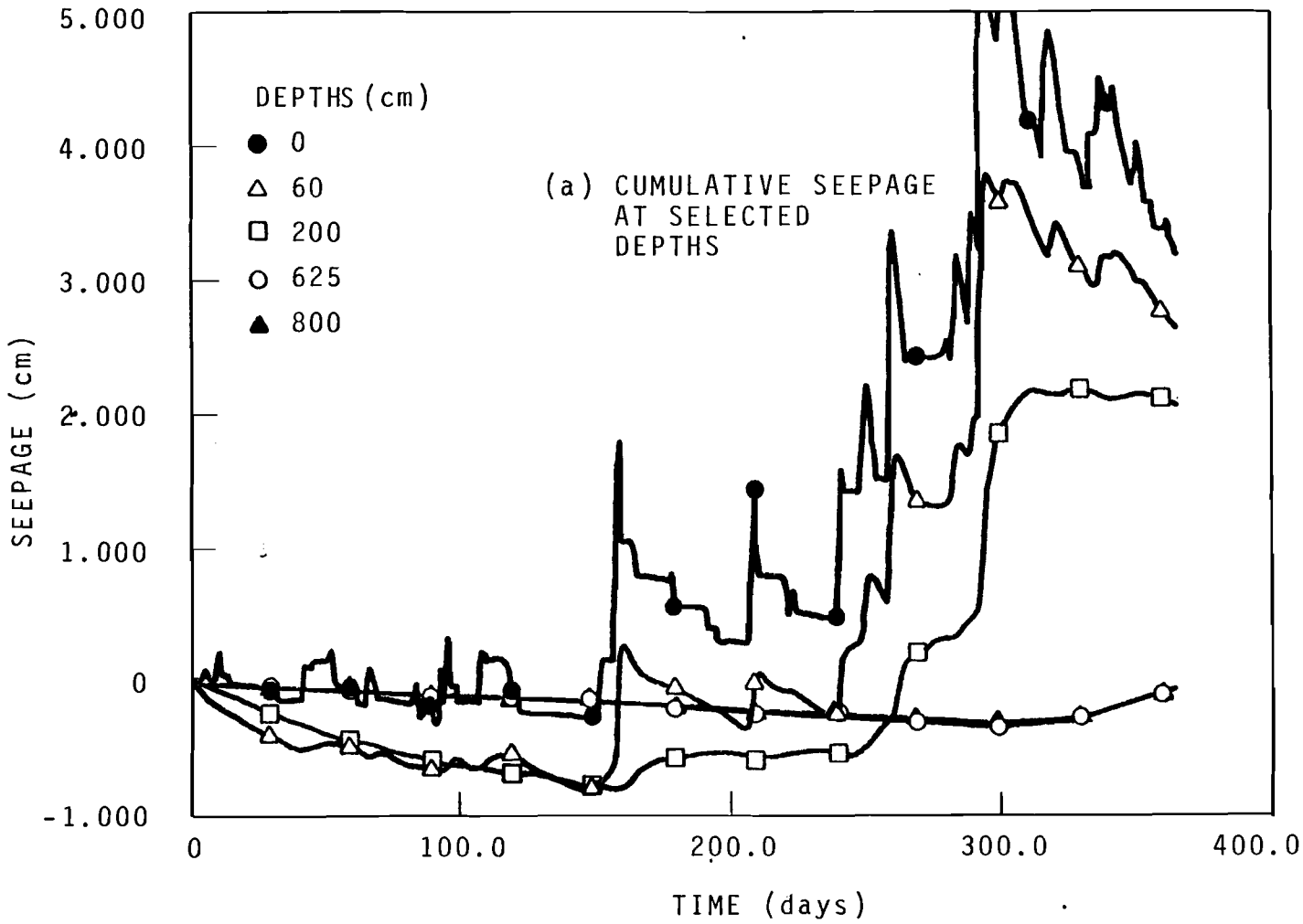

FIGURE 38. Simulation of Soil-Water Movement for a Three-Year Sequence Based on Consecutive 1947 and 1948 Climates with a Repeated 1948 Year: a) Cumulative Seepage at Selected Depths, b) Soil-Water Storage in the 800-cm Profile for Year 1

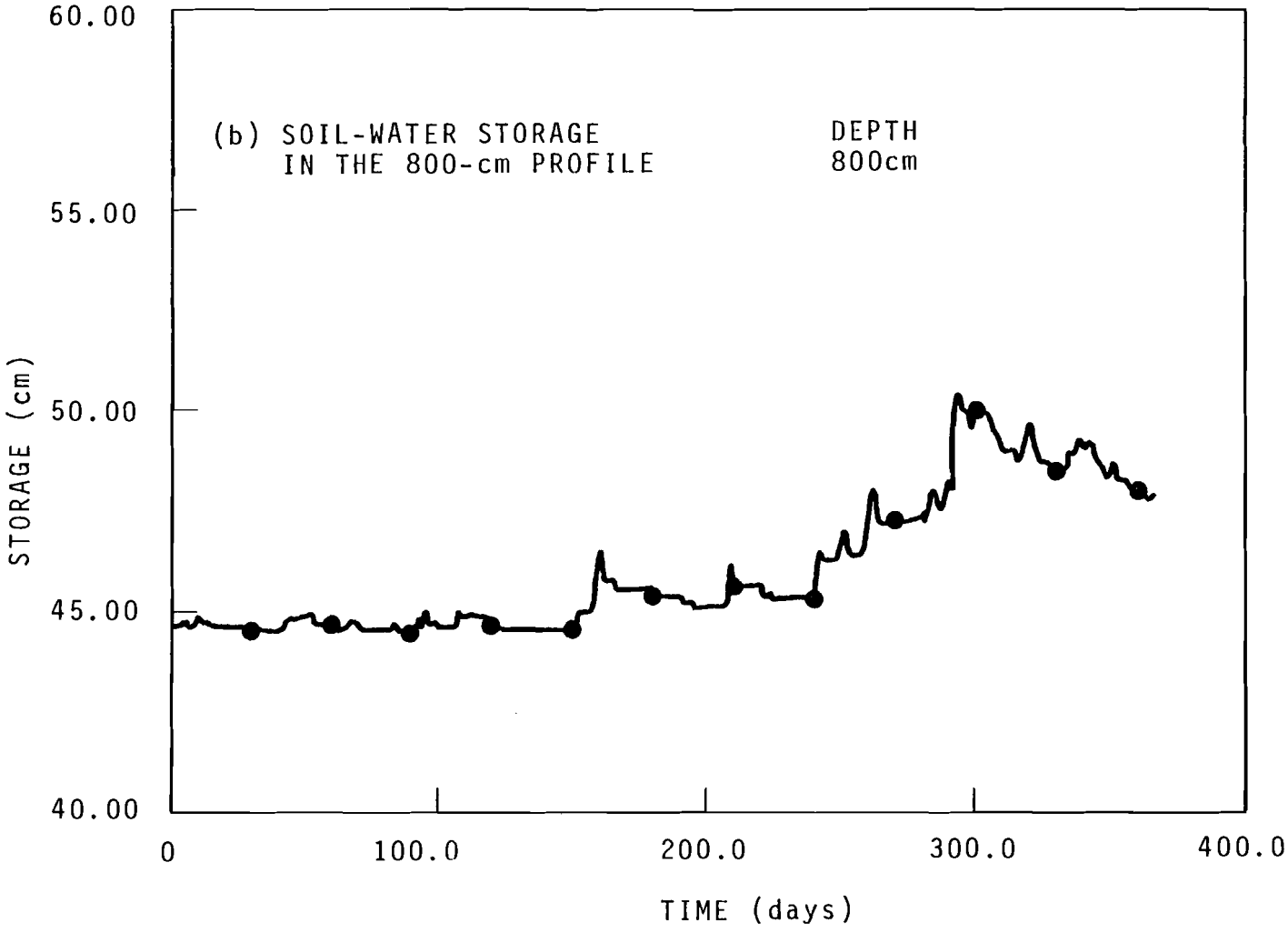

FIGURE 38. (contd)

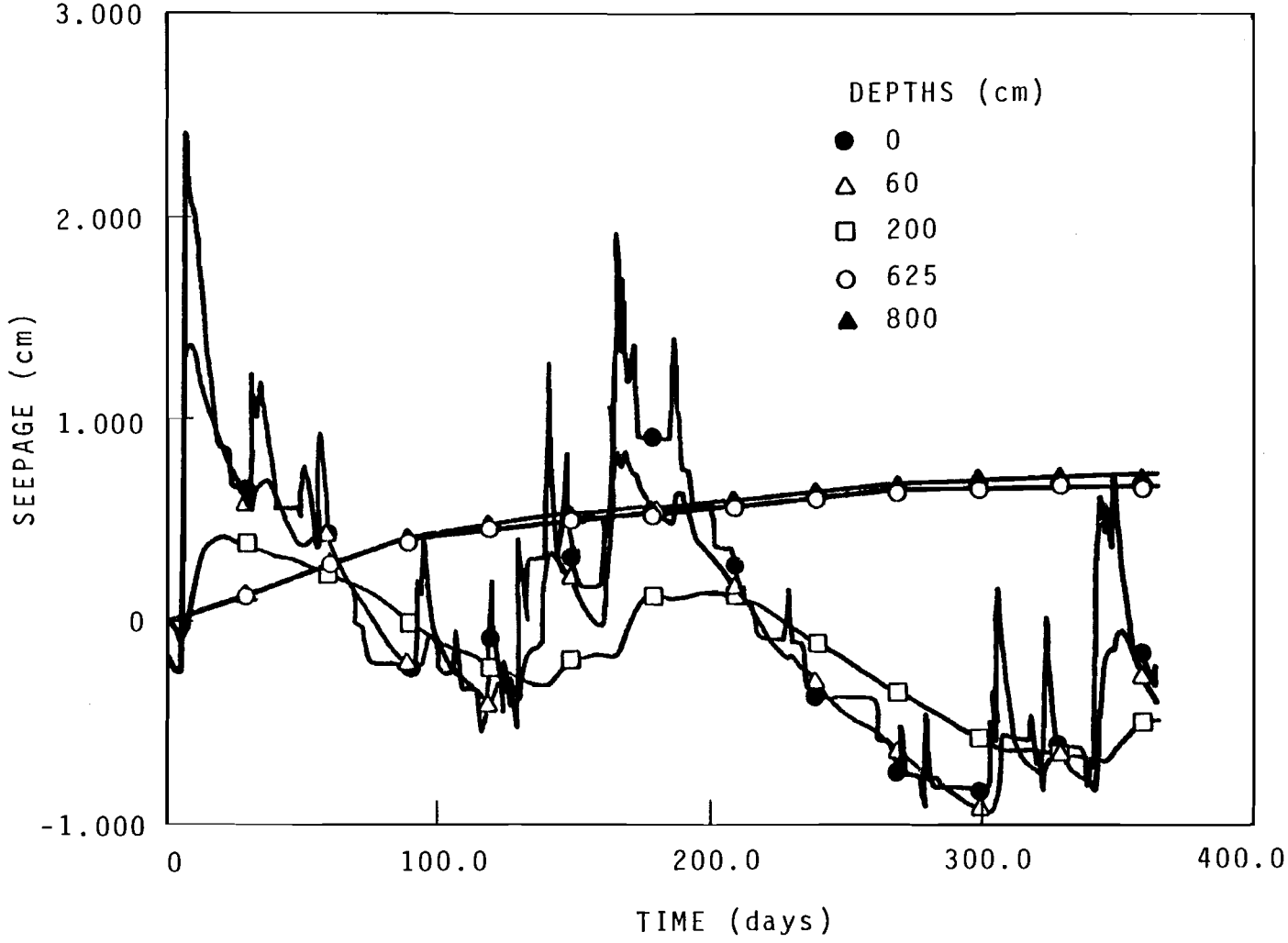

FIGURE 39. Year 2 of Figure 38: a) Cumulative Seepage at Selected Depths, b) Soil-Water Storage in the 800-cm Profile for Year 2 under Figure 38 Conditions.

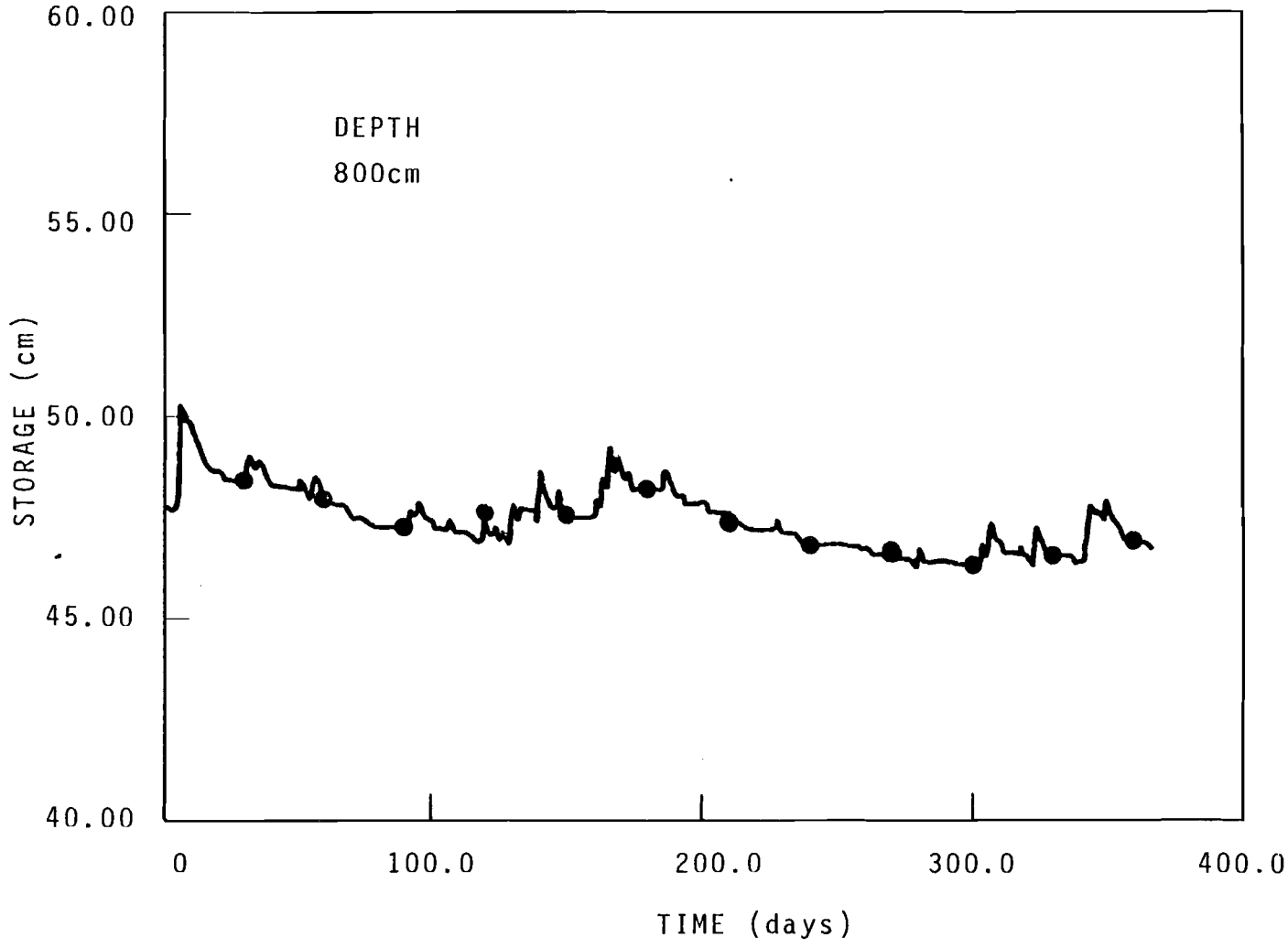

FIGURE 39. (contd)

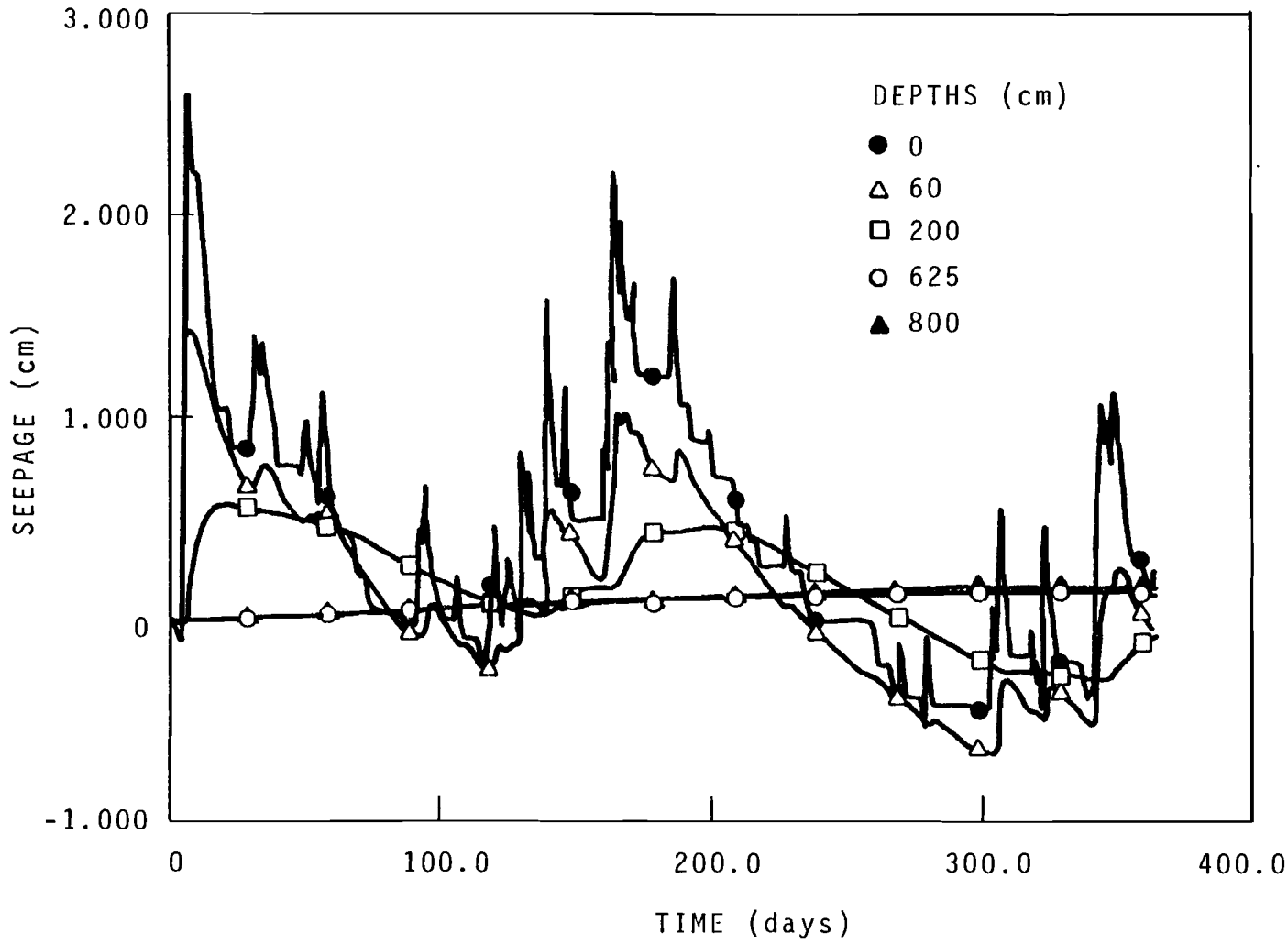

FIGURE 40. Year 3 of Figure 38: a) Cumulative Seepage at Selected Depths, b) Soil-Water Storage in the 800-cm Profile for Year 3 under Figure 38 Conditions.

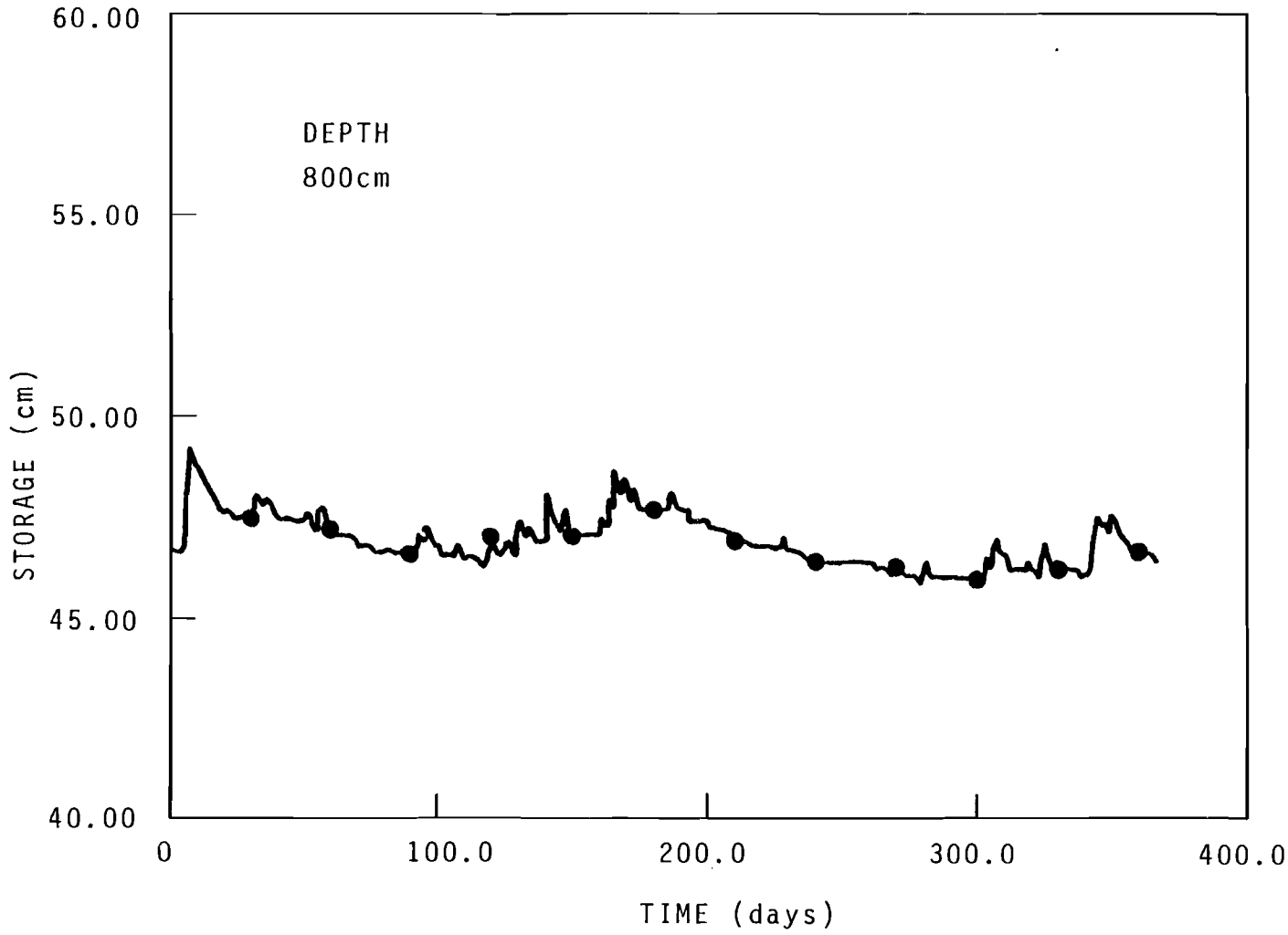

FIGURE 40. (contd)

TABLE 7. Simulation of a Three-Year Rainfall Sequence Based on Consecutive 1947 and 1948 Climates with a Repeated 1948 Year. Blaney-Criddle PET and presence of a hydrophobic surface layer are assumed. Standard initial conditions.

Year	Infiltration (cm)	Evaporation (cm)	Drainage (cm)	Storage (cm)
1947 (1)	23.47	20.13	-0.05	47.95
1948 (2)	24.56	25.02	0.73	46.70
1948 (3)	24.54	24.56	0.15	46.44

Average Mass Balance Error = 0.07 cm

Initial Storage: 44.62 cm

Potential Evaporation: 147.7 cm (1947)
131.2 cm (1948)

TABLE 8. Simulation of a Three-Year Rainfall Sequence Based on Repeated 1947 Climate. Assumptions are those of Table 7.

Year	Infiltration (cm)	Evaporation (cm)	Drainage (cm)	Storage (cm)
1947 (1)	23.47	20.13	-0.05	47.95
1947 (2)	23.47	21.97	1.15	48.23
1947 (3)	23.47	22.10	1.31	48.23

Average Mass Balance Error = 0.06 cm

Initial Storage: 44.62 cm

Potential Evaporation: 147.7 cm

conditions for which the pattern of soil-water movement is repeated, as shown by Figures 41 and 42. Apparently, about 1.3 cm of water would pass through the 800-cm soil profile each year if climate similar to 1947 repeated. On the other hand, repetition of 1948 climate would seem to produce negligible drainage even though potential evaporation is less and precipitation greater in 1948 than in 1947. In both cases, however, a steady state is approached in the sense that dependence on particular initial conditions diminishes with repetitions of climate.

EFFECTS OF SOIL PROFILE CONFIGURATION

Water-table depth and existence of heterogeneous soil layers are particularly important factors in regard to effect on possible drainage. Depth to the water table controls drainage time, as well as potential for increased surface evaporation as a consequence of upward water movement. In addition, it is known that in nonhomogeneous soils, discrete layering of materials with hydraulic conductivity properties different from the main soil body can retard water flow. Use of barriers in the form of coarse sand or gravel layers has important application to controlling water flow through buried waste deposit sites. These effects were examined by performing simulations with raised water table and with the coarse sand layer removed from the soil profile. For that purpose, the UNSAT model allows simulation of any number of soil layers, as long as hydraulic properties are provided.

Table 9 contains the summary of results for a 700-cm-deep water table and an 800-cm-deep profile with the coarse sand layer removed. Those simulations were made using 1947 climate and a hydrophobic surface layer, so that drainage could occur. Initial conditions were given in terms of suction head representing the required profile as a subset of standard initial conditions in Table 3. The coarse sand layers replaced by fine sand had water contents consistent with the head. Table 9 suggests an increased withdrawal from the shallow water table and an increased drainage without the layer, but these conclusions must be verified from detailed seepage for each depth. Figures 43 through 45 provide the necessary detail for selected depths. These figures

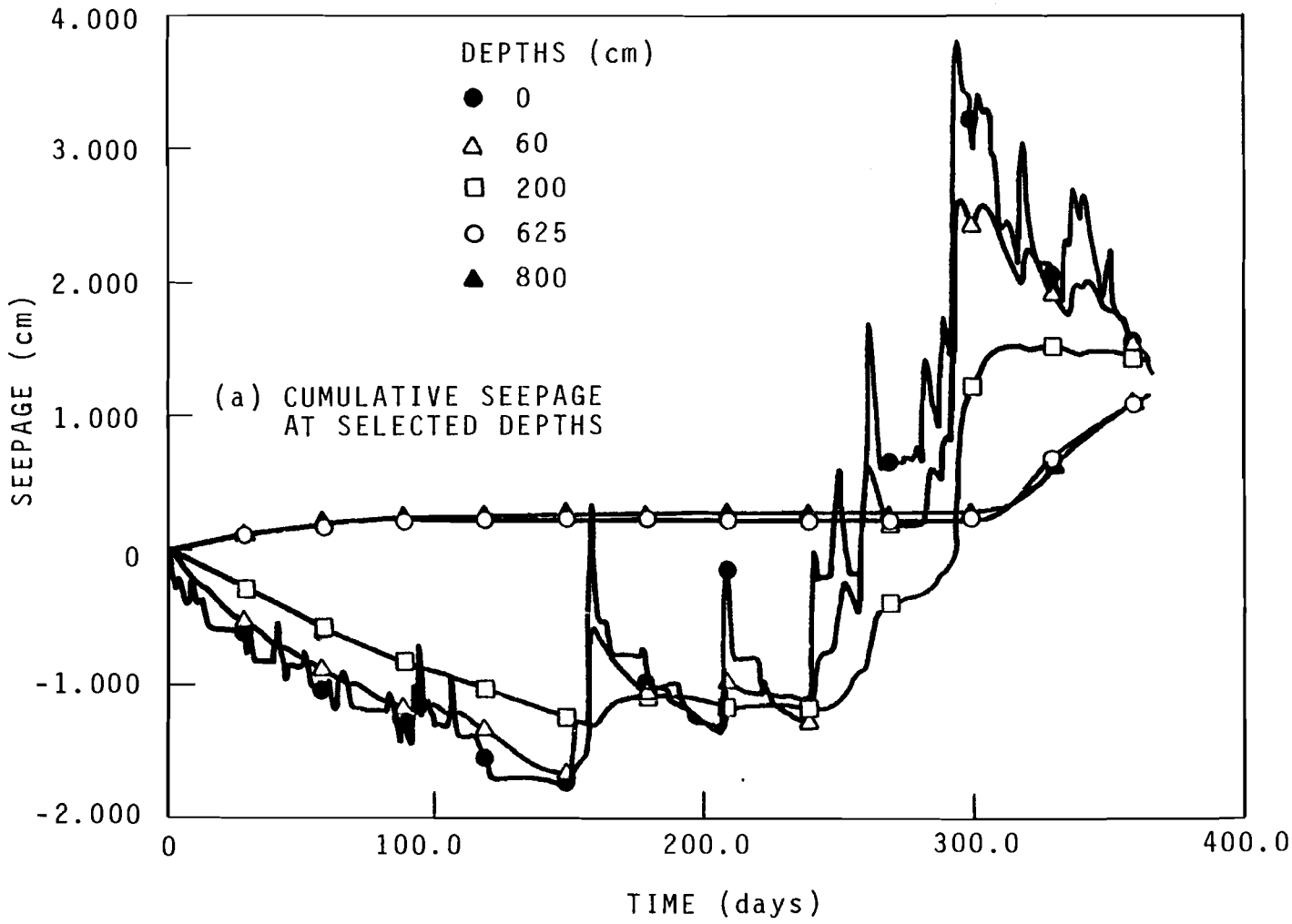

FIGURE 41. Simulation of Soil-Water Movement for a Three-Year Sequence Based on Repeated 1947 Climate: a) Cumulative Seepage at Selected Depths, b) Soil-Water Storage in the 800-cm Profile, Year 2.

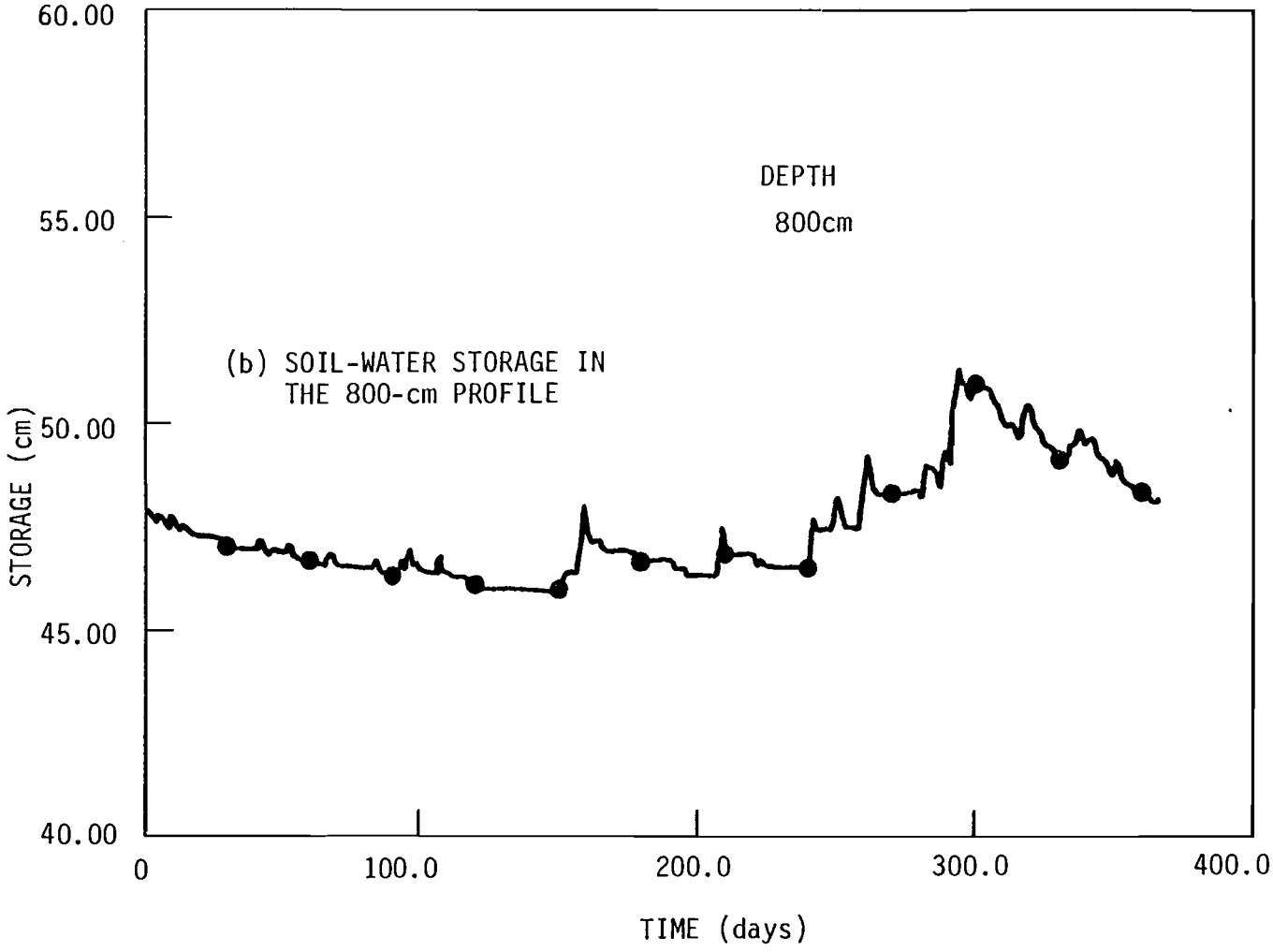

FIGURE 41. (contd)

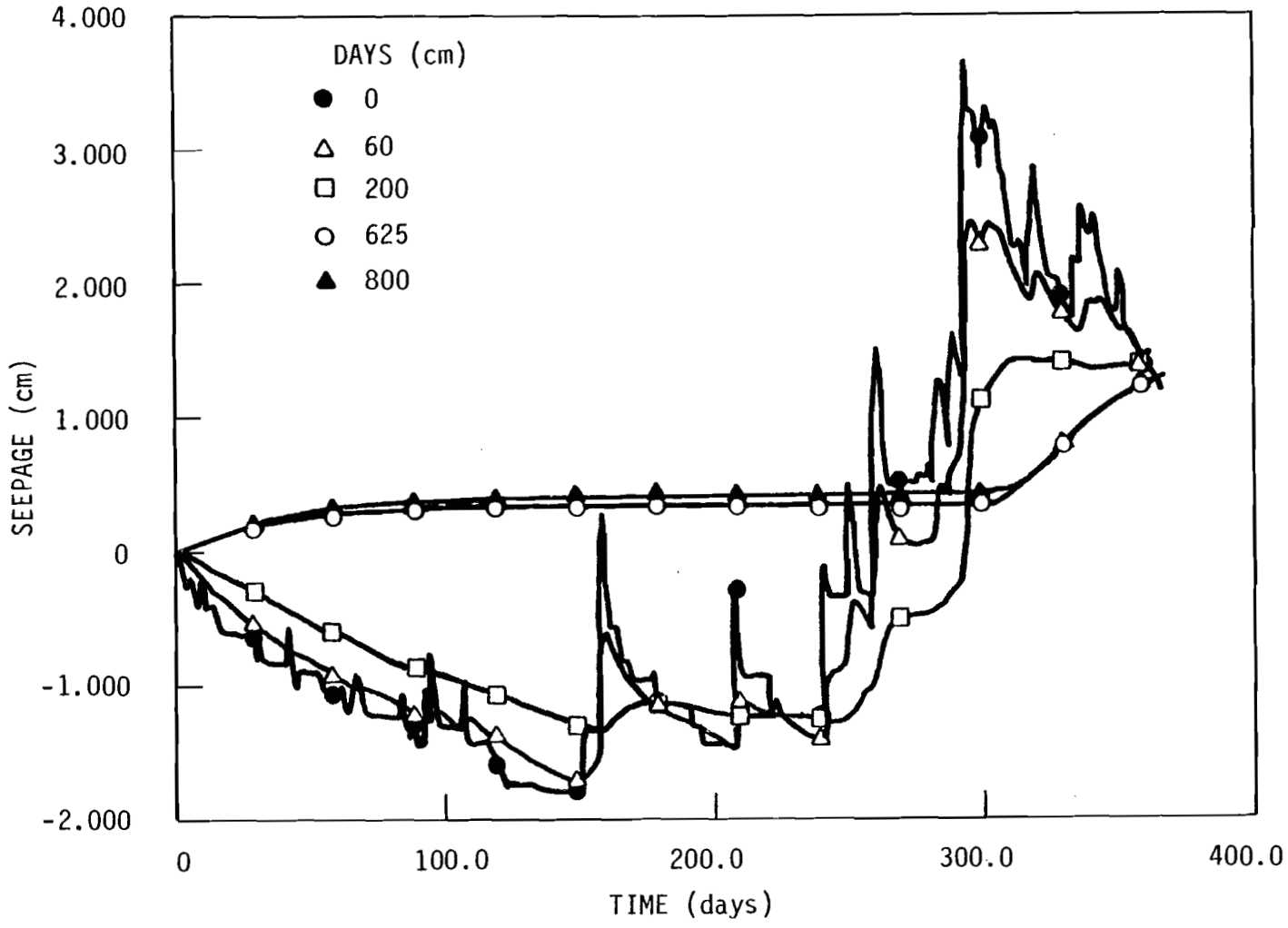

FIGURE 42. Year 3 of Figure 41: a) Cumulative Seepage at Selected Depths, b) Total Water Storage in 800-cm Profile

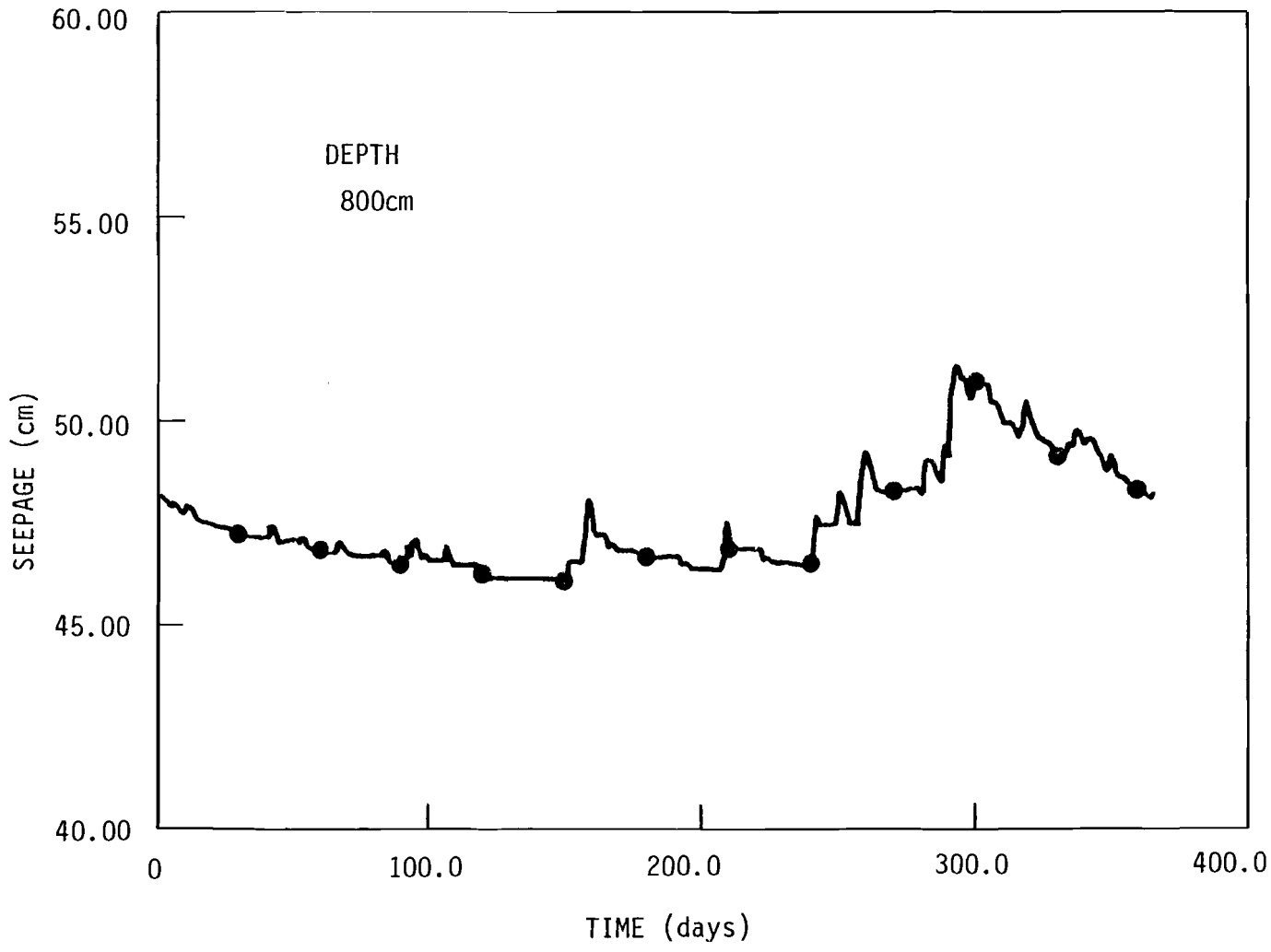

FIGURE 42. (contd)

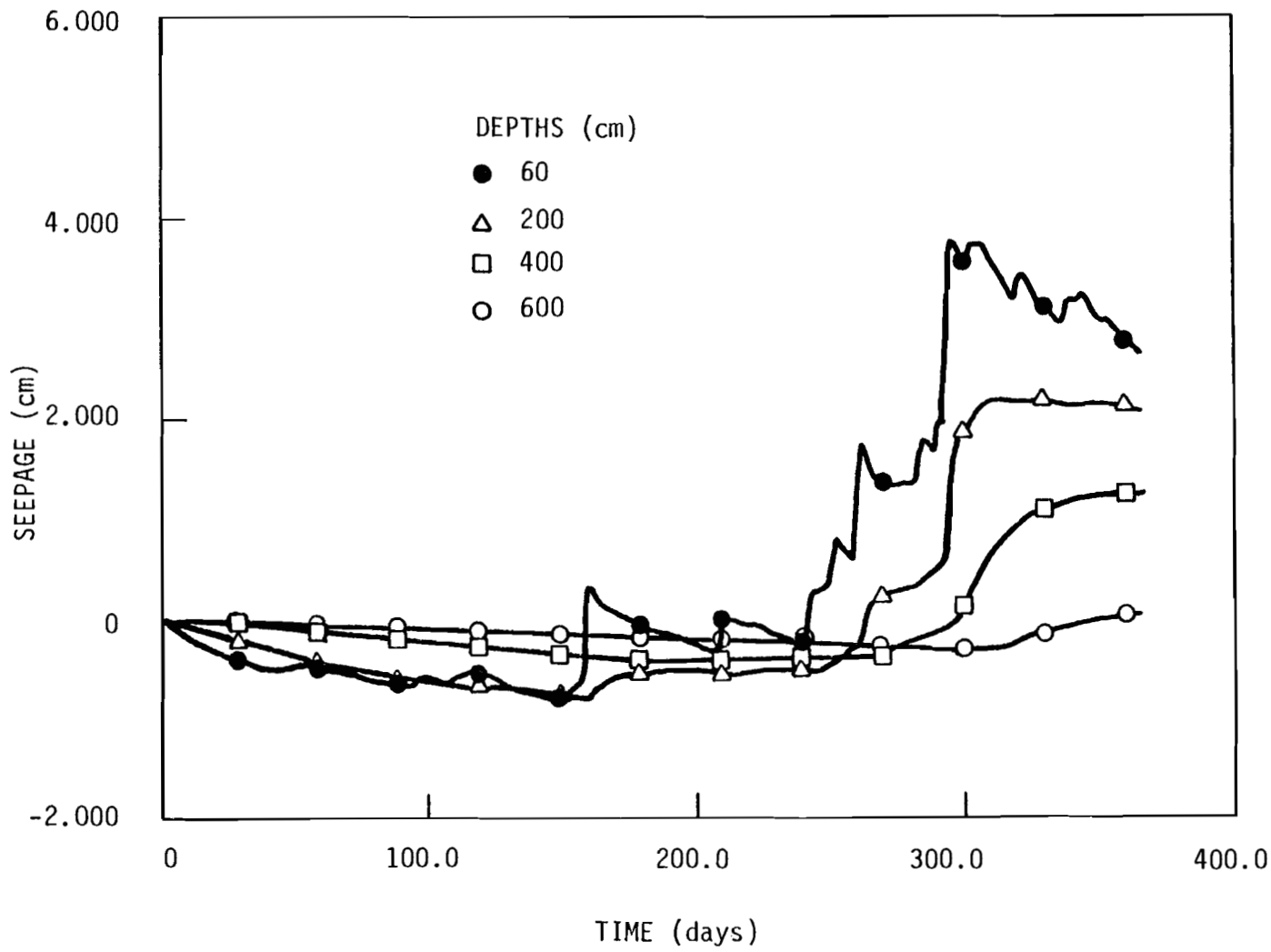

FIGURE 43. Cumulative Seepage at Selected Depths for 1947 Climate and Blaney-Criddle PET, 800-cm-deep Water Table.

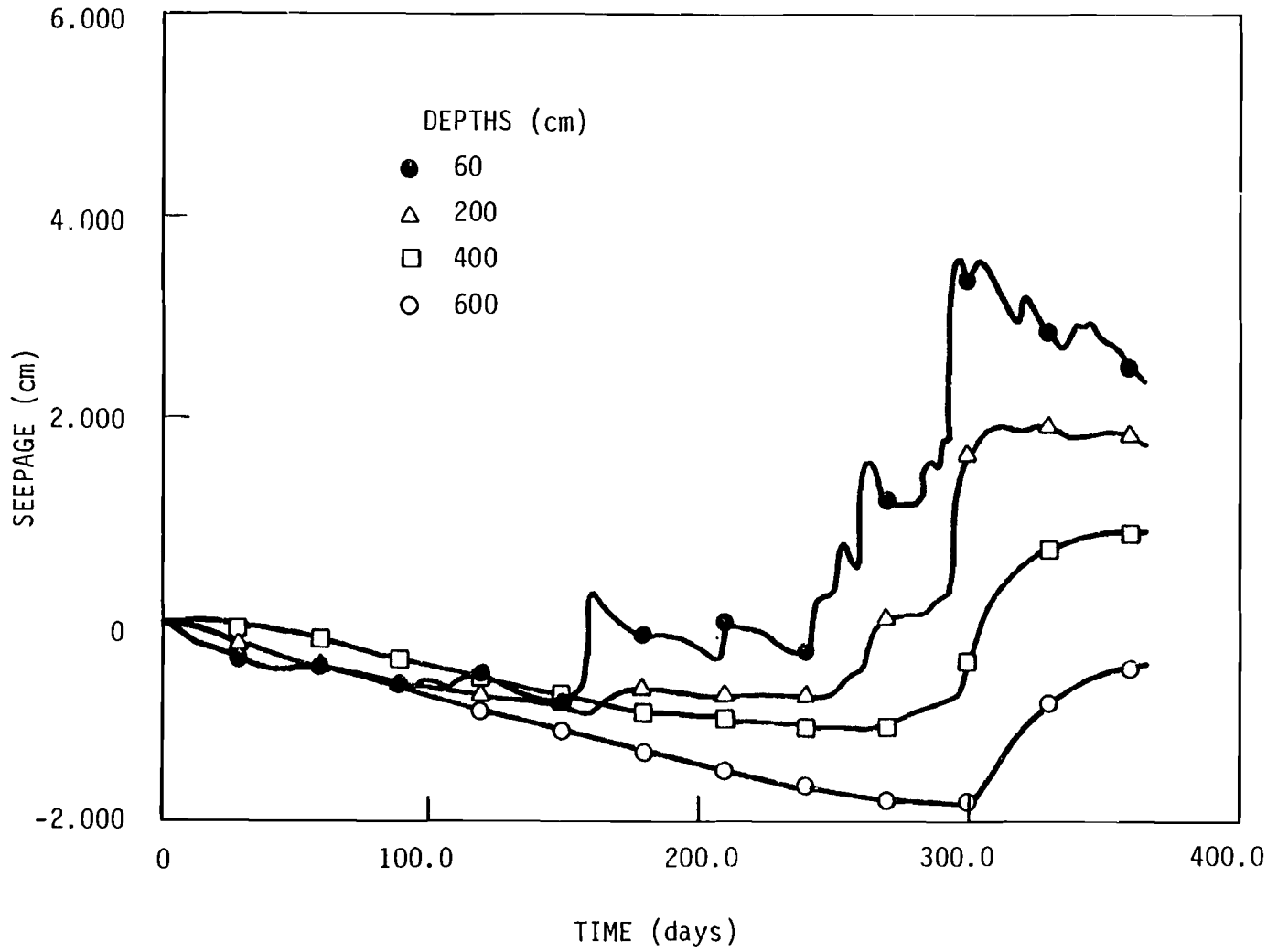

FIGURE 44. Cumulative Seepage at Selected Depths for 1947 Climate and Blaney-Criddle PET, 700-cm-deep Water Table

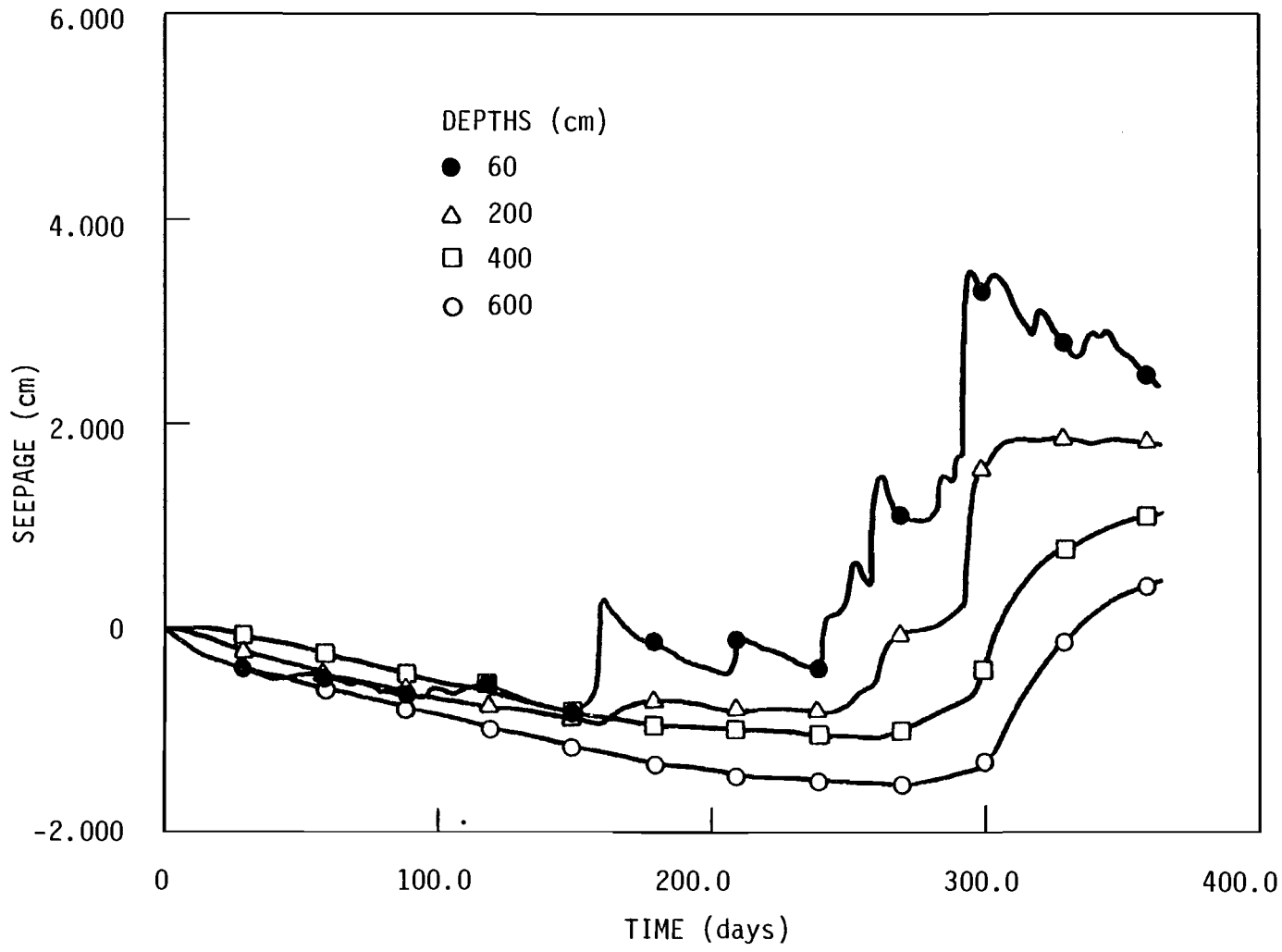

FIGURE 45. Cumulative Seepage at Selected Depths for 1947 Climate and Blaney-Criddle PET; Sand Layer Removed from Profile

TABLE 9. Simulations Using 1947 Climate and Blaney-Criddle PET Method, Assuming Presence of a Hydrophobic Layer for Three Cases

Water Table	Infiltration (cm)	Evaporation (cm)	Drainage (cm)	Storage (cm) Initial	Storage (cm) Final
(a)	23.47	20.13	-0.05	44.62	47.95
(b)	23.47	20.41	-0.73	37.77	41.45
(c)	23.47	20.43	0.26	50.03	52.72

Average Mass Balance Error = 0.09 cm

Potential Evaporation: 147.7 cm

(a) 800-cm water table including coarse sand layer 600 to 650 cm

(b) 700-cm water table including coarse sand layer 600 to 650 cm

(c) 800-cm water table without sand layer

seem to imply that rate of seepage both into and out of the water table is increased by either shallower water table or removal of the coarse sand layer. Although drainage decreased according to Table 9, the excess storage would flow into the water table more rapidly during the following year. Continued simulation, however, would be required to verify that behavior.

Differences in the water content profiles with and without a coarse sand layer at 600 cm are shown for some selected days in Figures 46 and 47. The selected days represent a period having 8.8 cm of rainfall with 2.5 cm remaining after evaporation. The wetting front is seen to be blocked by the layer in Figure 46.

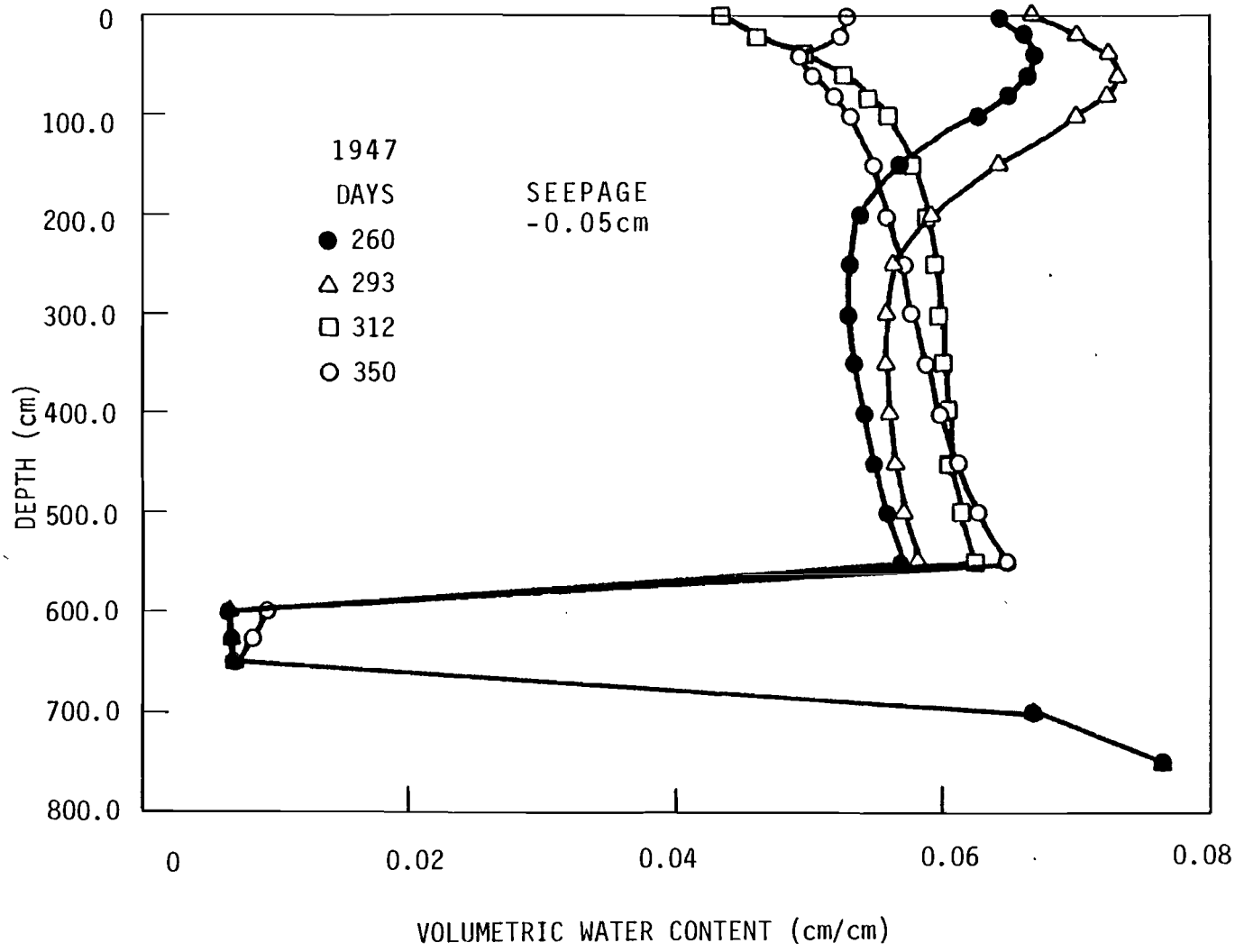

FIGURE 46. Water Content Profiles for Selected Days in 1947. Rainfall was 8.8 cm for the period.

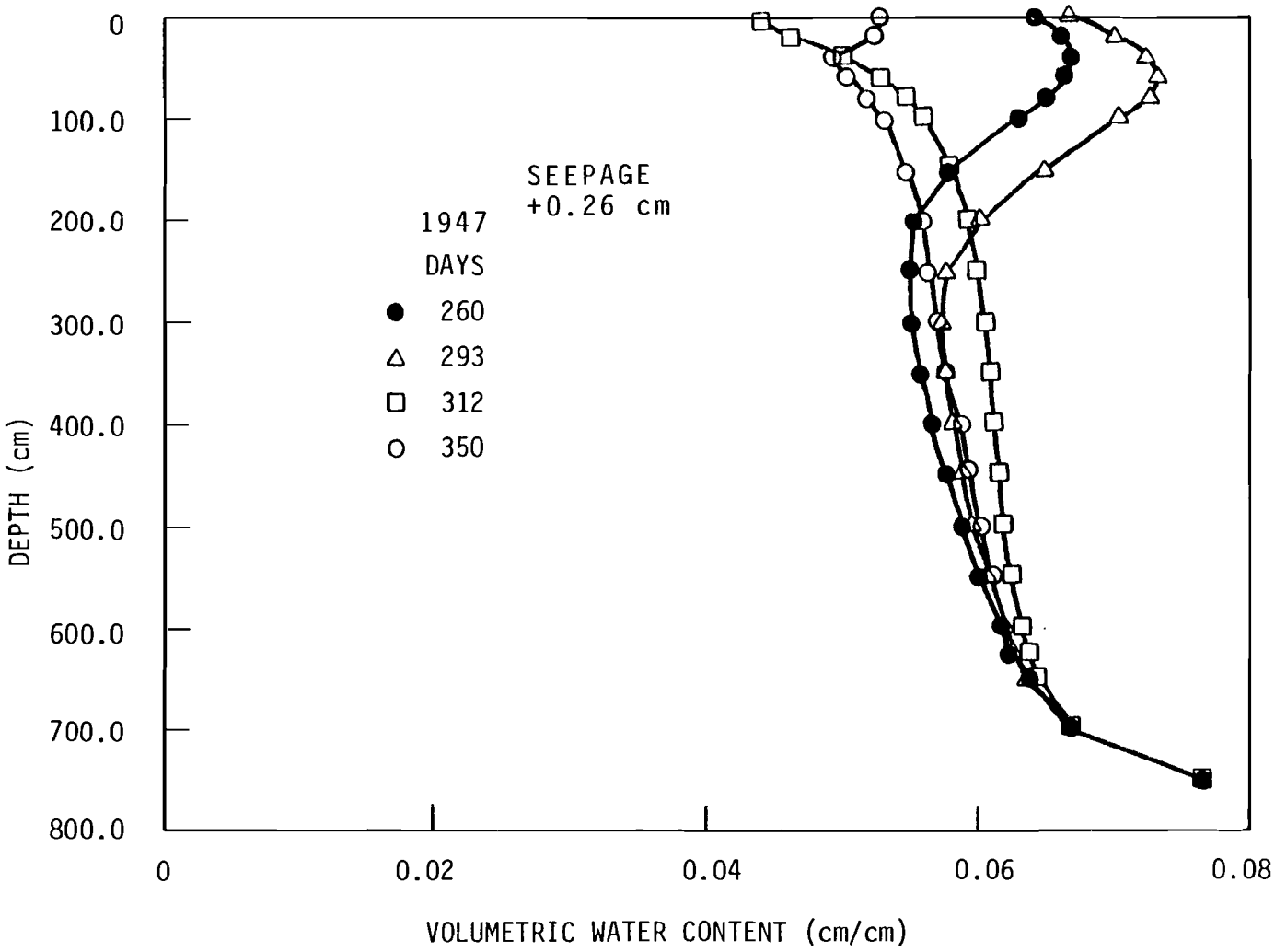

FIGURE 47. Water Content Profiles for Selected Days in 1947 with Coarse Sand Layer Removed

REFERENCES

Black, T. A., W. R. Gardner, and G. W. Thurtell. 1969. "The Prediction of Evaporation, Drainage, and Soil Water Storage for a Bare Soil," Soil Sci. Soc. Am. Proc. 33:655-660.

Blaney, H. F. and W. D. Criddle. 1962. Determining Consumptive Use and Irrigation Water Requirements. USDA (ARS) Tech. Bull. 1275. 59 pp.

Brownell, L. E., J. G. Backer, R. E. Isaacson and D. J. Brown. 1975. Soil Moisture Transport in Arid Site Vadose Zones. Part II. ARH-ST-123. 232 pp.

Cary, J. W. 1966. "Soil Moisture Transport Due to Thermal Gradients. Practical Aspects," Soil Sci. Soc. Am. Proc. 30:428-433.

Doorenbos, J. and W. O. Pruitt. 1975. "Guidelines for Predicting Crop Water Requirements," Irrigation and Drainage Paper 24:1-179. First Edition. Food and Agricultural Organization of the United Nations, Rome.

Enfield, C. G., J. J. C. Hsieh and A. W. Warrick. 1973. "Evaluation of Water Flux Above a Deep Water Table Using Thermocouple Psychrometers," Soil Sci. Soc. Am. Proc. 37:968-970.

Feddes, R. A. 1971. "Water, Heat and Crop Growth," Comm. Agric. Univ. 16:71-12, Wageningen, Netherlands,

Fuchs, M., G. S. Campbell and R. I. Papendick. 1978. "An Analysis of Sensible and Latent Flow in a Partially Frozen Unsaturated Soil," Soil Sci. Soc. Am. J. 42:379-385.

Gardner, H. R. and W. R. Gardner. 1969. "Relation of Water Application to Evaporation and Storage of Soil Water," Soil Sci. Soc. Am. Proc. 33:192-196.

Gilmore, W. R. 1977. Radioactive Waste Disposal; Low and High Level. Noyes Data Corp., Park Ridge, NJ. 364 pp.

Gupta, S. K., K. Tanji, D. Nielsen, J. Biggar, C. Simmons, and J. MacIntyre. 1978. Field Simulation of Soil-Water Movement with Crop Water Extraction. Water Science and Engineering Paper No. 4013. Dept. of Land, Air, and Water Resources, Univ. of Calif., Davis.

Hanks, R. J., H. R. Gardner and M. L. Fairbourn. 1967. "Evaporation of Water from Soils as Influenced by Drying with Wind or Radiation," Soil Sci. Soc. Am. Proc. 31:593-598.

Hillel, D. I., C. H. M. van Bavel, and H. Talpaz. 1975. "Dynamic Simulation of Water Storage in Fallow Soil as Affected by Mulch of Hydrophobic Aggregates," Soil Sci. Soc. Am. J. 39:826-833.

Hillel, D. I. 1977. Computer Simulation of Soil Water Dynamics. I.D.R.C. Box 8500, Ottawa, Canada. 215 pp.

Idso, S. B., R. D. Jackson, R. J. Reginato. 1975. "Estimating Evaporation: A Technique Adaptable to Remote Sensing," Sci. 189:991-992.

Jackson, R. D. 1973. "Diurnal Changes in Soil-Water Content During Drying," R. R. Bruce (ed) Field Soil Water Regime. Soil Sci. Soc. Amer. Special Pub. 5, pp. 37-55.

Jackson, R. D., B. A. Kimball, R. J. Reginato and F. S. Nakayama. 1973. "Diurnal Soil-Water Evaporation: Time-Depth-Flux Patterns," Soil Sci. Soc. Am. Proc. 37:505-509.

Jackson, R. D., R. J. Reginato, B. A. Kimball and F. S. Nakayama. 1974. "Diurnal Soil-Water Evaporation: Comparison of Measured and Calculated Soil-Water Fluxes," Soil Sci. Soc. Am. Proc. 38(6):861-866.

Jackson, R. D., B. A. Kimball, R. J. Reginato, S. B. Idso and F. S. Nakayama. 1975. "Heat and Water Transfer in a Natural Soil Environment," D. A. Devries (ed.) Heat and Mass Transfer in the Biosphere. Vol. I. Transfer Processes in the Plant Environment. Scripta Book Pub. Co., Washington, DC, pp. 67-76.

Jury, W. A. 1973. Simultaneous Transport of Heat and Moisture through a Medium Sand. Ph.D. Dissertation, Univ. Microfilms, Ann Arbor, MI, 191 pp.

Jury, W. A. and J. Letey. 1979. Water Vapor Movement in Soil. Reconciliation of Theory and Experiment (Submitted to Soil Science Society Am. J.).

Kimball, B. A., R. D. Jackson, R. J. Reginato, F. S. Nakayama and S. B. Idso. 1976. "Comparison of Field-measured and Calculated Soil-heat Fluxes," Soil Sci. Soc. Am. J. 40:18-25.

Letey, J. 1968. "Movement of Water Through Soil as Influenced by Osmotic Pressure and Temperature Gradients," Hilgardia. 39:405-418.

Lindberg, J. W. and F. W. Bond. 1979. Geohydrology and Groundwater Quality Beneath the 300 Area, Hanford Site, Washington. PNL-2949. Pacific Northwest Laboratory, Richland, Washington.

Makkink, G. F. 1957. "Testing the Penman Formula by Means of Lysimeters," J. Inst. Water Eng. 11:277-288.

Morton, F. I. 1976. "Climatological Estimates of Evapotranspiration," Proc. ASCE. J. Hydrol. Div. 102:275-290.

Paas, H. J. 1955. Unconfined Radioactive Waste and Contamination in the 300 Area and Miscellaneous Areas Not Included in Other Reports. HW-39076. 12 pp.

Penman, H. L. 1948. "Natural Evaporation from Open Water, Bare Soil and Grass," Royal Soc. London Proc. Ser. A. 193:120-146.

Phillips, S. J., A. E. Reisenauer, W. H. Rickard and G. A. Sandness. 1977. Initial Site Characterization and Evaluation of Radionuclide Contaminated Solid Waste Burial Grounds. BNWL-2154, Pacific Northwest Laboratory, Richland, Washington, 59 pp.

Reisenauer, A. E. 1972. Calculations of Soil Hydraulic Conductivity from Soil-Water Retention Relationships. Pacific Northwest Laboratory, BNWL-1710, Richland, Washington.

Ritchie, J. T. 1972. "Model for Predicting Evaporation from a Row Crop with Incomplete Cover," Water Resources Res. 8:1204-1213.

Rosenberg, N. J. 1974. Microclimate, The Biological Environment. John Wiley and Sons, New York, NY 315 pp.

Staple, W. J. 1974. "Modified Penman Equation to Provide the Upper Boundary Condition in Computing Evaporation from Soil," Soil Sci. Soc. Am. Proc. 38:837-389.

Tanner, C. B. and W. A. Jury. 1976. "Estimating Evaporation and Transpiration from a Row Crop During Incomplete Cover," Agron. J. 68:239-243.

Tanner, C. B. and M. Fuchs. 1968. "Evaporation from Unsaturated Surfaces: A Generalized Combination Method," J. Geophys. Res. 73:1299-1304.

Taylor, S. A. and J. W. Cary. 1964. "Linear Equations for the Simultaneous Flow of Matter and Energy in a Continuous Soil System," Soil Sci. Soc. Am. Proc. 28:167-172.

Thornthwaite, C. W. and J. R. Mather. 1955. "The Water Balance," Climatology. 8(1), Laboratory of Climatology, Centerton, NJ.

Wallace, R. W. 1978. "A Comparison of Evapotranspiration Estimates Using DOE Hanford Climatological Data," PNL-2698, Pacific Northwest Laboratory, Richland, Washington, 19 pp.

DISTRIBUTION

No. of Copies	OFFSITE
	A. A. Churm DOE Chicago Patent Group 9800 South Cass Ave. Argonne, IL 60439
27	DOE Technical Information Center
	G. W. Cunningham DOE Division of Waste Management Production and Reprocessing Washington, DC 20545
	C. R. Cooley DOE Division of Waste Management Washington, DC 20545
	G. H. Daily Division of Waste Management Production and Processing Washington, DC 20545
	J. E. Dieckhoner Division of Waste Management Production and Reprocessing Washington, DC 20545
	C. H. George DOE Office of Assistant Secretary for Energy Technology Washington, DC 20545

No. of Copies	OFFSITE
	D. R. Spurgeon DOE Office of Assistant Secretary for Energy Technology Washington, DC 20545
	L. Dressin DOE Office of Assistant Secretary for Energy Technology Washington, DC 20545
	G. K. Ortel DOE Office of Assistant Secretary for Energy Technology Washington, DC 20545
	A. F. Kluk Division of Environmental Control Engineering Nuclear Programs Washington, DC 20545
	W. E. Mott Division of Environmental Control Engineering Washington, DC 20545
	C. A. Heath DOE Division of Waste Management Washington, DC 20545
	S. Myers DOE Office of Nuclear Waste Management Washington, DC 20545

No. of
Copies

OFFSITE

R. W. Ramsey
Division of Environmental
Control Engineering
Washington, DC 20545

L. C. Braisley
DOE Office of Assistant
Secretary of the
Environment
Washington, DC 20545

W. A. Brobst
Environmental Control
Engineering
Environmental Control
Technology
Washington, DC 20545

Department of Energy
Albuquerque Operations
Office
Albuquerque, NM 87115

Department of Energy
Chicago Operations Office
Argonne, IL 60439

Department of Energy
Argonne National Laboratory
Argonne, IL 60439

Department of Energy
Brookhaven National Laboratory
Upton, NY 11973

Department of Energy
Idaho Operations Office
Idaho Falls, ID 83401

Department of Energy
Idaho National
Engineering Laboratory
Idaho Falls, ID 83401

No. of
Copies

OFFSITE

Department of Energy
Nevada Operations Office
Las Vegas, NE 89114

Department of Energy
Oak Ridge Operations Office
Oak Ridge, TN 37830

Department of Energy
Oak Ridge National Laboratory
Oak Ridge, TN 37830

Department of Energy
Savannah River Operations
Office
Aiken, SC 29081

Department of Energy
Savannah River National
Laboratory
Aiken, SC 29081

Department of Energy
Los Alamos National
Laboratory
Los Alamos, NM 87545

P. Columbo
Brookhaven National
Laboratory
Upton, NY 11973

E. L. Albenesius
Savannah River National
Laboratory
Aiken, SC 29081

H. Reno
Idaho National
Engineering Laboratory
Idaho Falls, ID 83401

No. of Copies

OFFSITE

P. A. Dickman
Idaho National Engineering Laboratory
Idaho Falls, ID 83401

J. G. Steger
Los Alamos Scientific Laboratory
Los Alamos, NM 87545

L. J. Johnson
Los Alamos Scientific Laboratory
Los Alamos, NM 87545

T. Tamura
Oak Ridge National Laboratory
Oak Ridge, TN 37830

F. A. Morris
HARC
4000 N.E. 41st Street
P.O. Box 5395
Seattle, WA 98105

R. F. Smith
HARC
4000 N.E. 41st Street
P.O. Box 5395
Seattle, WA 98105

Atomic Industrial Forum, Inc.
7101 Wisconsin Ave.
Washington, DC 20014

Beverly Rawles
Battelle Memorial Institute
Office of Nuclear Waste Isolation
505 King Ave.
Columbus, OH 43201

No. of Copies

OFFSITE

Environmental Protection Agency
Technology Assessment Division
Office of Radiation Programs
Washington, DC 20460

National Academy of Sciences
Radioactive Waste Management Committee
National Research Council
2101 Constitution Ave.
Washington, DC 20418

Nuclear Regulatory Commission
Division of Safeguards, Fuel Cycle and Environmental Research
Washington, DC 20545

C. Bishop
NRC Division of Fuel Cycle
Low Level Branch
Washington, DC 20555
Mail Stop 396-SS

FOREIGN

International Atomic Energy Agency
Kartner Ring II
P.O. Box 590
A-1011 Vienna,
AUSTRIA

No. of Copies	
ONSITE	
9	Richland Operations Office
	R. E. Austin O. J. Elgert R. E. Gerton R. B. Goranson J. L. Landon H. E. Ransom J. L. Rhodes F. R. Standerfer J. D. White
2	United Nuclear Industries
	T. E. Dabrowski J. F. Nemec
2	Rockwell Hanford Operations
	J. L. Deichman A. W. Graves
43	Pacific Northwest Laboratory
	L. L. Ames W. J. Bair D. B. Cearlock J. R. Eliason R. E. Fitzner K. A. Gano G. W. Gee D. E. Olesen S. J. Phillips (10) A. M. Platt W. H. Rickard L. E. Rogers G. A. Sandness R. J. Serne C. S. Simmons R. A. Walter W. R. Wiley Technical Information (5) Publishing Coordination (2) Water and Land Resources Library (10) Ro